

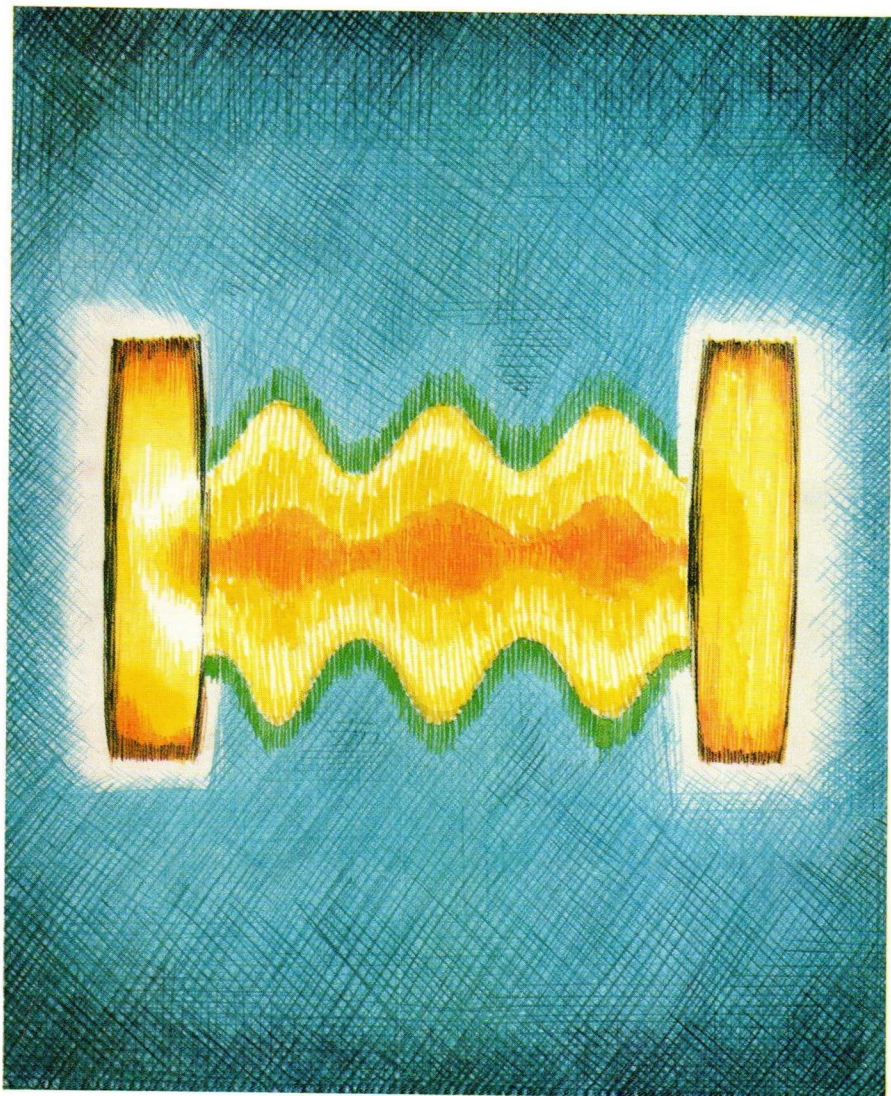
# PHILIPS

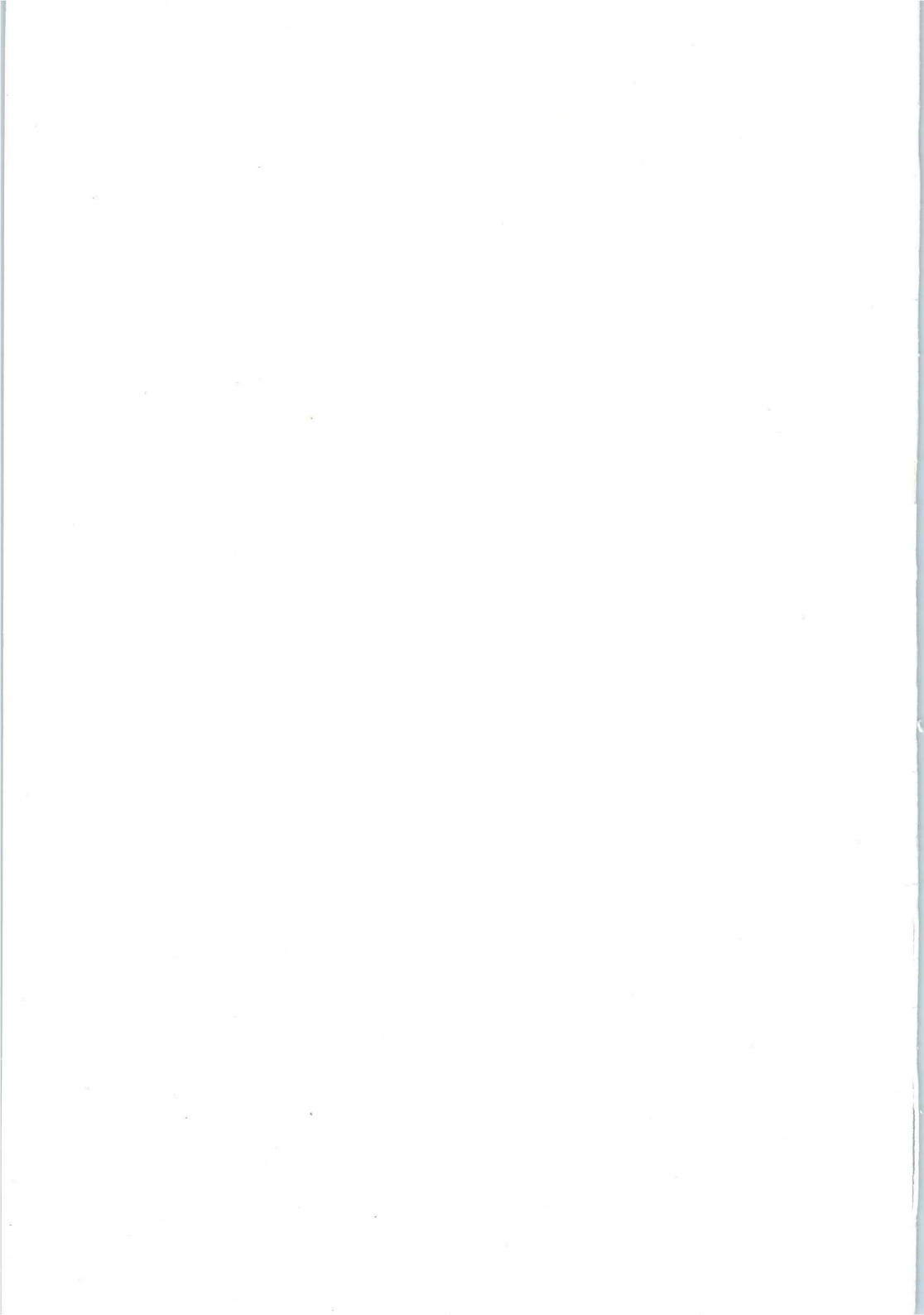
Application book



Electronic  
components  
and materials

## Piezoelectric ceramics





E12

## **Piezoelectric Ceramics**



# Piezoelectric Ceramics

*Edited by*

*J. van Randerlaat and R. E. Settrington*

PUBLICATIONS DEPARTMENT  
ELECTRONIC COMPONENTS AND MATERIALS DIVISION

© *N.V. Philips' Gloeilampenfabrieken, Eindhoven, The Netherlands*

*First edition June 1968*  
*Second edition January 1974*

*The publication of this document does not imply a licence under any patent*

# Contents

<b>1</b>	<b>Introduction</b>	<b>1</b>
<b>2</b>	<b>The piezoelectric effect in ceramic materials</b>	<b>4</b>
2.1	General	4
2.2	Examples	6
2.3	Theory and definitions of piezoelectric quantities	8
2.4	Depolarization	15
2.5	Stability	16
2.6	The range of PXE materials and their properties	17
<b>3</b>	<b>PXE ignition of gases</b>	<b>23</b>
3.1	General	23
3.2	PXE high voltage generation	23
3.3	Construction of an ignition unit	31
3.4	Static igniters (squeeze action)	35
3.5	Impact igniters	36
3.6	Considerations on ignition probability	38
<b>4</b>	<b>PXE flexure elements</b>	<b>40</b>
4.1	Operating principle	40
4.2	Support of flexure elements	42
4.3	Applications of flexure elements	43
4.4	Static and dynamic behaviour below resonance	44
4.5	Behaviour in the resonance range	49
4.6	Maximum output from PXE flexure elements	52
4.7	Application examples	54
<b>5</b>	<b>Ceramic resonators in electrical filters</b>	<b>64</b>
5.1	Mode of operation and construction	65
5.2	Encapsulation of the resonator	68
5.3	Resonator characteristics and measurements	68
5.4	Using resonators in filters	71
<b>6</b>	<b>PXE sound and ultrasound air transducers</b>	<b>78</b>
6.1	General	78
6.2	Applications	78
6.3	Construction and characteristics of ultrasound air transducers	81
6.4	Design and characteristics of a 36 kHz ultrasound air transducer	87
6.5	Transmitter circuits for 36 kHz ultrasound air transducers	92
6.6	Receiver circuits for 36 kHz ultrasound air transducers	95
6.7	A simple 3 kHz tone generator	103
6.8	Ultrasonic safety belt security system	105
6.9	PXE telephone microphone	106

<b>7</b>	<b>Echo sounders</b>	108
7.1	General	108
7.2	Characteristics of echo sounding systems	109
7.3	The ultrasound transducer in echo sounding systems	110
7.4	Electrical matching	113
7.5	Measurements on echo sounding transducers	114
7.6	Performance data of a typical echo sounder transducer	117
7.7	Transmitter and receiver circuits for echo sounding systems	118
<b>8</b>	<b>PXE high intensity transducers</b>	123
8.1	General	123
8.2	Advantages of composite transducers	124
8.3	Improving radiation intensity and bandwidth by means of different end sections	126
8.4	Performance of non-pre-stressed composite transducers	134
8.5	Pre-stressed composite transducers (with applications)	136
8.6	Disc transducers (bonded to a cleaning tank)	143
<b>9</b>	<b>PXE delay line transducers</b>	146
9.1	General	146
9.2	Solid delay lines	147
9.3	High coupling PXE transducers	148
9.4	Modes of vibration	150
9.5	Directivity of transducers	150
9.6	Bonds for shear wave transducers	153
9.7	PXE materials for shear wave transducers	153
9.8	Description of an actual delay line	154
Appendix A	Dynamic behaviour of PXE transducers	159
Appendix B	Bonding techniques	169
	B.1 Gluing	169
	B.2 Soldering	170
Appendix C	Temperature graphs	172
Appendix D	Coupling coefficient chart	190
Appendix E	Survey of seven important modes of vibration	193
Appendix F	S.I. units	196
<b>References</b>		<b>201</b>
<b>Index</b>		<b>202</b>

## **Contributors**

- C. M. v.d. Burgt – The Netherlands  
D. G. J. Fanshawe – United Kingdom  
J. F. Fiedeldij – The Netherlands  
I. Flinn – United Kingdom  
D. J. Grevink – The Netherlands  
G. D. van Grol – The Netherlands  
P. J. Hulyer – United Kingdom  
J. Koch – Germany  
W. Laurich – Germany  
A. Petersen – Germany

## List of symbols

$A$	= surface area
$B$	= bandwidth; volume
$C$	= capacitance
$D$	= dielectric displacement; diameter
$d$	= piezoelectric charge constant
$E$	= field strength
$F$	= force
$f$	= frequency
$f_M$	= maximum response frequency
$f_m$	= minimum-impedance frequency
$f_n$	= maximum-impedance frequency
$G$	= gain
$g$	= piezoelectric voltage constant
$h$	= height
$I$	= acoustic intensity
$J$	= Bessel function
$k$	= coupling coefficient
$L$	= inductance
$l$	= length
$M$	= piezoelectric figure of merit
$N$	= frequency constant
$n$	= arbitrary number
$P$	= power
$p$	= sound pressure
$Q$	= quality factor
$Q_e$	= electrical quality factor
$Q_m$	= mechanical quality factor
$R$	= resistance
$S$	= strain (relative deformation)
$s$	= elastic compliance
$T$	= mechanical stress; temperature
$T_c$	= stress amplitude
$t$	= time
$u$	= impact speed

$V$	=	voltage
$v$	=	propagation speed; velocity
$W$	=	energy
$w$	=	width
$Y$	=	elasticity modulus; electrical admittance
$Z$	=	impedance
$z$	=	deflection
$\tan \delta$	=	dielectric loss factor
$\varepsilon$	=	absolute permittivity
$\zeta$	=	radiation coefficient
$\eta$	=	efficiency
$\theta_c$	=	Curie temperature
$\lambda$	=	wavelength
$\rho_{et}$	=	electrical resistivity
$\rho_m$	=	mass density
$\sigma$	=	Poisson's ratio of lateral contraction
$\tau$	=	delay time
$\omega$	=	angular frequency

## Foreword

Although this book bears the same title as its predecessor it has been extensively rewritten and contains a great deal of new material in the form of data on the latest PXE types and descriptions of applications — from the most professional level to the everyday consumer item. Where useful information has been retained from the first edition it has been thoroughly revised and up-dated. The result is a practical guide for everyone concerned with piezoelectric materials.

One thing that has not changed over the years is our attitude toward service. We are, of course, able to offer a wider service as our knowledge expands — and our application support team are well versed — but it is impossible to foresee every use to which PXE will be put, or to imagine how customer requirements will shape the PXE types of the future. Constant interchange between user and manufacturer is a vital stimulus to improving the product and extending its scope. We look forward to it continuing.

J. F. Fiedeldij,  
Product Division  
Piezoelectric Ceramics.

## 1 Introduction

Piezoelectricity is the name for the phenomenon whereby electric dipoles are generated in certain anisotropic crystals when subjected to mechanical stress\*. The same materials exhibit the converse effect in that they suffer a dimensional change under the influence of an electric field. A few of the natural crystals, such as quartz, tourmaline and Rochelle salt, are the traditional piezoelectric materials. For many years these have served well as transducers for converting electrical energy into mechanical energy (and vice versa), and they will undoubtedly continue to be used as such in specific applications.

Ceramic piezoelectric materials were developed some years ago and have been constantly improved since then. These materials are finding a wide range of usage, which will be discussed in this Application Book. Prospects are that continued research will result in the addition of many more applications to the existing range.

Physically, ceramic piezoelectric materials are hard, chemically they are inert and immune to humidity and other atmospheric conditions. They have mechanical properties resembling those of the better known insulation ceramics and they are manufactured by much the same processes.

Thanks to their ceramic nature, these new piezoelectric materials can be given almost any shape or size with the direction of polarization freely chosen, as the Frontispiece shows. Consequently, ceramic piezoelectric materials offer greater versatility in transducer design than any single crystal material. Furthermore they are extremely "stiff", that is to say, they are capable of exerting or sustaining very great stresses.

By slightly changing the chemical composition of the materials it is possible to emphasize one or more specific properties so that special requirements can be met. For this reason several grades of piezoceramic are available, each tailored to suit a particular field of application and rigorously tested for its ability to meet the severest quality requirements (*PLATE I*).

\* This effect was discovered in 1880 by Jacques and Pierre Curie.

The range of application of these materials is immense and can be divided into the following groups:

- high voltage generators  
(for ignition purposes)
  - gas appliances;
  - cigarette lighters;
  - fuzes for explosives;
  - flash bulbs,
  - small petrol motors.
- high power ultrasonic generators
  - ultrasonic cleaning (industrial and domestic appliances);
  - sonar;
  - echo sounding;
  - underwater telephony;
  - ultrasonic welding and drilling of plastics and metals;
  - ultrasonic soldering;
  - atomization,
  - pulverization.
- transducers for sound and ultrasound in air
  - microphones (e.g., for telephones);
  - intruder alarm systems;
  - remote control;
  - loudspeakers (e.g., tweeters),
  - audio tone generators in signalling devices.
- pick-ups and sensors
  - record players;
  - accelerometers;
  - detection systems in machinery (e.g., textile);
  - medical equipment;
  - motor cars,
  - musical instruments.
- resonators and filters
  - radio;
  - television;
  - remote control,
  - telecommunications.

- delay lines

- keyboards

- miscellaneous

colour television,  
electronic computers.

teleprinters;

desk calculators and electronic  
computers;

slot machines,

telephones.

h.t. transformers;

small motors;

analogue memories;

fine movement control;

flow meters,

flaw meters.

## 2 The piezoelectric effect in ceramic materials

### 2.1 General

To gain an understanding of the piezoelectric effect in ceramics we must first consider the behaviour of the material on a microscopic scale. For a material to exhibit an anisotropic effect, such as piezoelectricity, it is a requirement that its crystal structure should have no centre of symmetry. This means that there is at least one axis in the crystal where the atomic arrangement appears different if one proceeds in opposite directions along it.

Piezoelectric ceramics are ferroelectric materials. Above a certain temperature, called the Curie temperature,  $\vartheta_c$ , the crystal structure of a ferroelectric *does* have a centre of symmetry and has therefore no electric dipole moment. Below this temperature it undergoes a phase change to a more complex structure which is non-centrosymmetric. In this phase the crystal has a built-in electric dipole which may be reversed, and also switched in certain allowed directions, by the application of a sufficiently high electric field. Such materials are termed ferroelectric because this electrical behaviour presents a physical analogy with the magnetic behaviour of ferromagnetic materials. They do not necessarily contain iron as an important constituent.

A single crystal cooled below the Curie temperature (in the absence of an electric field) contains many 'domains' in each of which the electric dipole is aligned in a specific allowed direction. Summed over the whole crystal the net electric dipole for the crystal is zero. But when the crystal is cooled in the presence of an electric field the domains tend to align in that allowed direction nearest to the electric field, with the result that the crystal as a whole exhibits an electric dipole. If this crystal is subjected to stress the lattice will be distorted and the stress will also cause some domains to grow at the expense of others, both of which result in a change in the total dipole moment of the crystal. Within a certain range of stress, which depends on the actual material, this variation of dipole moment with stress is approximately linear and reversible. This is the basis of piezoelectricity in ferroelectric materials.

Piezoelectric ceramics may be regarded as a mass of minute crystallites which are randomly oriented (Fig. 2.1(a)). After firing, a ceramic body is isotropic (on a macroscopic scale) and exhibits no piezoelectric effect because of this random orientation and because of the domain structure within the crystallites.

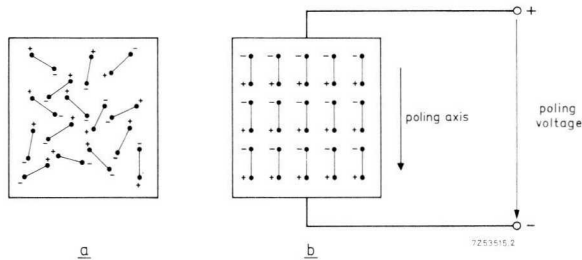


Fig. 2.1 Electric dipoles (of the domain) in piezoelectric materials (*a*) before and (*b*) after polarization (ideal conditions).

Components may be made piezoelectric in any chosen polar direction by a poling treatment which involves exposing the ceramic to a high electric field at a temperature not far below the Curie point.

Metallized electrodes are usually deposited on the surfaces of the material and a voltage applied between them. As a result the body elongates in the same direction. Because of the random orientation of the crystallites and the fact that only certain dipole directions are allowed within the crystal, it is not possible to get the perfect dipole alignment with the field (Fig. 2.1(*b*)). However, there are several allowed directions within every crystallite and so a reasonable degree of alignment with the field is possible.

After cooling of the product and removal of the poling field, the dipoles cannot easily return to their original positions, and we have now what is known as remanent polarization of the ceramic material. The ceramic body has become permanently piezoelectric and can convert mechanical energy into electrical energy, and vice versa. A poling treatment is therefore quite indispensable for these materials, and is usually the final operation to be carried out.

Fig. 2.2 illustrates the phenomenon of piezoelectricity in a cylinder of piezoelectric material. For clarity the magnitude of the effect has been exaggerated. Fig. 2.2(*a*) shows the cylinder under no-load conditions. If an external force is applied to produce compressive or tensile strain in the material, the resulting deformation causes a change in dipole moment so that a voltage appears between the electrodes. If the mechanical stress is such that the ceramic body resumes its original form, i.e., before poling (Fig. 2.2(*b*)), the measured voltage will have the same polarity as the voltage used for poling. When the mechanical stress is reversed, the voltage on the electrodes will also be reversed (Fig. 2.2(*c*)).

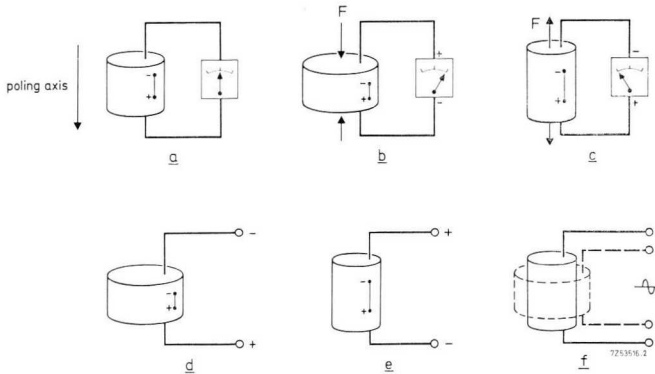


Fig. 2.2 The piezoelectric effect on a cylindrical body of piezoelectric ceramic. For the sake of clarity only one dipole is shown.

If a voltage of opposite polarity to that of the poling voltage is applied to the electrodes, the cylinder will shorten (Fig. 2.2(d)). If the polarity of the applied voltage is the same as that of the poling voltage, the cylinder elongates (Fig. 2.2(e)). When an alternating voltage is applied, the cylinder will become alternately longer and shorter (Fig. 2.2(f)).

### 2.2 Examples

It will be useful for us to know how great the conversion effect actually is. Let us first consider the generator action, i.e., the phenomenon of mechanical energy being transformed into electrical energy. A piezoelectric cylinder 20 mm long will serve as an example.

The graph of Fig. 2.3, in which the open circuit voltage is plotted against compressive stress, shows that the voltage (and hence the field strength  $E$ ) is linearly proportional to the stress applied up to a value of 25 kV at a stress of  $50 \cdot 10^6 \text{ Pa}^*$ , or  $500 \text{ kgf/cm}^2$ . This is expressed as:

$$E = -gT, \tag{2.1}$$

\* The International Committee of Weights and Measures has recommended the special name 'Pascal' (Pa) for the S.I. unit of pressure and stress ( $1 \text{ Pa} = 1 \text{ N/m}^2$ ). See Appendix F for S.I. units.

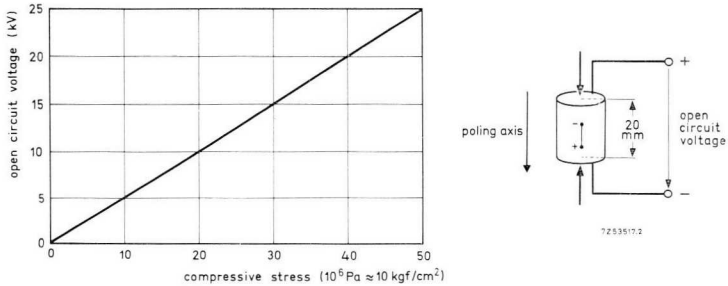


Fig. 2.3 Open circuit voltage of a 20 mm long piezoelectric ceramic cylinder as a function of compressive stress applied.

where  $T$  is the mechanical stress (in this case the stress is compressive and so  $T < 0$ ), and where  $g$  is a material constant. This material constant is the highly important piezoelectric voltage constant, i.e., the ratio between the field strength induced and the stress applied. The electric field strength is defined as being positive when it has the same sense as the poling field.

Stresses of this size can easily be applied with a simple press. Forces of a few kgf can be applied manually and, with this cylinder, only  $0,25 \cdot 10^6$  Pa ( $2,5$  kgf/cm<sup>2</sup>) is required to generate 125 V. (The total electrical energy developed is so low that experiments involve no personal danger whatsoever.)

Examples of the application of mechano-electrical conversion are the ignition of gases in cigarette lighters and various household appliances, gramophone pick-up heads, accelerometers, and sound receivers such as hydrophones and microphones.

Where the motor action (electro-mechanical conversion) of piezoelectric ceramics is concerned, we may use the simple formula:

$$S = dE, \quad (2.2)$$

where  $S = \Delta l/l$  and represents the strain (relative deformation) of the ceramic at a certain field strength  $E$  (Fig. 2.4). Once again we have an important material constant;  $d$  is known as the piezoelectric charge constant (see Section 2.3). If  $d$  is known, eq. 2.2 can be used, for instance, to calculate the deformation strain occurring at the maximum permissible voltage (see Section 4.6 for  $E_{max}$ ).

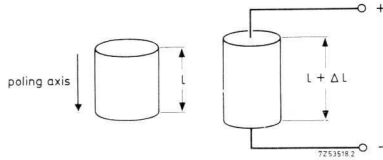


Fig. 2.4 Elongation of a cylindrical piezoelectric ceramic body caused by a d.c. voltage.

A typical value for  $S$  is  $2 \cdot 10^{-4}$  (for PXE5), which corresponds to an elongation of about  $4 \mu\text{m}$  of the 20 mm long cylinder. These figures refer to the static strain; under the influence of a dynamic (alternating) field the situation changes. For example, at the frequency of mechanical resonance the maximum amplitudes can be much greater than the static displacements. For still greater deflections ( $> 0,1 \text{ mm}$ ), there are special flexure elements (see Chapter 4).

Examples of applications where the motor effect is used are transducers for ultrasonic cleaning, ultrasonic air transducers, fine movement control, and many others.

## 2.3 Theory and definitions of piezoelectric quantities

### 2.3.1 PIEZOELECTRIC RELATIONS

The electrical condition of an unstressed medium placed under the influence of an electric field is defined by two quantities — the field strength  $E$  and the dielectric displacement  $D$ . Their relationship is:

$$D = \varepsilon E, \quad (2.3)$$

in which  $\varepsilon$  is the permittivity of the medium.

The mechanical condition of the same medium at zero electric field strength is defined by two mechanical quantities — the stress applied  $T$  and the strain  $S$ . The relationship here is:

$$S = sT, \quad (2.4)$$

in which  $s$  denotes the compliance of the medium.

Piezoelectricity involves the interaction between the electrical and mechanical behaviour of the medium. To a good approximation this interaction can be described by linear relations between two electrical and mechanical variables:

$$\left. \begin{aligned} S &= s^E T + dE; \\ D &= dT + \epsilon^T E. \end{aligned} \right\} \quad (2.5)$$

The choice of independent variables (one mechanical,  $T$ , and one electrical,  $E$ ) is arbitrary. A given pair of piezoelectric equations corresponds to a particular choice of independent variables. In a similar way it is possible to arrive at the following formulae:

$$\left. \begin{aligned} E &= -gT + \frac{D}{\epsilon^T}; \\ S &= s^D T + gD: \end{aligned} \right\} \quad (2.6)$$

$$\left. \begin{aligned} E &= -hS + \frac{D}{\epsilon^S}; \\ T &= c^D S - hD: \end{aligned} \right\} \quad (2.7)$$

$$\left. \begin{aligned} D &= eS + \epsilon^S E; \\ T &= c^E S - eE. \end{aligned} \right\} \quad (2.8)$$

In these equations,  $s^D$ ,  $s^E$ ,  $\epsilon^T$ ,  $\epsilon^S$ ,  $d$  and  $g$  are the main practical constants and they require further explanation. The superscripts to the symbols denote the quantity kept constant under boundary conditions. For instance, if by short-circuiting the electrodes the electric field across the piezoelectric body is kept constant, superscript  $E$  is used. By keeping the electrode circuit open, the dielectric displacement is kept constant and superscript  $D$  is used. So  $s^D$  and  $s^E$  are the specific elastic compliances (strain-to-stress ratio) for a constant electric charge density and constant electric field respectively. Terms  $\epsilon^T$  and  $\epsilon^S$  are the permittivities (electric displacement-to-field strength ratio) at constant stress and constant strain respectively.

It follows from eqs. 2.5 and 2.6 that there are two ways of defining the piezoelectric (strain) constants  $d$  and  $g$ . Thus  $d$  can be defined as a quotient of either  $S$  and  $E$  or  $D$  and  $T$ ; similarly  $g$  can be defined from two other quotients (see Table 2.1).

Table 2.1. Definition of the constants  $d$  and  $g$ .

constant	definition	S.I. units*		
$d$	$\frac{\text{dielectric displacement developed}}{\text{applied mechanical stress}}$ ( $E = \text{constant}$ )	$\frac{\text{coulombs/metre}^2}{\text{Pa}}$	or	$\frac{\text{C}}{\text{N}}$
	$\frac{\text{strain developed}}{\text{applied field}}$ ( $T = \text{constant}$ )	$\frac{\text{metres/metre}}{\text{volts/metre}}$	or	$\frac{\text{m}}{\text{V}}$
$g$	$\frac{\text{field developed}}{\text{applied mechanical stress}}$ ( $D = \text{constant}$ )	$\frac{\text{volts/metre}}{\text{Pa}}$	or	$\frac{\text{Vm}}{\text{N}}$
	$\frac{\text{strain developed}}{\text{applied dielectric displacement}}$ ( $T = \text{constant}$ )	$\frac{\text{metres/metre}}{\text{coulombs/metre}^2}$	or	$\frac{\text{m}^2}{\text{C}}$

Note: It can be shown that both units for the same constant are of the same dimensions. In the S.I. system of units they are also numerically identical.

\* See Appendix F for S.I. units.

Terms  $c^D$  and  $c^E$  are the elastic stiffnesses (stress-to-strain ratios) and  $h$  and  $e$  are piezoelectric (stress) constants. Equations 2.7 and 2.8 are seldom used in practice and therefore these four constants are not given in the material tables.

From eqs. 2.5 and 2.6 it follows that

$$d = e^T g \quad (2.9)$$

and

$$s^D = (1 - k^2)s^E \quad (2.10)$$

if  $k$  is defined by

$$\left. \begin{aligned} k^2 &= \frac{d^2}{s^E e^T} \\ \text{or} \quad \frac{k^2}{1 - k^2} &= \frac{g^2 e^T}{s^D} \end{aligned} \right\} \quad (2.11)$$

In a similar manner it can be found from eqs. 2.6 and 2.7 that

$$\varepsilon^S = (1 - k^2)\varepsilon^T. \quad (2.12)$$

Being introduced like this,  $k$  can be considered merely as a convenient numerical quantity. It has, however, a basic physical meaning. At frequencies far below the mechanical resonant frequency,  $k^2$  can be expressed as:

$$k^2 = \left[ \frac{\text{stored energy converted}}{\text{stored input energy}} \right]_{\text{low frequency}}$$

Hence  $k$  is referred to as the coupling coefficient.

This formula holds for electro-mechanical and mechano-electrical energy conversions. A study of the value of  $k$  quoted in Table 2.II shows that up to 50% of the stored energy can be converted at low frequencies. The value of  $k^2$  is the theoretical maximum, but in practical transducers the conversion is usually lower, depending upon the design.

Although a high value of  $k$  is desirable for efficient transduction,  $k^2$  should not be thought of as an efficiency. Eqs. 2.5 to 2.8 do not take dissipative mechanisms into account. In principle, the energy which is not converted can be recovered. For instance, in electro-mechanical action the unconverted energy remains as a charge in the capacitance of the PXE.

The efficiency is defined as the ratio of usefully converted power to the input power. Properly tuned and matched piezoelectric ceramic transducers operating at resonance can achieve efficiencies of well over 90%. When not operated at resonance, or if not properly matched, the efficiency can be very low indeed.

### 2.3.2 DIRECTION DEPENDENCE

In piezoelectric materials the constants depend on the directions of electric field, displacement, stress and strain, therefore subscripts indicating direction are added to the symbols.

For piezoelectric ceramic materials the direction of positive polarization is usually taken to be that of the  $Z$ -axis of a right-hand orthogonal crystallo-

graphic axial set  $X, Y, Z$ . Since these materials have complete symmetry about the polar axis, the senses of  $X$  and  $Y$  chosen in an element are not important. If the directions of  $X, Y$  and  $Z$  are represented as 1, 2 and 3 respectively, and the shear about these axes as 4, 5 and 6 respectively, the various related parameters may be written with subscripts referring to these (Fig. 2.5).

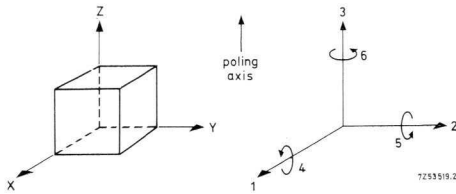


Fig. 2.5 Notation of axes.

*Permittivity  $\epsilon$*

The first subscript gives the direction of the dielectric displacement; the second indicates the direction of the electric field.

**EXAMPLES**

$\epsilon_{11}^T$  is the permittivity for dielectric displacement and field in the 1-direction under conditions of constant stress ( $T = 0$ ).

$\epsilon_{33}^S$  is the permittivity for dielectric displacement and field in the 3-direction under conditions of constant strain ( $S = 0$ ; clamped condition).

Table 2.II (in Section 2.6) gives values for the relative permittivity  $\epsilon/\epsilon_0$ , i.e., the ratio of the absolute permittivity  $\epsilon$  to the permittivity of vacuum  $\epsilon_0$ , the latter being  $8.85 \cdot 10^{-12}$  farad/metre.

*Compliance*  $s = 1/Y$

The first subscript refers to the direction of the strain, and the second subscript gives the direction of stress. ( $Y$  is the elasticity modulus.)

#### EXAMPLES

$s_{33}^E = 1/Y_{33}^E$  is the strain-to-stress ratio in the 3-direction at a constant electric field ( $E = 0$ ).

$s_{55}^D = 1/Y_{55}^D$  is the shear-strain to shear-stress ratio, at constant electric displacement ( $D = 0$ ), for shear about an axis perpendicular to the poling direction.

For further information see [1].

*Piezoelectric constants*  $d$ ,  $g$  and  $k$

The first subscript refers to the direction of the electric field or displacement, and the second subscript gives the direction of the mechanical stress or strain.

#### EXAMPLES

$d_{33}$  is the ratio of strain in the 3-direction to the field applied in the 3-direction, the piezoelectric body being mechanically free and not subjected to fields in the 1 and 2 directions. It also denotes the ratio of the charge per unit area flowing in the 3-direction when the electrodes are short-circuited, to the stress applied in the 3-direction (again the material should be free from any other stresses).  $g_{31}$  denotes the ratio of the field developed in the 3-direction to the stress applied in the 1-direction when there are no other external stresses and when there are no charges applied either in the 3-direction or in the 1 and 2 directions. It also denotes the ratio of the strain in the 1-direction to the density of the charge applied to the electrodes which are positioned at right angles to the 3-axis, provided the piezoelectric material is again free in all directions, and no charges are applied in the 1 and 2 directions.

$k_{31}$  denotes the coupling coefficient between the stored mechanical energy input in the 1-direction and the stored electrical energy converted in the 3-direction, or vice versa.

### Special cases $k_p$ and $k_t$

The planar coupling coefficient  $k_p$  of a thin disc denotes the coupling between the electric field in the 3-direction (thickness direction), and the simultaneous mechanical actions in the 1 and 2 directions (Fig. 2.6), which results in radial vibration; hence the term radial coupling ( $k_r = k_p$ ).

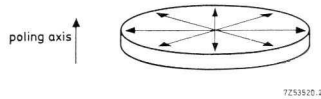


Fig. 2.6 Planar vibration of a thin disc of piezoelectric material.

The thickness coupling coefficient  $k_t$  of a thin disc with arbitrary contour denotes the coupling between the electric field in the 3-direction (thickness direction) and the mechanical vibration in the 3-direction. This is smaller than  $k_{33}$  because of the constraint imposed by the large lateral dimensions of the disc relative to the thickness.

### Frequency constant $N$

The frequency constant is the product of a resonant frequency and the linear dimension governing the resonance. If the applied electric field is perpendicular to the direction governing the vibration then the resonance is the series resonance (see Appendix A). If the field is parallel then it is the parallel resonant frequency. Thus for a 31 or 15 mode resonance, and for the planar or radial mode resonance, the relevant frequency constants are  $N_1^E$ ,  $N_5^E$  and  $N_p^E$ . On the other hand, for 33 mode resonance the frequency constant is  $N_3^D$ . Thus  $N_1^E$ ,  $N_5^E$  and  $N_p^E$  give the minimum impedance, or series resonant frequency, whilst  $N_3^D$  gives the maximum impedance, or parallel resonant frequency. If one wants to determine the length of a 33 resonator for a certain series resonant frequency, the equivalent parallel resonant frequency should first be determined using the coupling coefficient  $k_{33}$  and Fig. D.1 of Appendix D. The resonant length can then be determined using  $N_3^D$  and the parallel resonant frequency. (Should one require a certain parallel resonant frequency in 31, 15 or planar resonators, the reverse process must be followed using Fig. D.1.)

The frequency constant for longitudinal vibration of a long bar poled lengthwise is usually denoted by  $N_3^D$ . However, the frequency constant for extensional thickness vibration of a thin disc with arbitrary contour poled in the thickness direction is usually denoted by  $N_t^D$ . For a disc both  $N_t^D$  and  $N_p^E$  are of interest.

The frequency constants are equal to half the governing sound velocity in the ceramic body, except for the constant  $N_p^E$ . Thus  $N^D = \frac{1}{2}(s^D \rho_m)^{-\frac{1}{2}}$  and  $N^E = \frac{1}{2}(s^E \rho_m)^{-\frac{1}{2}}$ , where  $s^D = s^E(1 - k^2)$  and the various constants have appropriate subscripts.

## 2.4 Depolarization

As already mentioned in the foregoing, piezoelectric materials are permanently polarized (poled). However, when working with these materials, the following points should be borne in mind:

- (a) the temperature of the material should be kept well below the Curie point;
- (b) the material should not be exposed to very strong alternating electric fields, or direct fields opposing the direction of poling,
- (c) mechanical stress exercised on the material should not exceed specified limits.

Failure to comply with these three conditions may result in depolarization (depoling) of the material (the loss of the semi-permanently induced oriented structure of the electric dipoles), so that the piezoelectric properties become less pronounced or vanish completely. All three conditions are discussed below.

### 2.4.1 THERMAL DEPOLING

In the case of thermal depoling, that is, when the material has been exposed to excessive heat, the electric dipoles are able to regain their unaligned state. The piezoelectric performance deteriorates and eventually, at the Curie point, the elements suffer permanent and complete loss of their piezoelectric properties. For continuous operation without noticeable depoling it is therefore recommended to work well below the Curie point. A safe temperature limit is half way between  $0^\circ\text{C}$  and the Curie temperature.

### 2.4.2 ELECTRICAL DEPOLING

A strong electric field applied to a piezoelectric ceramic in a sense opposite to the original poling voltage will tend to cause depoling. The field strength necessary to cause serious depoling depends on the grade of the material, the duration of application and the temperature (and some other factors), but is typically in the range 500 V/mm to 1000 V/mm when applied statically. Alternating fields also have a depoling effect during the half cycles which oppose the poling field.

### 2.4.3 MECHANICAL DEPOLING

Mechanical depoling occurs when the mechanical stress on piezoelectric elements becomes too high. There is then the danger of the directional orientation in the ceramic being spoiled immediately, which in turn results in a much poorer piezoelectric performance of the elements. The safety stress limits vary considerably depending on the material (Fig. 3.2).

## 2.5 Stability

The properties of piezoelectric elements are more or less temperature dependent (see Appendix C) and time dependent (see Table 2.III). The stability as a function of time is of particular interest. Fortunately the poling ages approximately logarithmically (Fig. 2.7), so that the rate of change in permittivity, coupling factor, frequency constant and so on, reduces rapidly in the course of time. Powerful ambient influences (see Section 2.4) are likely to change the original aging pattern. This applies particularly to the permittivity, the mechanical quality factor, and the dielectric loss factor,  $\tan \delta$ .

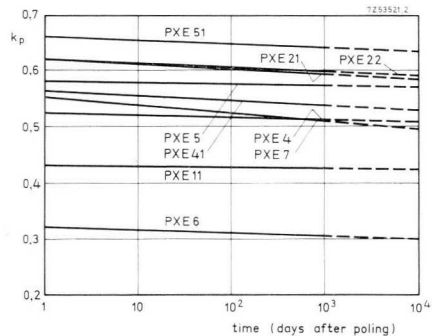


Fig. 2.7 Polarization decreases logarithmically with time, as is shown here for various piezoelectric materials.

## 2.6 The range of PXE materials and their properties

Our piezoelectric materials are marketed under the name PXE. Nearly all grades of PXE materials consist of a modified lead zirconate titanate, except PXE11 which is potassium sodium niobate. The various grades of PXE material are distinguished according to their electrical and mechanical properties and field of application. The following grades of PXE are currently available.

*PXE4* (Maintenance type only.) A grade particularly recommended for applications requiring large mechanical drive amplitudes and low mechanical and dielectric losses. As shown in Fig. 2.8 the hysteresis loop of PXE4 is much narrower than that of PXE5. Furthermore, PXE4 can be exposed to repetitive high quasi-static loads. This grade is used, for instance, for ultrasonic cleaning, sonar, and ignition (quasi-static operation).

*PXE5* This material combines a high coupling coefficient and high piezoelectric charge constant. It is ideally suited for low-power applications. Among these there are numerous non-resonant applications such as pick-up elements, fine movement control, feedback plates, microphones, pressure and acceleration sensors, and hydrophones. PXE5 can also be used for low-power resonant applications (e.g., air transducers for remote control purposes). This grade has an excellent time stability characteristic and a high electrical resistivity at high temperatures.

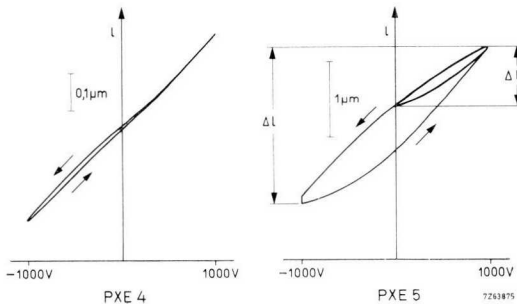


Fig. 2.8 The hysteresis effect in thin piezoelectric discs of PXE4 and PXE5 (16 mm diameter, 1,1 mm thick).

Table 2.II. Principal properties of present grades of PXE materials.

Unless otherwise specified the values given are nominal ones measured at  $20\text{ }^{\circ}\text{C} \pm 5\text{ }^{\circ}\text{C}$ .

property and symbol <sup>(1)</sup>	unit	PXE4 <sup>(2)</sup>	PXE5
<i>thermal data</i>			
Curie temperature <sup>(5)</sup>	$^{\circ}\text{C}$	265	285
specific heat	$\text{J}/\text{kg } ^{\circ}\text{C}$	420	420
thermal conductivity	$\text{W}/\text{m } ^{\circ}\text{C}$	1,2	1,2
<i>mechanical data</i>			
density $\rho_m$	$10^3 \text{ kg}/\text{m}^3$	7,50	7,60
compliance $\left\{ \begin{array}{l} s_{33}^E \\ s_{11}^E \\ s_{55}^E \end{array} \right\}$	$10^{-12} \text{ m}^2/\text{N}$	13,5 11,8	18,9 15,4 38,5
Poisson's ratio $\sigma$		$\approx 0,3$	$\approx 0,3$
mechanical quality factor for radial mode $Q_m^E$		$\approx 500$	$\approx 80$
frequency constants <sup>(7)</sup> $\left\{ \begin{array}{l} N_p^E \\ N_3^D = \frac{1}{2}v_3^D \\ N_1^E = \frac{1}{2}v_1^E \\ N_5^E = \frac{1}{2}v_5^E \end{array} \right\}$	$\left. \begin{array}{l} \text{Hz}\cdot\text{m} \\ \text{or} \\ \text{m}/\text{s} \end{array} \right\}$	2300 2050 1620	2000 1850 1460 930
compressive strength	$10^6 \text{ N}/\text{m}^2$	$> 600$	$> 600$
tensile strength		$\approx 80$	$\approx 80$
<i>electrical data</i>			
relative permittivity $\left\{ \begin{array}{l} \varepsilon_{33}^T/\varepsilon_0 \\ (\varepsilon_0 = 8,85 \cdot 10^{-12} \text{ F}/\text{m}) \\ \varepsilon_{11}^T/\varepsilon_0 \end{array} \right\}$		1750	1800 1800
resistivity $\rho_{el}$ (25 $^{\circ}\text{C}$ )	$10^{12} \text{ }\Omega\text{m}$	0,1	1
time constant $\rho_{el} \varepsilon_{33}^T$ (25 $^{\circ}\text{C}$ )	min	$> 25$	$> 250$
dielectric loss factor $\tan \delta$	$10^{-3}$	6	16
<i>electromechanical data</i>			
coupling factor $\left\{ \begin{array}{l} k_p \\ k_{33} \\ k_{31} \\ k_{15} \end{array} \right\}$		0,55 0,64 0,32	0,58 0,70 0,34 0,66
piezoelectric charge constants $\left\{ \begin{array}{l} d_{33} \\ d_{31} \\ d_{15} \end{array} \right\}$	$\left. \begin{array}{l} 10^{-12} \\ \text{C}/\text{N or} \\ \text{m}/\text{V} \end{array} \right\}$	292 - 138	384 - 169 515
piezoelectric voltage constants $\left\{ \begin{array}{l} g_{33} \\ g_{31} \\ g_{15} \end{array} \right\}$	$\left. \begin{array}{l} 10^{-3} \\ \text{Vm}/\text{N or} \\ \text{m}^2/\text{C} \end{array} \right\}$	18,8 - 8,9	24,2 - 10,7 32,5

*Notes*

<sup>(1)</sup> Product properties are dependent on the dimensions and technology of the product and measuring signal level. Therefore a meaningful translation of the material properties is best done in consultation with the supplier.

Properties in the planar mode are measured on discs 16 mm diameter and 1 mm thick.

Properties in the 33-mode are measured on cylinders 6,35 mm diameter and 16 mm long.

Properties in the 15-mode are measured on plates 10 mm by 12 mm and 0,2 mm thick.

<sup>(2)</sup> Maintenance type only.

PXE6 <sup>(3)</sup>	PXE7	PXE11 <sup>(3)</sup>	PXE21	PXE22	PXE41	PXE42 <sup>(4)</sup>	PXE51 <sup>(3)(4)</sup>
370	320	400(180) <sup>(6)</sup>	270	270	315	325	220
420	420	420	420	420	420	420	420
1,2	1,2	1,2	1,2	1,2	1,2	1,2	1,2
7,70	7,75	4,5	7,75	7,75	7,90	7,80	7,70
	15,8	9,5	18,6	18,6	14,6		17,8
10,2	12,5	8,1	15,1	15,1	12,2	11,8	14,5
	35,8	24,4			32,0		
≈ 0,3	≈ 0,3	≈ 0,3	≈ 0,3	≈ 0,3	≈ 0,3	≈ 0,3	≈ 0,3
≈ 1000	≈ 80	≈ 270	≈ 80	≈ 80	≈ 1000	≈ 750	≈ 50
2460 <sup>(8)</sup>	2200	3600	2000	2000	2200	2250	2050
	2000	2900	1900	1900	2000		1950
1800	1640	2650			1620		
	970	1500			1020		
> 600	> 600	> 600	> 600	> 600	> 600	> 600	> 600
≈ 80	≈ 80	≈ 80	≈ 80	≈ 80	≈ 80	≈ 80	≈ 80
600	700	400	1750	2250	1200	1300	2800
	1000	600			1130		
0,1	1	100	0,1	0,1	0,05		0,1
> 9	> 100	> 6000	> 25	> 30	> 7		> 40
8	20	25	16	16	2,5	2,5	16
0,32	0,52	0,43	0,62	0,62	0,56	0,55	0,66
	0,70	0,55	0,72	0,72	0,68		0,72
0,19	0,31	0,25	0,37	0,37	0,33	0,32	0,39
	0,66	0,65			0,66		
	220	100	385	438	268		480
- 44	- 86	- 47,5	- 180	- 202	- 119	- 120	- 234
	370	235			335		
	35,4	28,2	25	22,0	25,2		19,3
- 8,0	- 14,0	- 13,4	- 11,6	- 10,1	- 11,2	- 10,4	- 9,5
	42,0	44,0			33,5		

<sup>(3)</sup> Available on request.

<sup>(4)</sup> Preliminary data.

<sup>(5)</sup> Temperature at which the  $\varepsilon_{33}^T$  is maximum.

<sup>(6)</sup> In PXE11 there is a transition from the ferroelectric orthorhombic to the ferroelectric tetragonal phase at 180 °C. If the material passes through this temperature in either direction then it must be repoled.

<sup>(7)</sup> See Section 2.3.2.

<sup>(8)</sup> Fractional variation of  $N_p^E$  between 20 °C and 65 °C < 0,3 %.

Table 2.III. Time stability.

property and symbol	relative charge per time decade (%) <sup>(1)</sup>										
	PXE4	PXE5	PXE6 <sup>(2)</sup>	PXE7	PXE11 <sup>(2)</sup>	PXE21	PXE22	PXE41	PXE42	PXE51 <sup>(2)(3)</sup>	
coupling coefficient $k_p$	-2,5	-0,5	-1,6	-0,5	-0,1	-1,5	-1,2	-1,5	-2,5	-1,0	
relative permittivity $\epsilon_{3,3}^T$	-6	-1	-0,95	-0,5	-1,6	-2	-2	+1	-6,0	-1	
frequency constant $N_p^E$	+1,5	+0,5	+0,06	+1,0	+0,16	+0,5	+0,5	+0,5	+1,5	+1	
quality factor $Q_m^{E(4)(5)}$	+5		+1,5					+10			
$\tan \delta$ <sup>(4)</sup>	-5							-10			

## Notes

(1) Reference point of time: 24 hours after poling.

(2) Available on request.

(3) Preliminary data.

(4) The values of  $Q_m^E$  and  $\tan \delta$  at a given field are functions of time after poling or after any major disturbance such as exposure to a high temperature.

(5) Non-linear.

*PXE6* A grade developed for applications where the mechanical quality factor, as well as temperature and time stability, must meet stringent requirements. It is, therefore, the material particularly recommended for ceramic resonators in radio and television receivers. The material is available on request.

*PXE7* A grade with low permittivity and high temperature stability as well as a high shear coupling coefficient. Aging of the permittivity of this material, and hence phase distortion of the electrical resonance circuit, is extremely low so that this material is eminently suitable for h.f. shear resonance applications where phase is important, e.g., ultrasonic delay lines for colour television receivers; this is the main application for PXE7.

*PXE11* This material possesses an extremely low dielectric constant and relatively high frequency constants. It also has a high shear-mode coupling coefficient and is, therefore, the recommended material for shear-mode transducers (e.g., delay lines for professional use) in the frequency range 10 MHz - 100 MHz.

*PXE21* A grade which has been developed for ignition purposes. It has a high voltage constant which ensures a high voltage output. This material is extremely suitable for the dynamic loading mechanisms used for the ignition of gases and explosives.

*PXE22* A material characterized by a higher permittivity than PXE21. The output voltage of PXE22 is equivalent to that of PXE21. Combined high energy and high voltage output makes PXE22 most suitable for dynamic loading in single-slug devices for gas ignition purposes.

*PXE41* A grade with a lower permittivity than PXE4. In particular it is the extremely high mechanical quality and the extremely low loss factor (even at intensive drive) that make PXE41 suitable for high power ultrasound applications at medium range temperatures and pre-stresses. Furthermore, PXE41 can be exposed to high repetitive quasi-static loads and dynamic loads for ignition purposes.

*PXE42* A grade with a lower permittivity than PXE41 and is characterized by low mechanical and dielectric losses combined with a high mechanical quality factor, and can therefore be driven at high mechanical amplitudes. It is the recommended material for ultrasonic cleaning.

*PXE51* A material with a higher permittivity and a higher charge constant than PXE5. Due to its lower Curie temperature it also has a lower time and temperature stability. The material is suitable for sensitive detector applications and for fine movement control.

Tables 2.II and 2.III present the technical data needed for the design of transducers using PXE. It should be borne in mind that the realm of piezoelectric materials is still being explored, and that new grades may well be added to our existing range at any time; we recommend that designers keep themselves informed of our latest technological developments.

## 3 PXE ignition of gases

### 3.1 General

PXE transducers are capable of producing voltages sufficiently high to draw a spark across an electrode gap. Such a spark can be used for the ignition of combustible gases. In the following pages the requirements for optimum use of PXE materials for ignition will be dealt with. The grades suitable for ignition applications are PXE4, PXE41, PXE21 and PXE22.

Over the years quite a number of ignition systems have been developed. Whether they operate on the mains, a battery or a permanent magnet, most of them require transformers and, in some cases, capacitors. A piezoelectric ignition system is far less complex. The electrical part consists of only one or two cylindrical pieces of PXE material. The high voltage required for ignition is generated by subjecting the PXE to a mechanical stress.

By using PXE transducers, the volume of the ignition system is substantially reduced — an important factor in their applicability to domestic appliances such as gas-heaters and ovens, and in welding and soldering equipment, and even more so in table and pocket lighters.

### 3.2 PXE high voltage generation

#### 3.2.1 STATIC STRESS

##### *Behaviour under open circuit conditions*

Consider a cylindrical PXE transducer of length  $l$  poled in the axial direction and with electrodes on its ends. If an axial stress  $T_3$  is applied, the voltage between the electrodes,  $V_3$ , under open circuit conditions ( $D = 0$ ) is given by:

$$V_3 = -g_{33}lT_3. \quad (3.1)$$

If the stress is compressive (negative), the voltage is positive, i.e., it has the same sign as the original poling voltage. Fig. 3.1 shows the electric field strength (calculated with  $g_{33}$ ) as a function of  $T_3$  for the materials PXE4, PXE41, PXE21, and PXE22.

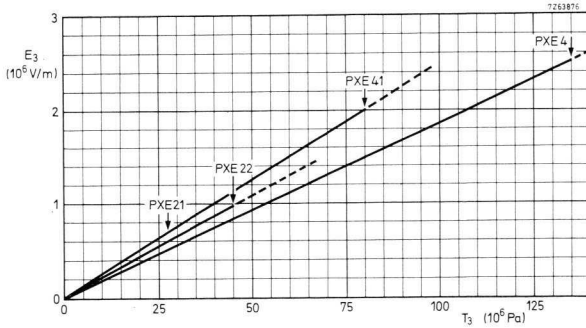


Fig. 3.1 Electric field strength (open circuit conditions) as a function of the quasi-static stress on PXE4, PXE41, PXE21 and PXE22 (calculated with  $g_{33}$ ).

Apart from the voltage level, the electrical energy dissipated in the spark is also an important factor in gas ignition. Let the total amount of energy produced by the mechanical source and fed into a PXE cylinder be  $W_T$  (under open circuit conditions). If the PXE cylinder remains open circuit and there are no losses, all of this energy could be withdrawn in mechanical form. But if an electrical load is connected, a part,  $W_e$ , may be withdrawn as electrical energy. Thus we may write:

$$W_T = W_e + W_m, \quad (3.2)$$

where  $W_e$  is the electrical energy, i.e., that fraction of the mechanical energy stored in the cylinder which may be withdrawn as electrical energy (in the clamped condition), and where  $W_m$  is the mechanical energy, i.e., that fraction of the mechanical energy stored which may only be withdrawn in mechanical form.

The energy  $W_T$  can be simply expressed in terms of the compliance  $s_{33}^D$  and the mechanical stress  $T_3$ :

$$W_T = \frac{B}{2} s_{33}^D T_3^2, \quad (3.3)$$

where  $B$  is the volume of the PXE element.  $W_e$  and  $W_m$  are found by means of the coupling coefficient  $k_{33}$ :

$$W_e = \frac{B}{2} k_{33}^2 s_{33}^D T_3^2; \quad (3.4)$$

$$W_m = \frac{B}{2} (1 - k_{33}^2) s_{33}^D T_3^2. \quad (3.5)$$

With eqs. 2.12 and 3.1,  $W_e$  can be expressed as:

$$\begin{aligned} W_e &= \frac{1}{2} \epsilon_{33}^T (1 - k_{33}^2) \frac{A}{l} V_3^2, \\ &= \frac{1}{2} \epsilon_{33}^S \frac{A}{l} V_3^2, \\ &= \frac{1}{2} (1 - k_{33}^2) C V_3^2 \end{aligned} \quad (3.6)$$

where  $A$  is the area of the PXE element and  $C$  is the capacitance of the PXE element at low frequency.

#### *Connecting a spark gap to a PXE cylinder*

If a spark gap is connected in parallel with the piezoelectric element, flashover will take place as soon as the breakdown voltage has been reached. Up to that moment the PXE cylinder behaves like an electrically open system (see above). During the flashover this system is loaded with the (real) resistance of the conducting spark. If at  $T_3$  the breakdown voltage,  $V_b$ , of the spark gap is reached, the electrical energy  $W_e$  (eq. 3.6 with  $V_3 = V_b$ ) of the cylinder is released in a flashover of very short duration ( $\approx 10^{-7}$  s). The actual time depends on the cylinder capacitance, the dimensions of the h.t. lead, and the resistance of the spark gap. If, as is done in practice, the cylinder remains connected to the mechanical source, and if the spark gap is still conductive, the PXE element is effectively short-circuited and so its compliance increases from  $s_{33}^D$  to  $s_{33}^E$ , where

$$s_{33}^E = \frac{s_{33}^D}{1 - k_{33}^2}. \quad (3.7)$$

Thus the compressive strain of the cylinder can now increase further with no increase of stress. This cannot occur instantaneously. What happens is that, as soon as the spark gap breaks down, acoustic shock waves begin to move in from the ends of the cylinder. Their propagation speed is about 4 mm/ $\mu$ s, so that this deformation is complete within a few microseconds (depending on the length of the cylinder). The additional mechanical energy fed to the cylinder for that purpose can be converted into additional electrical energy  $W_{ea}$ :

$$\begin{aligned} W_{ea} &= \frac{B}{2} s_{33}^E k_{33}^4 T_{33}^2, \\ &= \frac{1}{2} \epsilon_{33}^T k_{33}^2 \frac{A}{l} V_b^2. \end{aligned} \quad (3.8)$$

In practice the realizable value of  $W_{ea}$  will depend very much on the way in which the PXE cylinder is mounted, and on the way the compressive stress is applied. However, eq. 3.8 indicates the size of the effect. Thus the electro-acoustical energy  $W_{ea}$  can make a very important contribution to the total energy in the spark. Consequently, the maximum total amount of electrical energy,  $W_{tot}$  available for the spark is:

$$\begin{aligned} W_{tot} &= W_e + W_{ea}, \\ &= \frac{1}{2} \epsilon_{33}^T \frac{A}{l} V_b^2, \\ &= \frac{1}{2} C V_b^2. \end{aligned} \quad (3.9)$$

Thus we see that the maximum available spark energy corresponds to the field energy of a capacitor of value  $C$  and a voltage  $V_b$ , the latter being the flash-over voltage of the spark gap.

The corresponding energy density  $w_{tot} = W_{tot}/B$  can be derived from eqs. 3.1 and 3.9:

$$w_{tot} = \frac{1}{2} \epsilon_{33}^T g_{33}^2 T_3^2. \quad (3.10)$$

Fig. 3.2 shows  $w_{tot}$  as a function of  $T_3$  (for PXE4, PXE41, PXE21, and PXE22). The maximum permissible static and dynamic stresses for the various materials are given in the same illustration.

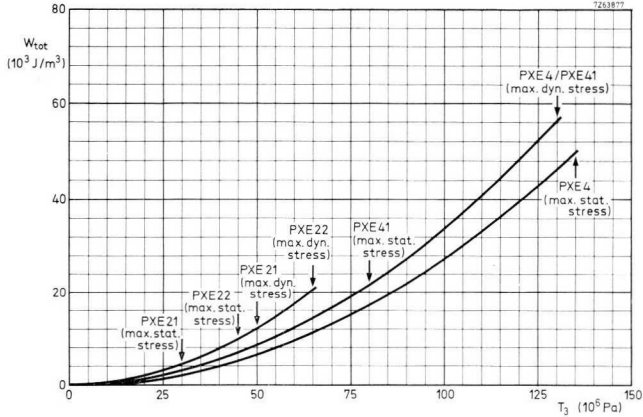


Fig. 3.2 Total electrical energy generated per unit volume in PXE4, PXE41, PXE21 and PXE22 as a function of stress  $T_3$  (linear effects only).

If, in a static system,  $n$  sparks are produced during one cycle, the maximum energy expressed by eq. 3.10 is available for each spark and the total energy amounts to:

$$\begin{aligned} W &= n \cdot \frac{1}{2} C V_b^2, \\ &= \frac{1}{2} C V_b \hat{V}, \end{aligned} \quad (3.11)$$

where  $\hat{V} = n \cdot V_b$  is the peak voltage of the system under open circuit conditions.

The theoretical aspects discussed so far were based on ideal piezoelectric materials stressed under ideal conditions. There are some practical limitations which modify performance and which must be taken into account.

- (a) If, as is usually the case, the PXE cylinder is compressed between steel cylinders, these will apply some lateral clamping to the PXE because of their lower compliance. Consequently the cylinder will assume a barrel shape instead of deforming homogeneously. This will tend to reduce the effective value of  $g_{33}$ . However, with the length-to-diameter ratio normally employed for high voltage generation, the effect will not be large.

- (b) Directly after the discharge, the voltage across the cylinder is not zero but equals the extinction voltage  $V_e$  of the spark gap, so that in eqs. 3.9 and 3.11 the value of  $\frac{1}{2}CV_b^2$  should really be reduced by  $\frac{1}{2}CV_e^2$ . Since  $V_e \ll V_b$ , here again the effect is small.
- (c) As indicated in eq. 3.1, a compressive stress on an open system produces a voltage of the same polarity as the poling voltage, so little or no depolarization will result. However, as soon as flashover takes place, the voltage becomes equal to the much lower extinction voltage and any residual mechanical stress may have a depolarizing effect (see (d) below). The materials used will have to meet stringent requirements as regards depolarization, particularly under quasi-static stress.
- (d) After flashover, when closed circuit conditions will prevail, even low values of  $T_3$  are sufficient to cause non-linear effects so that the electric charge is greater than would be expected on grounds of the linear piezoelectric effect. This is illustrated in Figs. 3.3(a) and 3.3(b) which give the charge displacements of PXE4, PXE41, PXE21, and PXE22 as functions of mechanical stress (under short-circuit conditions). The upper curves in these diagrams apply to conditions of increasing mechanical stress; the lower ones to conditions of decreasing stress after having discharged the PXE element by temporarily short-circuiting it. The broken lines indicate the tangents to the curves at the origin; they can be calculated with the aid of eq. 2.5 and the low signal values of  $d_{33}$  given in Table 2.II. The non-linear effects can be either reversible or irreversible. As long as the upward and downward curves coincide we are dealing with a reversible effect. At higher stresses the curves will no longer coincide, which means that the material has been partly depolarized. For multiple ignition applications it is essential that the peak stress be so chosen that depolarization remains within reasonable limits.
- From the curves we see that the grades PXE4 and PXE41 are the most suitable materials for ignition mechanisms based on the principle of quasi-static stressing. The non-linear effects result in a greater amount of electrical energy being released than might be expected from the simple theory (eqs. 3.9 and 3.11).
- (e) Owing to the electrical losses in the PXE material, the non-elastic deformations in both the PXE material and the pressure mechanism, the leakage resistance, parasitic capacitances, and so on (see Section 3.3), not all of the available electrical energy will be dissipated in the discharge.

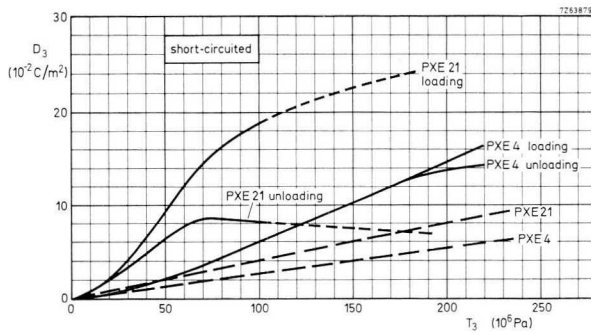
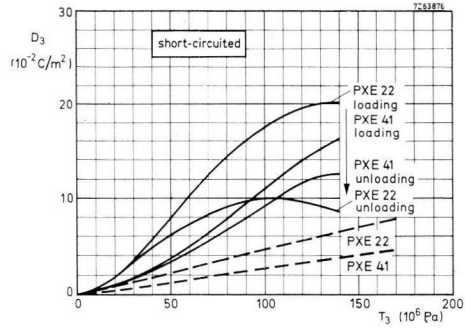


Fig. 3.3 Measured charge displacement as a function of stress  $T_3$  under loading and unloading conditions for (a) PXE22 and PXE41, and (b) PXE21 and PXE4. The tangents to the curves at the origin (broken lines) are characterized by:

$$d_{33} = 438 \cdot 10^{-12} \text{ C/N (PXE22);}$$

$$d_{33} = 268 \cdot 10^{-12} \text{ C/N (PXE41);}$$

$$d_{33} = 385 \cdot 10^{-12} \text{ C/N (PXE21),}$$

$$d_{33} = 292 \cdot 10^{-12} \text{ C/N (PXE4).}$$

## 3.2.2 DYNAMIC STRESS (IMPACT IGNITION)

In the so-called impact ignition system the PXE element is stressed dynamically with a spring-loaded hammer mechanism. When the hammer strikes, a pressure wave is generated in the PXE cylinder as well as in the hammer. The build-up of the mechanical stress, and consequently of the voltage, in the PXE depends on the acoustic properties of the components used for the ignition mechanism.

In the simplest case of free impact between a hammer with an area  $A_h$  and a PXE cylinder with an area  $A_c$ , and assuming that  $A_h$  and  $A_c$  are not too different, the maximum mechanical stress can be calculated to a close approximation with the formula:

$$\begin{aligned}
 T_3 &= u \frac{A_h Y}{A_c v + A_h v_{33}^D Y s_{33}^D}, \\
 &= u \frac{A_h Z_h Z_c^D}{A_h Z_h + A_c Z_c^D}, \tag{3.12}
 \end{aligned}$$

where  $u$  is the impact speed of the hammer;  $v$  is the propagation speed of the pressure wave in the hammer;  $v_{33}^D$  is the propagation speed of the pressure wave in the PXE material under open circuit conditions;  $Y$  is the modulus of elasticity of the hammer material;  $Z_h$  is the acoustic impedance of the hammer material ( $Z_h = \rho_h Y$  where  $\rho_h$  is the density of the striker material), and  $Z_c^D$  is the acoustic impedance of PXE under open circuit conditions ( $Z_c^D = \rho_m / s_{33}^D \approx 34 \cdot 10^6 \text{ kg/m}^2\text{s}$ , where  $\rho_m$  is the density of the PXE material).

This formula is no more than a rough indication of the mechanical stress that might be expected in a practical system. The actual mechanical stress can easily be derived from the open circuit voltage pulse (eq. (3.1)).

If the cylinder is connected to a spark gap with a flashover voltage  $V_b$ , the open circuit peak voltage being  $V$ , the energy available for the spark (from the linear piezoelectric effect only) lies between the two values:

$$\min \frac{1}{2} C V_b^2 \quad \text{and} \quad \max \frac{1}{2} C V^2. \tag{3.13}$$

The actual magnitude of the available energy depends on the level of the maintaining voltage, and hence on the impedance, of the spark. The share of charge displacement caused by non-linear effects depends to a large extent on the duration of the mechanical stress cycle. If the pulse duration is a few milliseconds or more the PXE cylinder still behaves quasi-statically and the charge displacement is non-linear (Fig. 3.3). However, if the pulse duration approaches a microsecond, this is short compared with the relaxation times of the ferroelectric domains and all non-linear effects disappear. The charge displacement then corresponds to the linear piezoelectric effect in that it becomes directly proportional to the mechanical stress (eq. 2.5). For pulses of intermediate length the contribution of the non-linear effect gradually decreases with pulse length. This means that higher stresses can be applied for short durations without depolarization occurring.

Since the requirements as regards depolarization caused by stress are less severe, materials with a higher energy output (high  $g_{33}$ , high  $\epsilon_{33}^T$ ) can be used for dynamic loads. PXE21 and PXE22 are materials developed for high stress operation normal size impact ignition mechanisms for domestic and industrial appliances. In small ignition mechanisms, such as are used in pocket lighters, the impact stress must be even higher to achieve the required voltage. PXE41 is therefore more suitable for this application.

### 3.3 Construction of an ignition unit

Ceramic piezoelectric materials are brittle and certain precautions must be taken when they are exposed to high stress. The best way to protect the PXE cylinders is to accommodate them in a housing, the so-called ignition unit. This also gives a more homogeneous field of forces within the PXE, acoustic matching between the various parts and proper insulation. The general directives concerning the design of ignition units will now be discussed with the aid of Fig. 3.4.

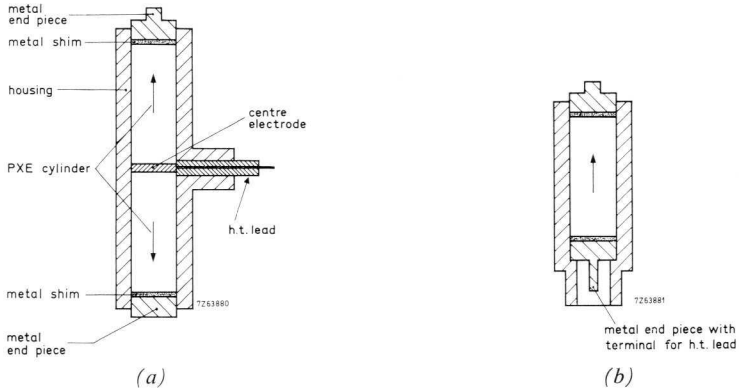


Fig. 3.4 Construction of an ignition unit with (a) two PXE cylinders and (b) one PXE cylinder.

### 3.3.1 PXE CYLINDERS

Most piezoelectric ignition units comprise two axially placed PXE cylinders with their polarities in opposite directions (Fig. 3.4(a)). The metal end pieces of the system are earthed, the high tension being tapped at the centre electrode. The cylinders are thus mechanically in series but electrically in parallel. This design offers two advantages: the energy dissipated in the spark is twice that dissipated by one cylinder, and also the insulation problem is limited to the h.t. terminal.

In practice it is sometimes possible to obtain sufficient energy from one PXE cylinder for a particular application. In this case an economy can be made by replacing one piece of PXE by a similar cylinder of insulating material such as alumina or porcelain. It is of course also possible to design an ignition unit to accommodate just one PXE cylinder (Fig. 3.4(b)).

The static and dynamic outputs of an ignition unit depend on the dimensions of the PXE cylinders as well as on the material properties (eqs. 3.1 to 3.12). Moreover, the useful life of the PXE element depends on the degree of depolarization caused by the mechanical stress. Other important factors in this respect are the mechanical strength and the conditions of the surface of the PXE cylinder. The end faces must be plane parallel, perpendicular to the axis, and as smooth as possible.

### 3.3.2 THE CENTRE ELECTRODE

A thin metal plate is inserted between the PXE cylinders to form a centre electrode. This plate is the terminal to which the h.t. lead can be connected by bonding, soldering, welding, or simply by means of a spring clip. The recommended materials for bonding are aluminium, copper, brass, steel, and nickel or nickel-iron. For soldered connections the choice is for copper or brass; for welding (spot-welding) copper, steel, nickel or nickel-iron are preferred. All these materials are also suitable for making the spring clip contacts.

### 3.3.3 THE HIGH TENSION LEAD

The high tension lead connects the centre electrode to the spark gap. This lead must meet the following requirements:

- (a) It must be suitable for connecting by bonding, soldering or welding, or for connection to a spring clip.
- (b) It must be made of stranded wire because shock loads entail vibrations which give rise to metal fatigue. This fatigue could lead to fracture of a single core at the place where it leaves the ignition unit.
- (c) The breakdown voltage of the lead should be twice as high as the peak voltage generated in the ignition unit.
- (d) The lead should be resistant to high temperatures.
- (e) The capacitance of the lead, as well as that of the spark gap, should be low compared with the capacitance of the PXE cylinder.
- (f) The leakage resistance of the fitted lead must be so high that the time constant of the lead and spark gap remains large in relation to the rise time of the voltage pulse.

Both the capacitance and the leakage resistance of the h.t. lead depend on the length of the lead and the quality of the insulation material used. Consequently, the lead must be kept as short as possible. Suitable insulation materials for the h.t. lead are neoprene, silicone rubber, and teflon. These materials can be used at temperatures up to 100 °C, 225 °C, and 300 °C, respectively. All contact between the h.t. lead and metal parts must be avoided. Furthermore, it is recommended that all electrical connections be immobilized and that sharp edges be removed from all connecting elements.

### 3.3.4 METAL END PIECE FOR THE PXE CYLINDER

If the PXE cylinders are exposed to high mechanical forces, these forces must be distributed uniformly across the end face of the cylinder to ensure maximum working life. This can be readily achieved by applying metal end pieces to the end faces of the PXE unit. A long life and good acoustic matching are achieved if steel is used for the end pieces. The steel surface facing the PXE cylinder will have to meet special requirements as regards flatness and smoothness.

### 3.3.5 THE METAL SHIM

As an extra protection for the PXE cylinder, a metal shim can be placed between the cylinder and the steel end piece. This shim is usually of copper, brass, or aluminium.

### 3.3.6 THE HOUSING

The various components are either fitted into a prefabricated plastic housing, or the plastic housing may be injection moulded around the assembled components. The latter method has some drawbacks when compared with the former:

- (a) For moulding, the various components must first be assembled to form a unit (by Araldite bonding, for instance).
- (b) To avoid possible depolarization, the temperature of the mould, and consequently the type of plastic being used, has certain limitations.
- (c) Since the plastic shrinks during the cooling-off process, it tends to grip the PXE cylinders too tightly and to absorb some of the applied mechanical energy during the passage of the acoustic wave, thus reducing the output.
- (d) Prior to moulding, the PXE cylinder must be lacquered (see also Section 3.3.7).

The housing must meet the following requirements:

1. Its breakdown voltage must be at least twice as high as the peak voltage generated in the ignition unit.
2. The housing should be impervious to water.
3. The housing must have adequate electrical and mechanical properties at the required operating temperature.

The most suitable materials are polyethylene for moulding, and polypropylene and nylon for prefabricated housings.

### 3.3.7 INTERNAL INSULATION

If the PXE cylinder is built into the ignition unit without further precaution, flashover along the cylinder wall is unavoidable. To eliminate such flashovers, and also to prevent the charge from leaking away, the cylinder must first be thoroughly cleaned, and its wall coated with an insulating material. Recommended materials are:

- (a) Lacquer (for moulding as well as for prefabricated housings).
- (b) Silicone grease or oil (only for prefabricated housings).

### 3.4 Static igniters (squeeze action)

In hand-operated igniters based on the principle of quasi-static high voltage generation, a force is exerted on one or two PXE cylinders by means of a lever system. Such a system can often be used to advantage when the usually larger volume required (as compared with dynamic systems) forms no objection.

A main characteristic of these mechanisms is the relatively long duration of the mechanical load applied for ignition. It lasts for about a half second and also depends on the person operating the ignition device. During that time the piezoelectric ceramic material is first loaded and then unloaded which results in one, or several, flashovers first in one direction and then in the other depending on the length of the spark gap. This can be of great advantage as regards ignition probability: if during one flashover the gas-air mixture is not favourable for ignition, there is the possibility that it will be when the next flashover occurs.

A drawback of the static ignition system is the long rise time of the voltage; it is about a quarter second, depending to some extent on the user. Under these conditions the time constant must be at least a half second if a leaking away of the charge and consequent energy loss are to be avoided. The capacitance of the ignition unit ranges from 50 pF to 100 pF, so that the leakage resistance of the entire system should be at least  $\sim 10^{10} \Omega$ , even under humid and soiled conditions. These requirements are not easily met if the apparatus must be equipped with a relatively long h.t. lead. That is the reason why static ignition units are used exclusively for hand-operated igniters that are equipped with spark gaps having short h.t. leads. It is thus possible to generate voltages of around 20 kV by applying a mechanical stress of about  $80 \cdot 10^6$  Pa to the piezoelectric material. In view of the consequent risk of depoling (see Section 3.2.1)

grades PXE4 and PXE41 are the recommended materials for purely static applications. The ultimate choice of material depends on the force that can be applied and also on the voltage and energy required (see Figs. 3.1 and 3.2).

### 3.5 Impact igniters

Gas appliances and cigarette lighters are equipped with ignition systems where a dynamic load is applied to the PXE cylinder by means of a spring-loaded hammer mechanism. The maximum mechanical stress (eq. 3.12) and therefore the generated voltage are functions of the impact speed and the area of the hammer. The rise times of the mechanical stress wave and the voltage peak are greater for a convex contact area of the hammer or the end face plate than for a flat contact area. In theory, the energy transfer from hammer to PXE cylinder is at a maximum when the acoustic impedance of the hammer and that of the PXE material are equal. However, experience shows that using steel also gives satisfactory results:

$$Z_{steel} \approx 46 \cdot 10^6 \text{ kg/m}^2\text{s};$$

$$Z_{PXE} \approx 34 \cdot 10^6 \text{ kg/m}^2\text{s}.$$

In theory, conditions are particularly favourable when the duration of the shock wave through the PXE cylinder is twice that through the hammer. Since the propagation speed in the PXE cylinder (with electrodes open circuited) is about 4 mm/ $\mu$ s, and in steel about 5,8 mm/ $\mu$ s, the hammer should be about 70% longer than the total length of the PXE element in the ignition unit.

Pulse durations calculated with these values do not occur in practice owing to interfering effects caused by the metal parts and the insulating material used in the ignition unit. Satisfactory results can be obtained with steel hammers with a length ranging from 30% to 100% of the overall length of the PXE material in the unit.

For longer ignition times the end of the cylinder facing the hammer, or both cylinders, should be shielded by a larger piece of metal (the anvil).

The oscillogram (Fig. 3.5) shows a voltage pulse (open circuit) generated in a well designed impact igniter. A smooth pulse shape has a favourable effect on the ignition probability and on the useful life of the PXE cylinder. In this respect it is essential that the ignition unit is statically pre-stressed.

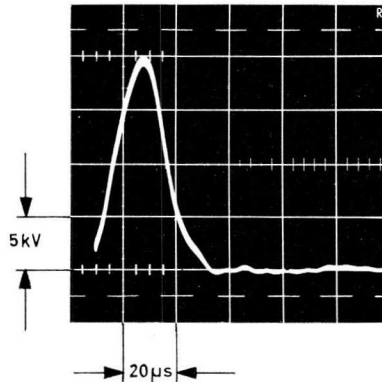


Fig. 3.5 Voltage pulse shape occurring in an impact igniter under open circuit conditions.

Table 3.I gives some typical values of parameters important for the design of normal size and small size impact igniters for domestic appliances and pocket lighters respectively.

Table 3.I. Impact mechanism data.

parameter	unit	normal size for domestic appliances	small size for pocket lighters
material		PXE21, PXE22	PXE41
dimensions of PXE cylinder (diameter $\times$ length)	mm	6,35 $\times$ 16	3,7 $\times$ 5
mass of hammer (steel)	g	13 to 18	2,5 to 4
hammer length	mm	10 to 25	10 to 15
potential energy of hammer stroke	mJ	90 to 160	80 to 90
static load on ignition unit (pre-stress)	N	7 to 40	10
mass of anvil (steel)	g	15 to 35	
maximum voltage (open circuit)	kV	15 to 25	10 to 16
pulse duration (open circuit)	$\mu$ s	40 to 60	20
available electrical energy	mJ	8 to 20	4 to 7

The impact igniter has the following advantages over static or quasi-static systems:

- (a) Owing to the short rise time of the voltage pulse (beyond the user's control), a leakage resistance of  $1\text{ M}\Omega$  for the entire system is adequate.
- (b) Since the load durations are short, the PXE cylinders can be exposed to greater loads without the danger of depolarization.
- (c) Coupling the ignition mechanism to the gas valve permits a more accurate determination of the time elapsing between the opening of the gas valve and the occurrence of the spark.

In practice about 6% to 17% of the potential energy of the hammer is converted into electrical energy. These percentages apply only if the effect is purely linear. Whether a sufficiently high ignition probability is thus obtained depends largely on the efficiency of the circuit design. In general, impact igniters are suitable for small ignition systems. The traditional wheel and flint construction in pocket lighters, for instance, can be replaced by a PXE unit whose dimensions are no more than 8 mm diameter and 22 mm long. The overall dimensions of the lighter remain the same. As mentioned in Section 3.2.2, the materials PXE21 and PXE22 are suitable for normal size impact igniters for domestic and industrial appliances, and PXE41 is the recommended grade for ignition units in pocket lighters.

### 3.6 Considerations on ignition probability

The unfavourable influences that the leakage resistance and the parasitic capacitance have on the ignition probability can be minimized by a suitable construction of the ignition unit (Sections 3.3.1 and 3.3.7). The rather low impedance of the spark gap is then the only cause that not all of the available energy (eqs. 3.9 and 3.11) is dissipated in the spark. In spite of this unavoidable effect, the energy fed to the spark gap is usually sufficient to ignite the combustible gases with a high degree of probability.

The discharge in the spark takes place in the form of numerous rapid flashovers. If the ignition unit is very small, and consequently the energy low (pocket lighters, for instance), the energy of one flashover can be too low to ensure sufficient ignition probability. In such cases it will be necessary to combine the energies of these numerous flashovers into one discharge to increase the ignition probability.

The simplest solution to the problem is to increase the time constant of the system by inserting a series resistor (a composition resistor) in the load as close to the spark gap as possible. As a result the spark is prolonged while at the same time fluctuations in the current-voltage characteristic are suppressed. The optimum resistance to be used depends on the construction of the igniter. In practice resistances of 20 k $\Omega$  to 40 k $\Omega$  give satisfactory results. A further solution, albeit a usually expensive one, is to connect an inductance in the h.t. lead. The ignition probability also depends on the following characteristics:

- flow rate of the gas;
- air supply;
- the time between the opening of the gas valve and the appearance of the spark;
- position of the spark,
- electrode distance.

The ignition probability is very strongly dependent on these parameters and optimum conditions are best found by experiment.

## 4 PXE flexure elements

### 4.1 Operating principle

Simple PXE transducers operating in the '31' or the '33' mode (Sections 2.2 and 2.3.2) have a very low compliance. This means that the displacements obtainable with these transducers are far too small for many applications and that the voltages and forces required to produce these displacements are very high. For example, in the '33' mode one can only obtain a movement of about  $4 \mu\text{m}$  with an applied voltage of  $\sim 10 \text{ kV}$ . Furthermore, the low compliance results in relatively high resonant frequencies for such elements and this is not always desirable.

A much more compliant type of structure is available operating in a bending mode. This is seen in its simplest form as the bilaminar cantilever illustrated in Fig. 4.1. It consists of two thin PXE strips bonded together. In the arrangement shown in Fig. 4.1 the strips are poled in opposite directions so that, when the voltage  $V$  is applied between the electrodes on their outer surfaces, the upper strip expands lengthways by the '31' action while the lower one contracts. This differential strain causes the cantilever to bend and the free end is displaced by a distance  $z$ . The action is to some extent analogous to that of a heated bimetal strip. The bilaminar flexure element described here is known as a 'bimorph'.

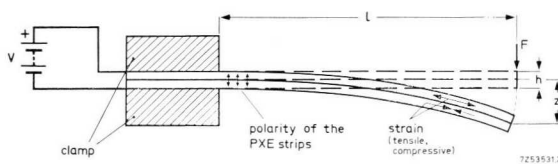


Fig. 4.1 PXE cantilever flexure element with oppositely polarized strips.

The robustness of these thin ceramic components can be improved by using a metal centre layer so that a trilaminar construction is obtained. The presence of this layer actually improves the electromechanical coupling, provided that it is not much thicker than either ceramic strip. Such trilaminar elements are

also commonly referred to as bimorphs. For many applications the central metal strip is extended beyond the PXE strips to provide simple mounting and to allow electrical contact to be made to the central plane, if required, as in Fig. 4.2. The performance of flexure elements will be substantially reduced if any slippage occurs between the layers. Good thin, rigid, stable bonds are therefore essential (see Appendix B).

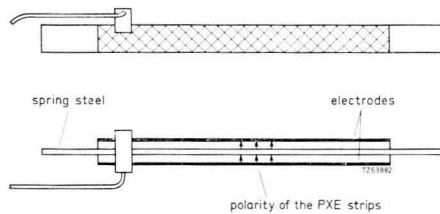


Fig. 4.2 Bimorph flexure element with protruding central metal strip. In this version the strips are poled in the same direction.

Another form of flexure element is the ‘multimorph’ shown in Fig. 4.3 which is made in one piece. The holes in the middle are silver-coated and form an effective centre electrode, which is only used for poling the element. Multimorphs operate in the same manner as bimorphs. Their construction is attractive as no bonding is necessary and therefore production is simpler.

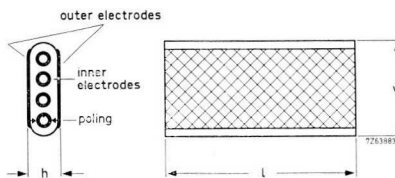


Fig. 4.3 PXE multimorph flexure element (usual dimensions are  $h = 0,67$  mm and  $w = 1,6$  mm).

Beside the flexure elements described so far, another commonly used structure is the flexure disc or diaphragm. These elements operate in exactly the same way as other flexure elements, and are useful for obtaining higher forces, though with smaller displacements, than can be obtained with strips. Their geometry and relatively high compliance make them well suited for coupling to gases which have a low specific acoustic impedance. These applications are dealt with separately in Chapter 6.

During the manufacture of flexure elements, the PXE components are poled for either series or parallel operation. For series operation the electrical input (or output) connections are made between the two outer electrodes (Fig. 4.1), the two PXE laminae having been poled in opposite directions. Multimorphs are used in this way (Fig. 4.3). For parallel operation the directions of polarization are the same; the centre electrode is used as one terminal while the two outer electrodes together form the other. The bimorph illustrated in Fig. 4.2 is of this type. The choice between series and parallel operation is governed by the voltage and impedance required. Multimorphs are suitable for series operation only.

## 4.2 Support of flexure elements

There are various ways in which flexure elements can be mounted. The principal methods are illustrated in Fig. 4.4. Cantilever mounting, as shown in Fig. 4.4(a), gives maximum deflection and compliance. It also has the lowest possible resonant frequency because it is a 'quarter-wave' resonator. Smaller displacements are obtained with both ends pinned, i.e., fixed in position but able to rotate freely, as shown in Fig. 4.4(b), but the structure is less compliant and is therefore able to support, or exert, greater forces. Rigid clamping (Fig. 4.4(c)) is not recommended because it entails an extremely low electromechanical coupling with fully electroded elements. If the flexure element is mounted at the vibration nodes (nodes supported, see Fig. 4.4(d)), the supporting structure can be very light and compact and the losses in the mounting are reduced to a minimum. This is particularly important if the device is to be used as a resonator in an electrical filter network, in which case a high quality factor is usually desirable. In a uniform bar the nodes for the fundamental flexure resonance are situated symmetrically  $0.55l$  apart, where  $l$  is the total length of the bar. Foam rubber can be used for nodal support. Since this material is extremely compliant, accurate positioning of the support is not so necessary.

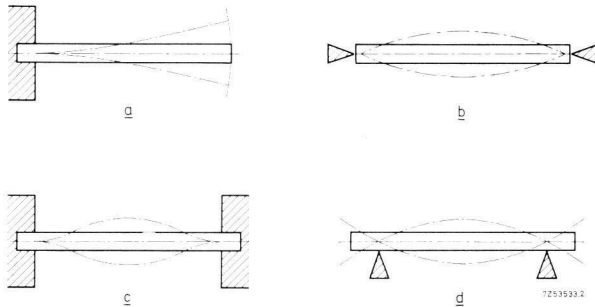


Fig. 4.4 Various methods of mounting flexure elements:  
 (a) cantilever; (b) ends pinned;  
 (c) rigid clamping, (d) nodes supported.

### 4.3 Applications of flexure elements

Flexure elements have a wide range of application. Examples where they serve as electrical-to-mechanical transducers are:

- sound generators (e.g., loudspeakers and buzzers);
- small vibratory motors;
- fine movement control;
- optical scanners, choppers and deflection devices,
- relays and switches.

The same elements can be used in the converse manner: a force applied to a flexure element produces a voltage. The following applications are based on this mechanical-to-electrical principle:

- microphones;
- gramophone pick-up cartridges;
- accelerometers,
- stress and strain gauges.

In some applications both the electro-mechanical and mechano-electrical transducer actions are exploited. For example:

- ultrasound air transducers;
- liquid level sensors,
- low-frequency filters.

Broadly speaking, these applications can be divided into three types:

- static and quasi-static applications;
- dynamic (but non-resonant) applications,
- dynamic applications within the resonance range\* of the transducer.

In the first group of applications, all three types occur. The second are all dynamic, and the third are all resonant.

#### **4.4 Static and dynamic behaviour below resonance**

As mentioned in Section 4.3, flexure elements are used in both an electro-mechanical and a mechano-electrical mode. To cover these different applications, one therefore needs information on the force and deflection available when a given voltage is applied, and also on the charge or voltage generated when the elements are subjected to given forces or deflections. The operation of flexure elements is somewhat more complex than is the case with simple '33' or '31' mode transducers and therefore one cannot easily use the material constants given in Table 2.II to derive their performance. For this reason some practical data are given below to indicate what may be expected.

\* Resonance range is understood to mean a frequency range in the neighbourhood of a resonance and including both the minimum impedance frequency and the maximum impedance frequency. (See Appendix A.)

#### 4.4.1 ELECTRO-MECHANICAL BEHAVIOUR

For static and dynamic non-resonant applications we are interested in the relationship between the deflection  $z$  of the flexure element, the applied voltage  $V$  and the resultant force  $F$ . Simple theory predicts that these are linearly related. The deflection of the cantilever flexure element (Fig. 4.1) can then be expressed as:

$$z = Al^3F + Bl^2V/h, \quad (4.1)$$

where  $A$  and  $B$  are constants depending on the cross-sectional dimensions as well as on the piezoelectric and elastic properties of the element.

Under static conditions eq. 4.1 is not too well obeyed because the ceramic exhibits creep after the voltage or stress has been applied, and this introduces hysteresis. Creep increases the deflection for a given applied voltage or force. This is illustrated in Figs. 4.5 and 4.6 which show respectively the static deflection of unloaded cantilever elements as a function of the voltage, and of the force, applied. Such hysteresis effects are also observed under dynamic conditions at low frequencies. There is a remanent deflection after the voltage or force is removed and this decays slowly to zero.

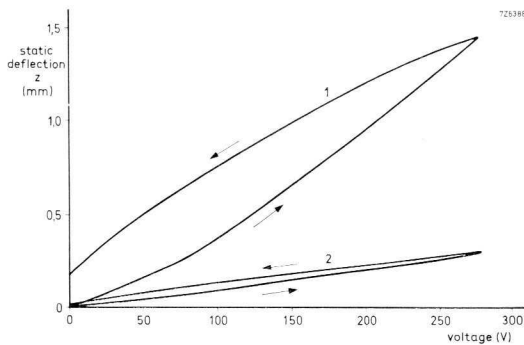


Fig. 4.5 Static deflection of two unloaded cantilever flexure elements as a function of voltage. Curve 1: multimorph bar, free length 60 mm,  $h = 0,67$  mm,  $w = 1,6$  mm. Curve 2: bimorph bar, free length 40 mm,  $h = 0,9$  mm,  $w = 3,5$  mm.

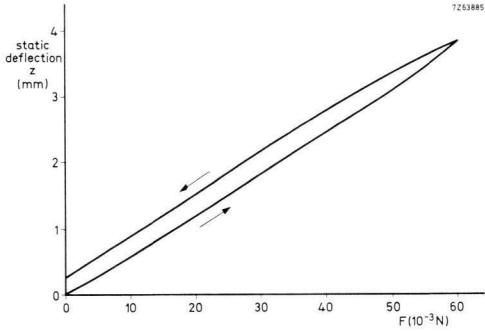


Fig. 4.6 Static deflection of a multimorph cantilever bar as a function of force (short-circuit conditions, electrodes interconnected). Free length 60 mm,  $h = 0,67$  mm,  $w = 1,6$  mm.

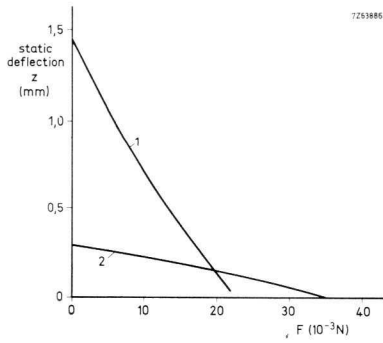


Fig. 4.7 Static deflection of two cantilever flexure elements as a function of the available force at a constant voltage of 275 V. The curves are related to the flexure elements described in Fig. 4.5.

In many applications the force developed through a deflection at a certain voltage is the main point of interest. Fig. 4.7 shows the relationship between the available force and the corresponding deflection for the same two cantilever flexure elements as in Fig. 4.5 ( $V = 275$  V). Note that the forces available from cantilever flexure elements are quite small. An increase of force at the expense of deflection may be achieved by supporting the beam at both ends, as in Fig. 4.4(b), or by using a bimorph diaphragm, as in Fig. 4.8. Here a thin PXE disc is bonded to each side of a thin steel diaphragm which is supported around its edge.

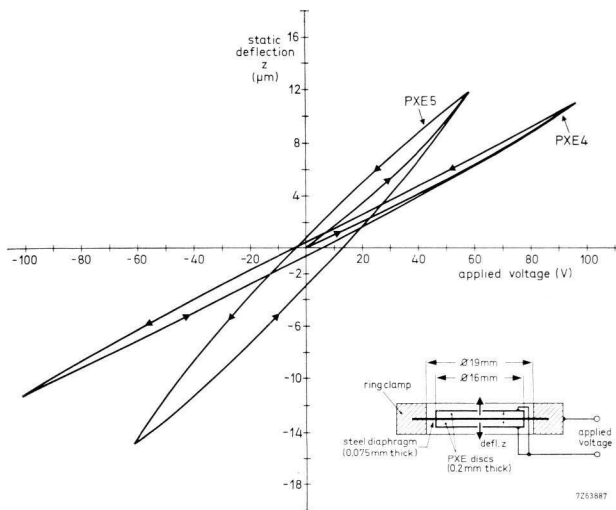


Fig. 4.8 Static deflection as a function of applied voltage for a bimorph diaphragm transducer.

## 4.4.2 MECHANO-ELECTRICAL BEHAVIOUR

As mentioned in Section 4.3, flexure elements are often used as detectors for various purposes and so one needs data on the electrical output which may be obtained when a certain deflection or force is applied. In this mode of operation flexure elements are charge generators and Table 4.1 gives formulae for calculating the charge sensitivity of PXE5 and PXE51 bimorphs and multimorphs as a function of applied force and displacement. To calculate the voltage output of an element one must use the total capacitance of the flexure element plus the input capacitance of the detector circuit. (Any resistive load must, of course, be such as to give the required  $RC$  time constant.) Formulae are also given in the table for calculating the capacitance of the element. In calculating the charge sensitivity one uses  $l$ , the active or bent length of the element. This may be considerably shorter than the total length  $l'$  which must be used for calculating the capacitance. This may be seen by reference to Figs. 4.4(a) and 4.4(d). In the cantilever mounting (Fig. 4.4(a)) a length of the bimorph is clamped and therefore piezoelectrically inactive but it does contribute to the capacitance.

Table 4.1. Sensitivity of flexure elements.

element and parameter	cantilever support (see Fig. 4.4(a) ) end drive		ends pinned support (see Fig. 4.4(b) ) centre drive	
	PXE5	PXE51*	PXE5	PXE51*
<i>Multimorph</i>				
capacitance (pF)	$21 l'w/h$	$32 l'w/h$	$21 l'w/h$	$32 l'w/h$
output vs force ( $\mu\text{C}/\text{N}$ )	$0,33 \cdot 10^{-3} (l/h)^2$	$0,45 \cdot 10^{-3} (l/h)^2$	$0,082 \cdot 10^{-3} (l/h)^2$	$0,11 \cdot 10^{-3} (l/h)^2$
output vs displace- ment ( $\mu\text{C}/\text{mm}$ )	$5,3 wh/l$	$7,8 wh/l$	$21 wh/l$	$31 wh/l$
<i>Bimorph</i>				
capacitance (pF)	$24 l'w/h$	$37 l'w/h$	$24 l'w/h$	$37 l'w/h$
output vs force ( $\mu\text{C}/\text{N}$ )	$0,35 \cdot 10^{-3} (l/h)^2$	$0,48 \cdot 10^{-3} (l/h)^2$	$0,087 \cdot 10^{-3} (l/h)^2$	$0,12 \cdot 10^{-3} (l/h)^2$
output vs displace- ment ( $\mu\text{C}/\text{mm}$ )	$5,5 wh/l$	$8,1 wh/l$	$22 wh/l$	$32 wh/l$

$l'$  = total length of element;  
 $l$  = active (bent) length of element,  
 $l'$ ,  $l$ ,  $h$  and  $w$  in mm.

\* Still in development, preliminary data only.

The same is true of the knife-edge support (Fig. 4.4(d)) where the ends outside of the knife edges do not undergo bending, but the 'ends pinned' formulae of Table 4.I may be used to calculate the charge generated by the bent region between the knife edges.

The output of a flexure element is, of course, dependent on the details of construction. In Table 4.I it is assumed that the diameter of the central holes in the multimorph is one third of the total thickness of the strip, and that the bimorph has an inert central layer of one third the total thickness. Furthermore, these formulae only give approximate low-level sensitivities. Especially at high forces and displacements the same effects of non-linearity and hysteresis, which have been mentioned in Section 4.4.1, are evident to an increasing degree. Care must be taken not to exert too great a force or bending: the limits are discussed in Section 4.6.

#### 4.5 Behaviour in the resonance range

Considering their dimensions, flexure elements have very low resonant frequencies which makes them convenient for many low-frequency applications. Fig. 4.9 shows the fundamental resonant frequency  $f_{s0}$  of a PXE5 multimorph cantilever flexure element as a function of its free length. For many non-resonant applications of flexure elements, such as gramophone pick-up cartridges,

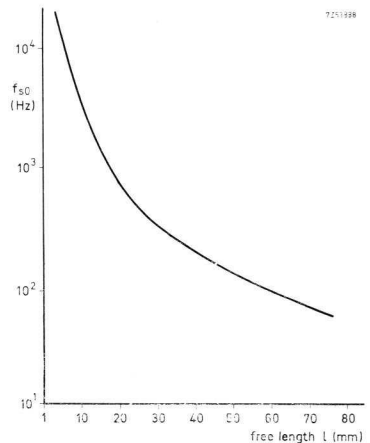


Fig. 4.9 Fundamental resonant frequency of a bimorph PXE5 cantilever bar as a function of free length ( $h = 0,67$  mm,  $w = 1,6$  mm).

this frequency can lie within or near to the frequency range of the equipment. In such cases resonance is suppressed by mechanical damping. Hence a knowledge of the resonance behaviour can be important for both resonant and non-resonant devices.

The fundamental resonant frequency of the flexure bar element depends on its length  $l$  and its thickness  $h$ , the material properties, and the way the element is mounted. The width has little effect unless it becomes more than  $l/2$ , in which case a transverse mode coupling might occur which could change the frequency response and resonant frequency of the fundamental longitudinal mode.

The resonant frequency of a PXE flexure bar ( $l \gg w$ ), under short-circuit conditions, is given (to a good approximation) by the general formula:

$$f_{s(n)} = \frac{\beta_n h}{l^2} \sqrt{\frac{1}{s_{11}^E \rho_m}} = 2\beta_n \frac{h}{l^2} N_1^E \quad (n = 0, 1, 2, 3, \dots), \quad (4.2)$$

where  $\beta_0 = 0,16$  for cantilever mounting (Fig. 4.4(a));

$\beta_0 = 1,03$  for node-supported mounting,  $p = 0,55l$  (Fig. 4.4(d)),

$\beta_0 = 0,45$  for ends pinned (Fig. 4.4(b)).

Table 4.II gives the formulae for calculating the fundamental resonant frequencies ( $f_{s0}$ ) of PXE5 and PXE51 bimorph elements for three different methods of support. The flexure bar elements may be simple single-piece bars or bilaminar bars with rigid thin bonds.

*Table 4.II. Mechanical resonant frequency,  $f_{s0}$ , of flexure bar ( $l \gg w$ ) elements of PXE5 and PXE51.*

mounting	$f_{s0}$
cantilever	$0,48 (h/l^2) 10^6 \text{ Hz}$
nodes supported ( $p = 0,55l$ )	$3,1 (h/l^2) 10^6 \text{ Hz}$
ends pinned ( $p \approx l$ )	$1,35 (h/l^2) 10^6 \text{ Hz}$

$l$  and  $h$  in mm.

For a multimorph these frequencies are about 5% higher. For a trilaminar flexure element whose centre strip is  $h/3$  thick, the frequency increases are about 2%, 7% and 14% for centre strips of steel, aluminium and epoxy resin respectively. For PXE51 ceramic they are about 3% higher.

The cantilever beam flexure element has the lowest fundamental resonant frequency for a given length, but also the disadvantage of needing a substantial clamp at the end. Moreover, the resonant frequency and the sensitivity depend on the rigidity of the clamp. In any practical design the clamping is far from ideal and this is particularly true in non-resonant applications where rubber mountings (needed for the suppression of flexural resonance) entail a loss of sensitivity.

In general, the overtone frequencies of flexure resonators are not harmonics, that is integral multiples, of the fundamental frequency. The factors by which the fundamental frequency must be multiplied to calculate the overtone frequencies depend on the mounting system used. These factors are given in Table 4.III.

Note that the values in the 'nodes supported' column are related to the distance  $p$  between symmetrically positioned mounting points. This spacing coincides with a pair of excursion nodes, and hence there should be very small loss or effect from the mountings with this mode.

The resonant frequencies given in Fig. 4.9 and in Tables 4.II and 4.III apply to unloaded flexure elements only. For many applications the flexure elements carry some additional mass, such as the stylus linkage in a pick-up cartridge. This naturally contributes to the total resonant mass and results in a lower fundamental resonant frequency as well as changing the frequencies of the overtones.

In the case of the trilaminar bar of Fig. 4.2, the central metal layer protrudes at the ends for mounting purposes. Here mounting will not be of the simple types shown in Fig. 4.4. However, if both metal end layers are clamped, the behaviour will approximate to the both ends pinned condition of Fig. 4.4(b).

Table 4.III. Overtone frequencies for flexure bar elements ( $l \gg w$ ) relative to the fundamental resonant frequencies.

overtone	mounting		
	cantilever	nodes supported at distance $p$	ends pinned ( $p \approx l$ )
1	6,3	2,8 ( $p = 0,55l$ )	4,0
2	18	5,4 ( $p = 0,95l$ )	9,0
3	34	8,9 ( $p = 0,67l$ )	16,0

## 4.6 Maximum output from PXE flexure elements

### 4.6.1 NON-RESONANT OPERATION

In non-resonant applications the power produced by flexure elements is not usually the most important consideration and, in any case, it is very small. One is usually more interested in the deflection which can be obtained by applying a certain voltage or, alternatively, how much deflection may be tolerated when a force is applied.

With electrical input it is recommended that the following limiting values of field strengths are observed for flexure elements in static non-resonant applications:

$$\left. \begin{array}{l} \text{PXE4} - E_{\max} \approx 900 \text{ V/mm} \\ \text{PXE5} - E_{\max} \approx 450 \text{ V/mm} \end{array} \right\} \text{ peak values.}$$

If the flexure element is subjected to an external force the bending must not be so great that the tensile stress in the surface of the PXE causes fracture (see Table 2.II for tensile strength). However, one must set even lower limits for the surface stress otherwise the piezoelectric properties of the PXE will deteriorate due to irreversible depolarization. For static applications the following limiting values are recommended:

$$\left. \begin{array}{l} \text{PXE4} - T_{1 \max} \approx 55 \cdot 10^6 \text{ Pa} \\ \text{PXE5} - T_{1 \max} \approx 14 \cdot 10^6 \text{ Pa} \end{array} \right\} \text{ peak values.}$$

In the present case the stress is in direction 1 (perpendicular to the direction of poling) and these values are lower than those for direction 3. Likewise the strength of the bonding layers must receive due consideration.

### 4.6.2 RESONANT OPERATION

Fig. 4.10 shows the equivalent circuit of a flexure element in resonant operation (see Appendix A). In applications near resonance one may be interested in obtaining maximum deflection, in which case losses are minimized by proper choice of material and mounting. In applications where power is used for driving a mechanical or an acoustic load, the mechanical quality factor  $Q_{mL}$  will inevitably be much lower.

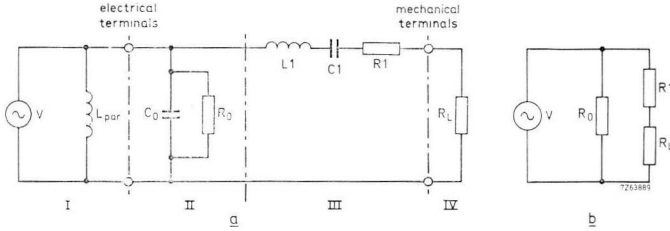


Fig. 4.10 (a) Equivalent circuit of an electrically tuned PXE flexure element (for the meaning of the symbols refer to Appendix A).

- I External tuning inductance;
- II Electrical side of the flexure resonator;
- III Mechanical side of the flexure resonator,
- IV External mechanical or acoustic load.

(b) The same circuit at resonance.

The useful acoustical or mechanical output power is either mechanically limited by the maximum permissible alternating stress  $T_{\max}$  in the surface of the ceramic material, or electrically limited by the maximum permissible alternating field in the PXE layers. For PXE flexure elements it is found that the acoustic or mechanical output power is limited mechanically if  $Q_{mL} > 2$ , and electrically if  $Q_{mL} < 2$ . This value of 2 also (roughly) constitutes the 'matched' load condition. In practice the  $Q_{mL}$  of a flexure element is usually higher than 2 so that, in general, the acoustic output power is mechanically limited by  $T_{\max}$ .

It can be derived, and it has been confirmed experimentally, that the maximum power output is proportional to the product of  $(f_r T_{\max})$  and volume (or weight) of the flexure element. A figure of about 50 mW per  $\text{cm}^3$  is typical for the output power of practical resonating PXE flexure elements designed to operate in the region of 50 Hz.

## 4.7 Application examples

### 4.7.1 PICK-UP ELEMENTS

Hitherto the most important application of PXE flexure elements has been in pick-up heads for record players. *PLATE II* shows such a pick-up equipped with piezoelectric elements. Both multimorph and bimorph elements can be used here. The materials usually preferred are PXE5 and PXE51 because these grades combine a high voltage sensitivity with a low mechanical  $Q$ . The latter is desirable to suppress any resonances which occur in the relevant frequency range. The  $Q$ -factor is further reduced by mounting the element in a lossy rubber.

### 4.7.2 PXE ELECTRIC MOTOR

Synchronous motors derive their power and time accuracy from an alternating current source whose frequency is kept constant. The synchronous clocks used so far employ a conventional synchronous motor operating electromagnetically; now a piezoelectric synchronous motor has been designed which incorporates a PXE flexure element.

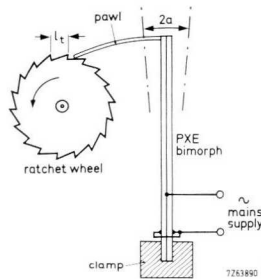
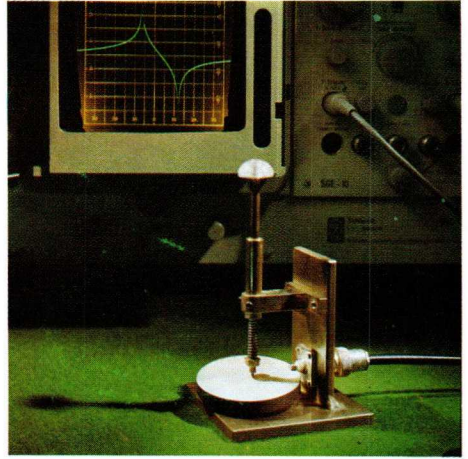


Fig. 4.11 PXE synchronous motor.

*PLATE I*

*Quality control of PXE products. Measuring the resonance and antiresonance characteristics.*



*PLATE II Stereo pick-up head with PXE elements*

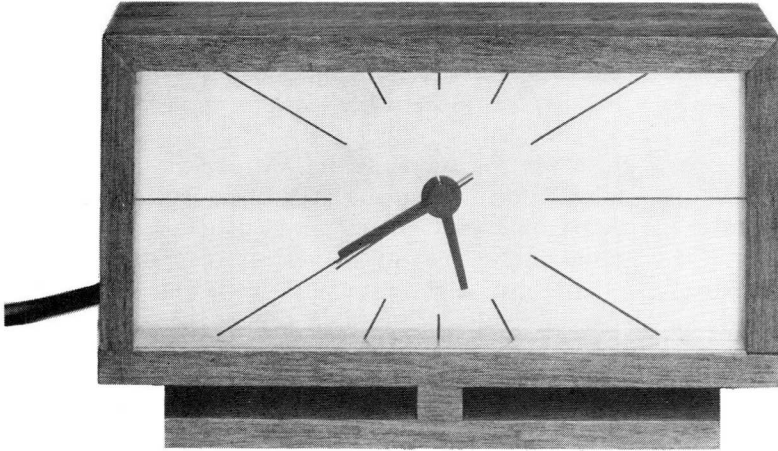


The principle of operation is illustrated in Fig. 4.11. A PXE element is mounted as a cantilever and the tip vibrates at mains frequency. A pawl mounted on the tip engages a ratchet wheel and the amplitude of vibration of the bimorph is so adjusted that the ratchet wheel advances just one tooth per stroke of the pawl.

A very high degree of reliability is required for this mechanism to be acceptable as a clock. There must be uninterrupted synchronous operation in spite of mains voltage and temperature fluctuations, production tolerances, some contamination with dust and dirt, changes of frictional resistance due to wear of bearings and aging of lubricants, slight wear on the pawl and ratchet, and aging and variation in the properties of the PXE flexure element. The last requirement immediately suggests that the flexure element should be driven at a frequency well below its resonance; if the resonant frequency varies slightly and is close to the driving frequency, large changes of amplitude could occur. When driven well below resonance the amplitude is also less affected by variations in the friction of the clock mechanism.

Tolerance to variations of vibration amplitude is greatest if the motion of the ratchet wheel is heavily damped, i.e., the ratchet should not act as a flywheel. To achieve this it is necessary to have some friction in the bearing, but this requirement is minimized if the moment of inertia is kept low by reducing both the radius of the wheel and its density. Under these conditions the amplitude of vibration  $2a$  may vary in the range  $l_t < 2a < 2l_t$  ( $l_t$  is the tooth spacing of the ratchet wheel) and synchronism will still be maintained when the wheel loses its velocity in a time which is short compared with the drive waveform period. A value slightly above the middle of this range is usually chosen,  $2a \approx 1.6l_t$ , to allow for voltage fluctuations and loss of amplitude with time due to normal aging.

731003-04-03



31003-04-02

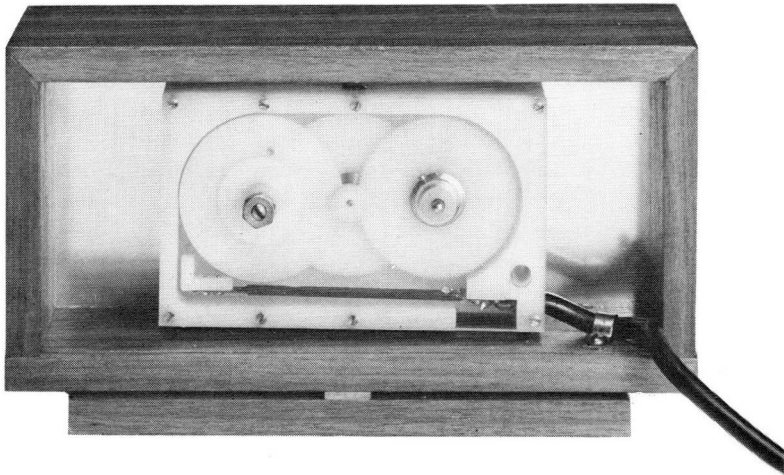


Fig. 4.12 Synchronous clock mechanism.

Fig. 4.12 shows a practical realization of the synchronous clock mechanism. The ratchet wheel (on the left) and the gears are made of plastic. The bimorph lies along the bottom, and the pawl (a loop of fine wire) can be seen bearing against the ratchet. Friction in the bearing of the ratchet may be adjusted by means of the screw at its centre. The ratchet wheel has a diameter of 1,2 cm and there are 500 teeth, each with a length of 75  $\mu\text{m}$ . With these dimensions the operation of the clock is virtually silent and the power consumption is about 1 mW.

#### 4.7.3 PXE LIQUID LEVEL SENSORS

Many machines, both industrial and domestic, are fitted with liquid level sensors for monitoring and for automatic control of liquid level in tanks and reservoirs. There are many different principles of operation for these devices. PXE flexure elements make excellent level sensors. Their short response time (a few milliseconds) makes them very useful where the liquid level changes rapidly. They have a low power consumption and so do not dissipate much heat, thus they are very suitable for use with flammable liquids. Furthermore they operate reliably over a wide temperature range.

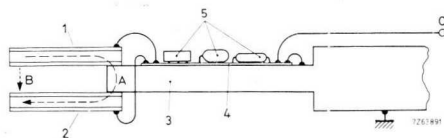
Two different types of PXE sensors are described below; the first relies on the liquid forming an acoustic path and the second uses the liquid as a damping medium.

##### *Tuning fork liquid level sensor\**

Fig. 4.13 shows a liquid level sensor which depends on the coupling between two short PXE multimorph cantilever resonators (free length  $\approx 12$  mm,  $f_r \approx 1,7$  kHz). These are mounted as the tines of a tuning fork by bonding with epoxy resin to either side of a metal tongue, and form a three-terminal piezoelectric filter element which is connected in an oscillator circuit (Fig. 4.14).

\* British Patent Application number 24070/73 filed on 21 May, 1973.

Tine 1 is connected to the output of the single-stage transistor amplifier  $TR_1$ ; tine 2 is connected to the input and provides feedback. There are two possible acoustic coupling routes between the tines, as indicated in Fig. 4.13. Route *A* is the constant coupling through the solid which is present in any tuning fork. This causes the tines to vibrate with a  $180^\circ$  phase difference; with the connections as shown it provides positive feedback and causes the circuit to oscillate. Route *B* depends on the medium between the tines and, as the path length is arranged to be short compared with the wavelength of sound, it tends to cause the tines to vibrate in phase. When the tines are in air, this coupling is weak and the coupling through route *A* is dominant so the circuit oscillates; if it is now immersed in a liquid route *B* is dominant and the feedback is negative so the oscillation will cease. It is a simple matter to arrange for the a.c. voltage to be rectified by diodes  $D_1$  and  $D_2$  to and use the resultant d.c. voltage on  $C_3$  to control a relay or other device through transistor  $TR_2$ .



- (1) and (2) 15,5 mm long PXE5 multimorphs;
- (3) metal tongue;
- (4) printed circuit,
- (5) electronic components.

Fig. 4.13 Tuning fork liquid level sensor.

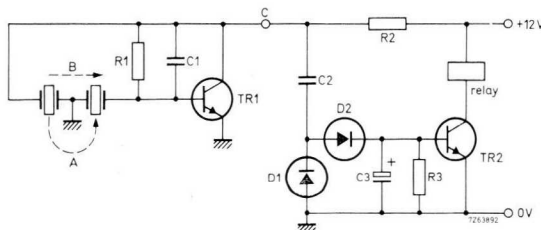


Fig. 4.14 Drive circuit for tuning fork level sensor.

The connections to the multimorphs can also be arranged so that the system oscillates when immersed and stops oscillating when the liquid falls away, making it easy to design 'fail-safe' systems for any eventuality.

#### *Liquid damped PXE level sensor*

Owing to its small size the damping of a multimorph in a liquid is not very great. Better damping is obtained with a flexure diaphragm transducer and, if space is available, it may be used in a level sensor. It has the advantages that the PXE does not come into direct contact with the liquid and is somewhat more rugged than the tuning fork transducer.

Fig. 4.15 shows the construction of a suitable diaphragm transducer which operates at about 25 kHz. It incorporates a three-electrode PXE5 disc 16 mm in diameter and 1,1 mm thick, having two concentric electrodes on one face. The transducer is connected in a circuit similar to Fig. 4.14. Oscillation is suppressed by the damping of the resonance when the diaphragm is in contact with the liquid, which reduces the positive feedback below the level for maintaining oscillation.

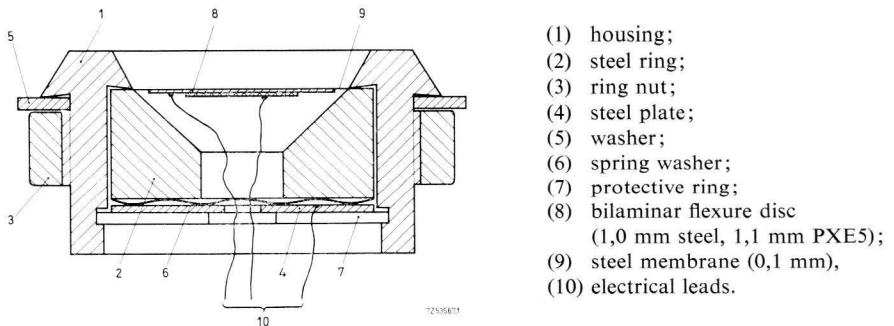


Fig. 4.15 Liquid damped PXE level sensor.

## 4.7.4 LIGHT BEAM DEFLECTION WITH FLEXURE ELEMENTS

If a small mirror is fitted to the free end of a cantilever flexure element (or connected to it by some arrangement of mechanical linkage) it can be made to execute rotational oscillations about an axis in its own plane. This arrangement can be used for deflecting a light beam. The largest deflections are obtained with a resonant system, but the bandwidth is then small and this can be a disadvantage for some applications.

Fig. 4.16(a) shows a practical arrangement of a flexure element for resonant operation fitted with a mirror. The element is a bimorph cantilever and the mirror is connected to its free end by means of two steel (or phosphor bronze) wires. The arrangement represents a system of two coupled resonators. If the system is designed so that the two resonant frequencies coincide, the mirror can be made to execute large oscillations. A particularly good arrangement is to have the resonant mode as shown in Fig. 4.16(b). The PXE bimorph is in its first overtone, with a node located near the free end. Another node is located at the mirror which, as a result, will only be tilted without being swept to and fro. Mirror rotations of about  $23^\circ$  have been achieved by using a PXE5 multimorph 0.67 mm thick and of 30 mm free length with this arrangement; the light beam deflection will, of course, be twice as large. The resonant frequency was 2.5 kHz at an applied a.c. voltage of 30 V (peak value).

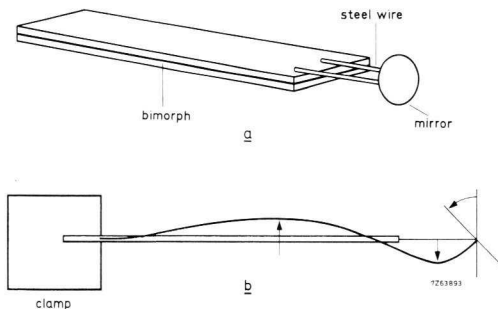


Fig. 4.16 (a) PXE bimorph flexure bar fitted with a mirror for deflecting light beams (resonant mode). (b) Resonant vibration of the system.

Fig. 4.17 shows a flexure element fitted with a mirror for non-resonant operation. Here a flexible link connects the free end of a cantilever bimorph to a pivoted mirror which is thus rotated through a small angle,  $\theta$ , when a voltage is applied to the bimorph. The deflection of the mirror is constant with a given input voltage for frequencies well below the fundamental resonance of the system. The moment of inertia of the mirror should be minimized to obtain the highest possible resonant frequency. Fig. 4.18 shows the frequency response of a system functioning with a 24 mm free length cantilever multimorph; the resonant frequency of the system is about 320 Hz.

Frequency response can be improved by increasing the damping. This is done by attaching to the mirror a small vane which is immersed in oil of suitable viscosity. Fig. 4.18 shows that the mirror deflections are now fairly constant up to about 400 Hz.

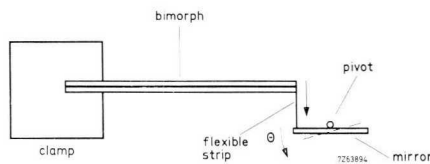


Fig. 4.17 PXE bimorph flexure bar fitted with a mirror for deflecting light beams (non-resonant mode).

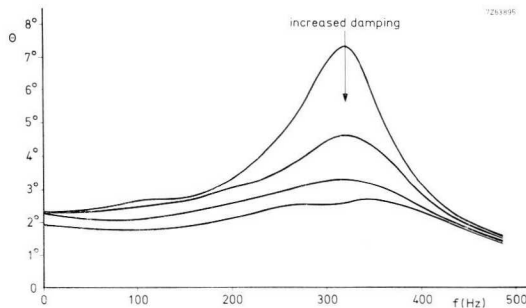


Fig. 4.18 Frequency behaviour of the system shown in Fig. 4.18 (deflection angle as a function of frequency) at a voltage of 100 V (peak value) at various dampings.

## 5 Ceramic resonators in electrical filters

It has long been possible to use quartz resonators for making highly stable filters of small relative bandwidth ( $< 0,1\%$ )\*.

With the ceramic resonators that have become available in the last few years, two of them are illustrated in Fig. 5.1, filters can be built that have a relative bandwidth of  $1\%$  to  $2\%$ . This opens up useful applications in radio and telecommunications equipment.

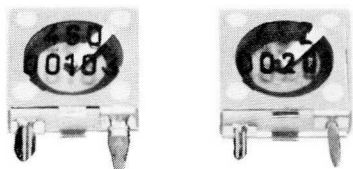


Fig. 5.1 Ceramic resonators.

To improve selectivity in radio receivers, for instance, it is often desirable to employ filters incorporating more than two resonant circuits. This is difficult with normal  $LC$  circuits because of their rather low quality factors (typically 100 to 400). However, ceramic resonators have relatively low losses and they can easily be made with quality factors of 1000 and more. This makes them very suitable for incorporation in multi-stage filters.

Piezoelectric resonators have the following advantages over  $LC$  types:

- no trimming necessary after assembly;
- higher quality factors;
- smaller dimensions;
- immunity to stray magnetic fields;
- no inherent magnetic field,
- low cost.

Good stability of properties is a prime requirement for this application. PXE6 is the recommended grade of material; the frequency constant  $N_p^E$  is stable with regard to temperature and time (see Table 2.III for aging data).

\* The possibility of enlarging this relative bandwidth with the aid of coils is not considered here.

## 5.1 Mode of operation and construction

### 5.1.1 RESONATORS FOR 450 kHz TO 480 kHz

The resonator consists of a thin disc of ceramic material with an electrode on either side (Fig. 5.2(a)). This disc is polarized axially, i.e., perpendicular to the parallel surfaces. An alternating voltage applied to the electrodes of the PXE disc causes it to vibrate. With the dimensions shown, the first resonance is in the radial, or planar, mode and it occurs in the frequency range 452 kHz to 480 kHz. That is to say that the disc expands and contracts radially at this frequency (see Fig. 5.2(b)). The relevant frequency constant and coupling coefficient are  $N_p^E$  and  $k_p$  (see Table 2.II).

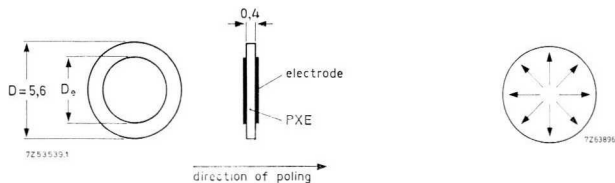


Fig. 5.2 (a) Ceramic disc resonator with an electrode on either side (dimensions in mm). (b) Radial vibration mode.

Electrical contact with the electrodes of the PXE disc must be made in such a way that the mechanical vibration of the resonator is not noticeably affected. The centre of the disc constitutes a nodal point with respect to the radial excursion and is, therefore, the position where the resonator should preferably be supported. To combine mechanical rigidity and minimum damping, the resonator is suspended between two central point contacts.

Apart from the behaviour in the vicinity of the nominal frequency, every resonator is characterized by a number of overtones which are typical for the mode of vibration under consideration. For a true half-wavelength type of resonator (e.g. a thin bar in length resonance driven in the 31-mode) the series resonant frequencies of the overtones occur at 3, 5, 7, and so on, times the series resonant frequency. However, for the thin disc in radial vibration discussed here, these ratios are not integers, but have the values  $\alpha_n/\alpha_1$  shown in Table 5.I.

Table 5.1. Coefficients  $\alpha_n$  to be used in eq. 5.1.

coefficient	fundamental resonance		overtones		
	0	1	2	3	4
$\alpha_n$	2,05	5,39	8,57	11,73	14,88
$\alpha_n/\alpha_1$	1,00	2,63	4,18	5,72	7,26

The series resonant frequency for the  $n^{\text{th}}$  overtone of thin discs in the radial mode of vibration is expressed as:

$$f_{s(n)} = \frac{\alpha_n}{2\pi r} \sqrt{\frac{1}{s_{11} E \rho_m (1 - \sigma^2)}} \quad (5.1)$$

These partly unavoidable overtones are not usually harmful because the corresponding series resonant frequencies are a sufficient distance away from the fundamental series resonant frequency. If necessary, the (effective) piezoelectric coupling corresponding to a certain overtone can be eliminated by a proper choice of the electrode diameter ( $D_e < D$ : see Fig. 5.2(a) and Section 5.1.2).

### 5.1.2 RESONATORS FOR 10,7 MHz

The resonant frequency of the resonator shown in Fig. 5.2 is governed by its diameter. If a PXE6 resonator is required to operate at  $f_s = 450$  kHz for instance, its diameter will have to be 5,6 mm. If a resonator vibrating in the same mode is required to operate at  $f_s = 10,7$  MHz, the corresponding diameter of the PXE disc will have to be about 200  $\mu\text{m}$ . This is beyond the capability of even the most up-to-date technology. The obvious solution is to choose other modes of vibration for resonators operating at these frequencies.

There is, for instance, the so-called thickness-mode of vibration (shown in ideal form in Fig. 5.3), where the thickness constitutes a half wavelength at the resonant frequency, and the disc is effectively clamped in the radial direction because the radial mode resonance is at a far lower frequency. The relevant frequency constant is  $N_t^D$  (see Section 2.3.2). In principle, the same disc as shown in Fig. 5.2 can be used. In contrast to a radial-mode resonator, the resonant frequency is now governed by the smallest dimension of the disc instead of the

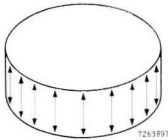


Fig. 5.3 Fundamental vibration mode of an 'ideal' thickness-mode resonator.

largest. In practice things are not quite so simple as this, and the resonant behaviour is also dependent on the diameter (for finite diameter) in the region of the thickness-mode resonance. Without further precautions a thickness resonator will produce a whole series of anharmonic spurious resonances in addition to the fundamental frequency. As Fig. 5.4 shows, these unwanted resonances can be suppressed by careful selection of the electrode diameter.

It is impossible here to make contact by supporting the resonator at a node (as is done with radial resonators). However, if the contact pressure is sufficiently low, the thickness resonator can be supported in any position.

It is also possible to have resonators operating in the thickness-shear mode for operation in this frequency range. Here the direction of polarization lies in the plane of the PXE plate but, again, the frequency-determining dimension is the plate thickness. In this case the relevant frequency constant is  $N_5^E$  (see Table 2.II).

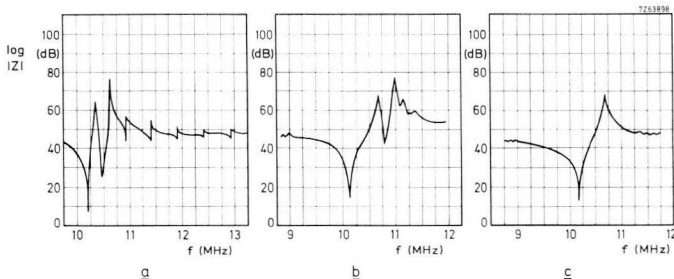


Fig. 5.4 Suppression of anharmonic spurious resonances by a suitable choice of electrode diameter, shown by means of the impedance curve of a thickness-mode resonator of 5,6 mm diameter.

- (a) Electrode covering the entire disc area.
- (b) Central electrode of 1,7 mm diameter.
- (c) Central electrode of 1,2 mm diameter.

## 5.2 Encapsulation of the resonator

It has been found from experiment that, in principle, the same method can be used for encapsulating both radial-mode and thickness-mode resonators (Sections 5.1.1 and 5.1.2 respectively).

Resonators are encapsulated for the following reasons:

- protection against external mechanical damping,
- enabling connections to other elements to be made.

*PLATE III* shows the parts of the complete resonator.

## 5.3 Resonator characteristics and measurements

The graph in Fig. A.2(b) (see Appendix A) shows the impedance of a piezo-electric resonator in the vicinity of the fundamental resonance plotted as a function of the frequency\*. As explained in Appendix A, the specific frequencies at which the impedance of a resonator reaches a minimum or a maximum are termed the minimum-impedance frequency  $f_m$  and the maximum-impedance frequency  $f_n$  respectively. They lie close to the particular series and parallel resonance frequencies ( $f_s$  and  $f_p$ ) at which the impedance becomes zero or infinite respectively when there are no dissipative elements in the equivalent circuit. The series resonant frequency and  $N_p^E$ , the frequency constant for the planar vibrational mode, are related to the disc diameter  $D$ :

$$f_s = \frac{N_p^E}{D}. \quad (5.2)$$

In practical applications it is important to know the values of the various elements in the equivalent circuit of the resonator. Fig. 5.5 shows the equivalent circuit in its simplest form. Since the four elements of this circuit, i.e., inductor  $L_1$ , resistor  $R_1$ , capacitor  $C_1$  (in the so-called dynamic or mechanical branch of the circuit) and capacitor  $C_0$  do not exist as individual elements, their respective values must be determined by indirect measurement. There are various methods, one of which is to measure the following quantities:

\* The terms resonant frequency and antiresonant frequency ( $f_r$  and  $f_a$ , defined by a real impedance) should not be used here because the deviations from the actual minimum and maximum frequencies are often great.

- the capacitance at a frequency below  $f_s$ ;
- series resonant frequency  $f_s$ ;
- series resonant frequency  $f_{sL}$  with a load capacitance  $C_L$  connected in series,
- resistance  $R_1$  at the series resonant frequency.

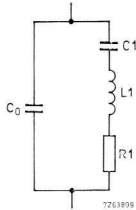


Fig. 5.5 Simplified equivalent circuit of a PXE resonator.

If the capacitance of the resonator is measured at a frequency far below the resonant frequency, say 1 kHz, the value found is, to a good approximation:

$$C_{lf} \approx C_0 + C_1. \quad (5.3)$$

The series resonant frequencies  $f_s$  and  $f_{sL}$  are best measured with the circuit of Fig. 5.6 which reduces the effect of stray capacitance. The generator frequency is adjusted to maximum transmission whilst the resonator is connected to the terminals *A* and *B* of the circuit. This frequency is equal to the maximum transmission frequency of the circuit and, as a first approximation, also equal to the minimum impedance frequency and the series resonant frequency  $f_s$  of the resonator.

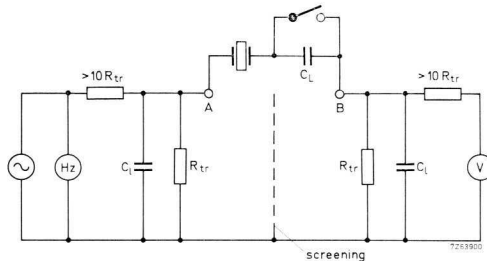


Fig. 5.6 Transmission circuit for determining the series resonant frequencies  $f_s$  and  $f_{sL}$  as well as the resistance  $R_1$ . The reactances  $1/\omega C_1$  ( $C_1$  is the leakage capacitance) must be high compared with  $R_{tr}$ . This condition is fulfilled, for instance, when  $C_1 \approx 2$  pF,  $f_s \approx 460$  kHz, and  $R_{tr} = 10 \Omega$ .

The same method is used to determine the maximum transmission frequency when an additional load capacitance  $C_L$  is connected in series with the resonator. Here again, as a first approximation, this frequency is equal to the corresponding minimum-impedance frequency and the series resonant frequency  $f_{sL}$  of the loaded resonator. The dynamic capacitance and inductance are then calculated as:

$$C_1 = (C_L + C_{1f}) \frac{f_{sL}^2 - f_s^2}{f_{sL}^2}; \quad (5.4)$$

$$L_1 = \frac{1}{4\pi^2 f_s^2 (C_L + C_{1f})} \cdot \frac{f_{sL}^2}{f_{sL}^2 - f_s^2}. \quad (5.5)$$

Once  $C_1$  is known,  $C_0$  is easily derived with sufficient accuracy from eq. 5.3. Resistance  $R_1$  can be determined by replacing the resonator by a reference resistor  $R_{st}$  giving the same indication as the resonator at the same frequency and at maximum transmission. Resistance  $R_{st}$  equals the minimum impedance as a first approximation, and is equal to  $R_1$ .

### Example

The following values were measured on a PXE6 resonator:  $C_{1f}$ , 194,7 pF;  $f_s$ , 460,44 kHz;  $f_{sL}$ , 469,34 kHz, and  $R_1$ , 19,5Ω. The load capacitance,  $C_L$ , was 200 pF. Inserting these values into eqs. 5.4 and 5.5 gives:

$$C_1 = 14,85 \text{ pF}$$

$$\text{and } L_1 = 8,05 \text{ mH.}$$

The value of  $C_0$  can now be deduced from eq. 5.3 as

$$C_0 = 179,9 \text{ pF.}$$

The mechanical quality factor,  $Q_m$ , is now calculated as:

$$Q_m = \frac{1}{\omega_s C_1 R_1} = 1200.$$

## 5.4 Using resonators in filters

As already mentioned in the introduction to this chapter, filters incorporating several resonant circuits are often used if, for instance, a high attenuation is required outside the passband. In the following sections three different methods of incorporating ceramic resonators in multi-stage filters will be described.

### 5.4.1 THREE-STAGE HYBRID FILTER

Fig. 5.7 shows the circuit diagram of a three-stage hybrid filter comprising two  $LC$  circuits and a resonator complete with signal source and load resistor. Leaving the parallel capacitor  $C_0$  of the resonator out of consideration, the filter consists of three selective resonant circuits:

- circuit 1, consisting of capacitor  $C_1$ , inductor  $L_1$  and resistor  $R_1$  in parallel;
- circuit 2 (the resonator), consisting of  $C_2$ ,  $L_2$  and  $R_2$  in series,
- circuit 3, consisting of  $C_3$ ,  $L_3$  and  $R_3$ .

The frequency response of the first circuit depends also on the losses in  $C_1$  and  $L_1$ , which are represented by resistance  $R_1$ . Its response is also influenced by the source impedance, i.e., the output impedance of the supply transistor (usually the mixer stage). All capacitive and inductive source effects can be compensated by adjusting the values of  $C_1$  and  $L_1$ . The real part of the output impedance is represented as  $R_s$ . The frequency response of the third circuit depends entirely on  $C_3$ ,  $L_3$ , the losses of these components (represented as  $R_3$ ) and the input impedance  $R_L$  of the following transistor.

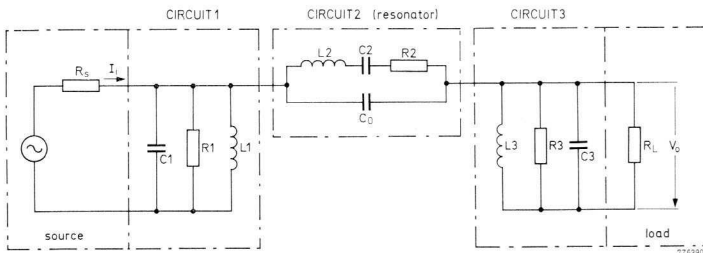


Fig. 5.7 Circuit diagram of a three-stage filter with source and load.

One of the most important characteristics of a filter is its transfer impedance:

$$Z_T = \frac{V_o}{I_i}, \quad (5.6)$$

which is the ratio of the output voltage to the input current. A filter is unambiguously defined by its transfer impedance in the middle of its passband ( $Z_{T0}$ ) and by  $\alpha$  the relative frequency dependence of the transfer impedance:

$$\alpha = \frac{Z_{T0}}{Z_T}. \quad (5.7)$$

Given a proper definition of the quality factors,  $Q$ , of the three circuits and the coupling factors,  $k$ , between them, the value of  $\alpha$  is uniquely determined by these  $Q$  and  $k$  values just as in the case of other filter configurations. Existing methods of filter synthesis can therefore be used for hybrid filters.

Fig. 5.8 shows a three-stage hybrid filter circuit that has been tested in practice. Capacitor  $C_n$  compensates the asymmetry of the passband caused by the parallel resonance of the resonator (neutralization of capacitance  $C_0$ ). Fig. 5.9 shows the passband curve.

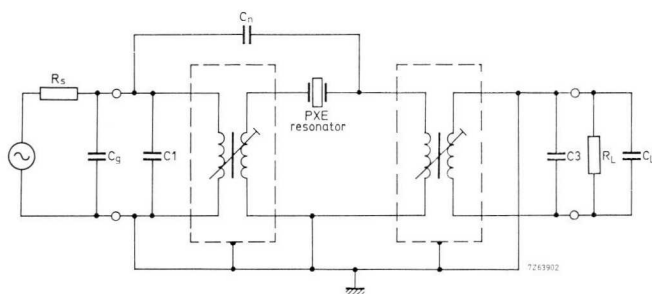
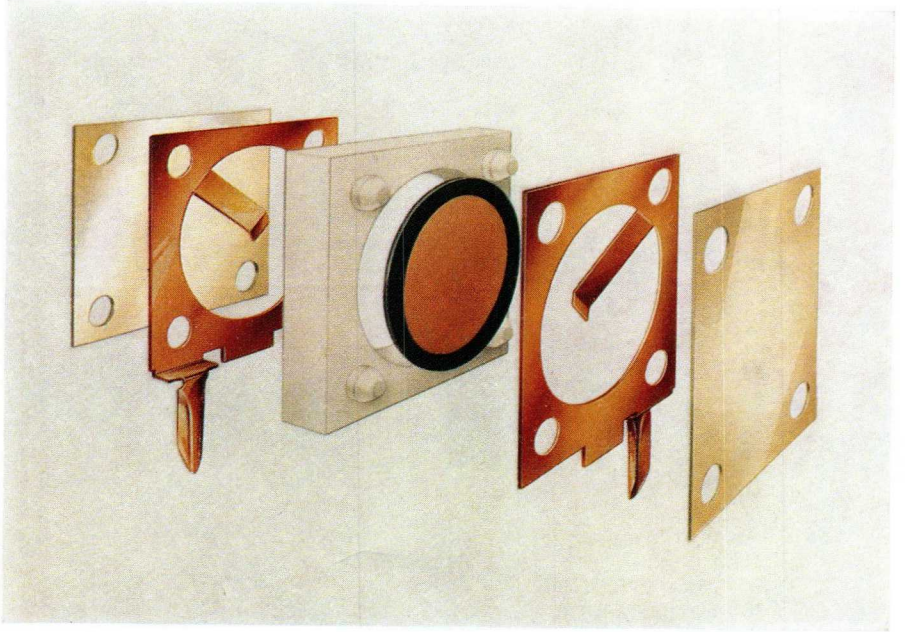


Fig. 5.8 Practical circuit of a three-stage hybrid filter with the following characteristics:

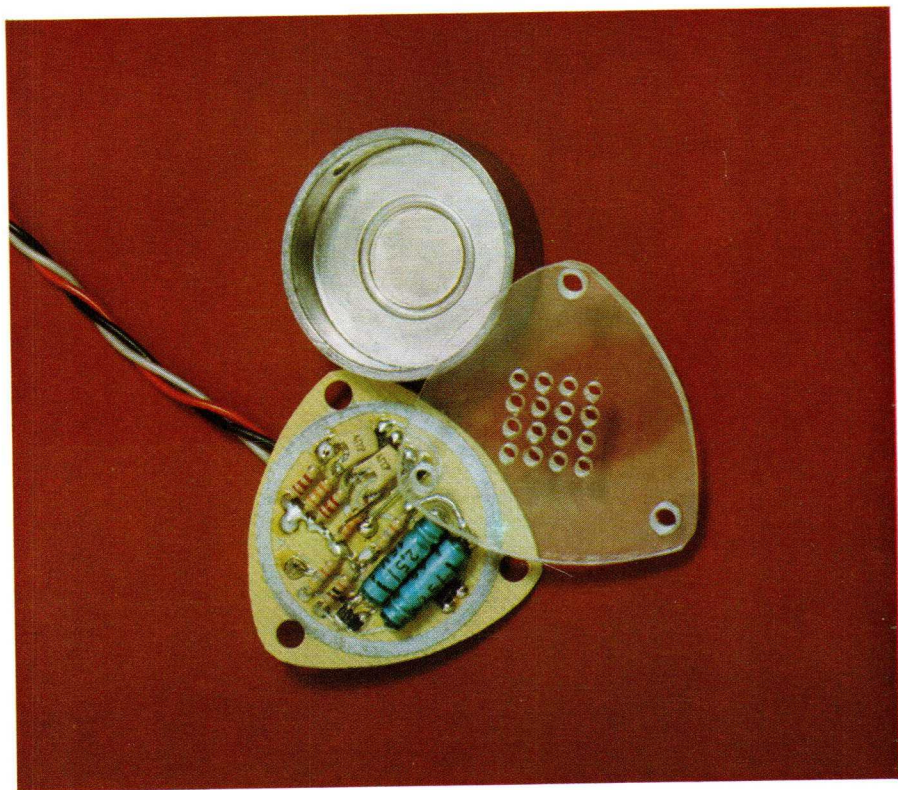
centre frequency $f_0$	460 kHz $\pm$ 1 kHz;
3 dB bandwidth	4,5 kHz;
insertion loss	13 dB;
saddling	< 0,5 dB;
ultimate attenuation at	
(a) $f_0 \pm 9$ kHz	about 35 dB,
(b) $f_0 \pm 50$ kHz	about 80 dB.

PLATE III



*Exploded view of complete resonator. The PXE is the disc in the centre; it is provided with a gold electrode on either side. By means of gold-plated springs a high-quality electrical contact is ensured even under hostile conditions.*

PLATE IV



*Piezoelectric air transducer for 2,85 kHz together with generator circuit.*

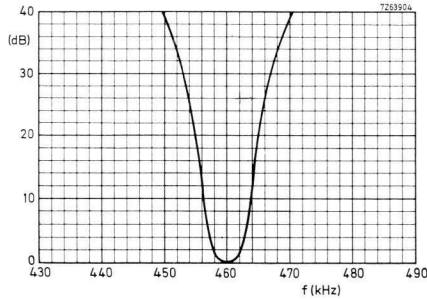


Fig. 5.9 Frequency response curve of a three-stage hybrid filter.

#### 5.4.2 ALL-CERAMIC FILTERS

Ceramic piezoelectric resonators that have a sufficiently high coupling coefficient  $k_p$  can be used for making filters without the need of conventional  $LC$  circuits.

Fig. 5.10 shows the circuit diagram of an all-ceramic filter consisting of three resonators. The coupling is provided by means of capacitors  $C_{1,2}$  and  $C_{2,3}$ . The input of the filter is loaded with the source resistance  $R_s$ , and its output with a resistance  $R_L$ . The additional resistance  $R_i$  serves to adjust the first resonant circuit to the required  $Q$  factor, and also forms the d.c. path required for biasing the preceding transistor.

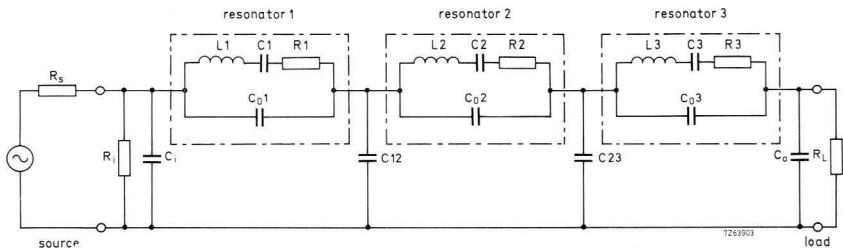


Fig. 5.10 Equivalent circuit of a three-stage all-ceramic filter.

For a narrow frequency band, say the passband, the frequency response of the filter can be determined from the three capacitively coupled resonators. Just as with hybrid filters, the frequency dependence of the transfer impedance is given by the (suitably defined) quality factors of the three resonators and their mutual coupling coefficients.

All-ceramic filters have a few advantages over multiple hybrid filters:

- the resonant circuits (resonators) all have the same temperature coefficient;
- they take up less space;
- no trimming required after assembly,
- they have a better stability.

#### 5.4.3 MONOLITHIC FILTERS

In the description of the 10,7 MHz resonator in Section 5.1.2 it was stated that the unwanted anharmonic vibrations can be eliminated by appropriate choice of the size of the electrodes. The idea is that the principal vibration mode in the area under the electrodes builds up a resonance, and that all other vibrations (with higher frequencies) move out of this area to the edge of the resonator where they are attenuated without building up a resonance. This is known as 'energy trapping'.

Obviously the distortion pattern of the main vibration mode in this type of resonator cannot break off abruptly at the edge of the electrode. The vibration amplitude will decrease exponentially outside the electrode area.

It is possible to apply a number of resonators to one chip of material which are sufficiently far apart to avoid any interference between them.

Conversely, two resonators can be placed very close to one another. In such a case, the excursion outside the electrode area of resonator 1 will not be negligibly small at the position of resonator 2, with the effect that the latter is set in vibration (Fig. 5.11(a)). This is analogous to the coupling of two pendulums by a small spring, or the coupling of two  $LC$  circuits by means of their mutual inductance. The resultant filter of coupled resonators on a single chip is known as a monolithic filter.

A possible equivalent circuit of a two-section filter is shown in Fig. 5.11(b). The degree of coupling between the two circuits is determined by the distance  $D$  between the electrodes, finally resulting in a particular value of  $C_{12}$  in the equivalent circuit.

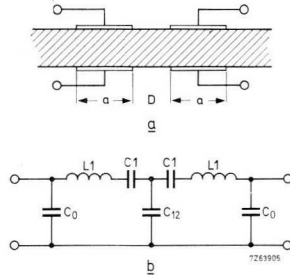


Fig. 5.11 (a) Monolithic filter of two sections.  
(b) Electrical equivalent circuit.

Fig. 5.12 shows the measured passband characteristics of two monolithic filters of the type in Fig. 5.11(a) coupled by a capacitor.

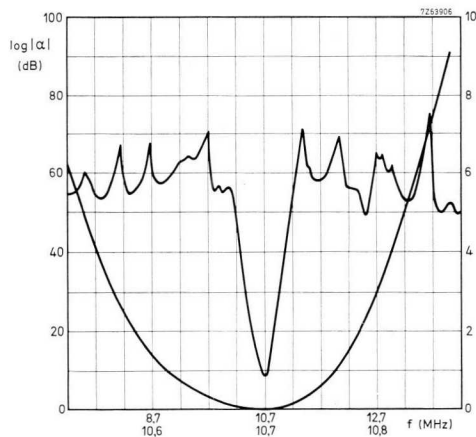


Fig. 5.12 Attenuation of filter consisting of two capacitively coupled monolithic filters, as a function of frequency. Passband is also shown enlarged.

## **6 PXE sound and ultrasound air transducers**

### **6.1 General**

Piezoelectric ceramic materials possess all the qualities for making sound and ultrasound air transducers of such reliable design that they will continue to function satisfactorily even under hostile atmospheric conditions. Such transducers can be used both for generating and receiving ultrasound. They have numerous applications, not only because ultrasound lies beyond the perception range of the human ear (most welcome in intruder alarm systems), but also because they operate on short wavelengths of no more than a few millimetres. This means that good directional beams of ultrasound can be formed with quite small transducers.

Sound transducers for lower frequencies (within the audible range) are usually smaller than the wavelength of the sound for which they are used, so that they have a spherical radiation pattern. At higher frequencies the situation changes: the wavelength becomes smaller than the size of the transducer. That is when the transducer assumes pronounced directivity characteristics. Likewise, as the frequency increases, the diffraction or bending of the sound path around obstructions becomes less and less, until finally sound is radiated along an almost straight line, much the same as light. The comparison goes even further: like light signals in light beam installations, the received and transduced sound signals can be used for counting, monitoring, and control purposes. Whereas transducers used within the audible range often have a large bandwidth, the resonant transducers used in ultrasound applications should have a relatively narrow bandwidth.

An ultrasound installation operating with a separate transmitter and receiver requires an a.c. generator (with a power amplifier, if necessary), and a microphone amplifier. The a.c. generator must be able to produce the required transmitter frequency, which is achieved by means of an adjustable oscillator or a suitable feedback arrangement.

### **6.2 Applications**

Important applications of ultrasound air transducers are, for instance, remote control of slide projectors and television receivers. Compared with radio control

systems, ultrasound systems have the advantage that they do not produce electromagnetic radiation, and hence they can never interfere with nearby radio-controlled installations or other radio sensitive equipment. Ultrasound control of a slide projector requires four channels (frequencies), *viz*: one for the forward shift and one for the backward shift of the slides, and two for focussing (for the circuits see Sections 6.5.2 and 6.6.3). A colour television receiver needs as many as fifteen channels for remote control, e.g., increase volume, decrease volume, more colour, less colour, increase brightness, decrease brightness, up to eight for channel selection, and switching on and off. The range of such a remote control system is usually about 10 m, but in any case effectiveness is limited by any surrounding walls, so that an ultrasound generator operating in a closed space is most unlikely to affect receivers beyond the walls of that space. An additional requirement is that the bulk as well as the power consumption of a battery-driven ultrasound transmitter must be kept to a minimum.

Another interesting application is the sound beam installation as used for intruder alarm systems (for circuits see Section 6.6.2). To obtain the required directivity, sound beam installations are preferably operated at high frequencies. The sound receiver (microphone) and the transmitter can be mounted facing each other, or side by side if a suitable sound reflector is available. As ultrasound can be led through arbitrarily curved narrow ducts, even measuring points which would otherwise remain inaccessible can be reached. Any objects interrupting or restoring the sound beam are registered, even transparent ones to which light beam installations do not respond. The dimensions of the registered objects must be large compared with the wavelength of the ultrasound used. A further advantage over light beam installations is that sound beam installations can be given a very rugged structure which makes them insusceptible to soiling and dust. Reliability is much higher due to the absence of an incandescent lamp and, finally, it is absolutely necessary for intruder alarm systems that the beam be invisible.

In its simplest form the ultrasound beam installation consists of an amplifier and two ultrasound transducers which are acoustically coupled and form a self-resonant system with the amplifier (for circuits see Section 6.6.1). As soon as the coupling between the two transducers is disturbed, the entire system stops oscillating. The rectified a.c. voltage can be used to light a lamp, or operate a relay, or to trigger a thyristor.

Transducers with a large bandwidth allow modulation of the ultrasound beam, and installations of this nature are characterized by their insusceptibility to noise interference. Furthermore, modulated ultrasound beams can be used for remote control: practical tests have given satisfactory results over distances of more than 10 m. The ultrasound beam can also be speech-modulated, permitting the transducers to be used advantageously for intercom systems, which can be exceptionally useful in noisy surroundings.

By making use of the Doppler effect, ultrasound can be used for measuring velocity. If the sound beam from the transmitter hits a moving reflecting body, the receiver will register a frequency shift that is to a good approximation directly proportional to velocity. If it is sufficient only to sense the presence of moving persons or objects (e.g., intruder alarm systems or safety systems), the equipment need only respond to the frequency shift without indicating its amount (movement detectors; particulars and circuits are given in Section 6.6.2). In such cases the transmitter and receiver usually share one housing.

Other interesting applications are leak detection in evacuated or pressurized vessels, and locating corona discharges. In and out flowing gases, and electric discharges, produce ultrasound which can be converted into an electrical signal by an ultrasound transducer or, alternatively, can be made audible after frequency transformation. A circuit designed for such an installation is described in Section 6.6.4.

Wideband transducers are also quite suitable for pulsed operation. Distances can be measured by means of the pulse-echo method, for instance, levels in bunkers and silos. Ultrasound provides an excellent means of measuring wind velocity with remote indication. If a beam of ultrasound travels through moving air, the propagation velocity of the sound increases and decreases in accordance with the direction, up-wind or down-wind, of the wind component. The phase shift (at higher wind velocity, the frequency shift) between transmitter and receiver provides a measure of wind velocity. With three orthogonal measuring trajectories, all three wind components can be determined. The same principle can be adapted to measure the flow rates of gases and liquids.

In several applications, frequency dependence of diffraction and absorption must be taken into account. For example, if the wavelength of the sound and the size of the object to be located are nearly the same, the sound diffracted into the 'shadow area' can impede location. In such cases it is advantageous to work with higher frequencies. On the other hand, absorption of ultrasound by

air increases rapidly with frequency. For practical purposes, half-value distances are used. These are the distances at which the sound pressure has dropped by 50%. The half-value distances given in Table 6.I are useful for practical design.

These half-value distances depend largely on humidity, temperature and pollution of the air. In addition to this shortening of the ultrasound range at higher frequencies, it should be noted that the sound pressure also reduces owing to the required smaller dimensions of the sound transducer.

*Table 6.I. Half-value distances for practical design.*

frequency (kHz)	half-value distance (m)
20	10
50	3
100	2

### 6.3 Construction and characteristics of ultrasound air transducers

Thin metal disc flexure resonators, driven by glued-on PXE discs, and PXE5 bimorph flexure plates, have been found to be excellent devices for producing and receiving ultrasound. The main reason for this is that they can be well matched to the low acoustic impedance of air. Consequently a relatively high electroacoustic efficiency is obtained (about 10%).

Let us first consider metal disc transducers and diaphragm transducers and then deal with a special square bimorph plate 36 kHz transducer (see Section 6.4).

#### 6.3.1 METAL DISC AND DIAPHRAGM TRANSDUCERS

Fig. 6.1 shows some radially symmetrical types of ultrasound air transducers plus their respective modes of vibration. In each case the PXE disc is bonded to a metal plate so that the composite assembly deflects in the manner shown during operation (broken lines). If the (mechanical) resonant frequency of this resonator corresponds to the frequency of the voltage applied, the amplitude of deflection, and hence the ultrasound radiation into the ambient air, are at a maximum.

Without further precaution, the resonator shown in Fig. 6.1(a) will exhibit simultaneous counterphase amplitudes which partly suppress the radiated sound waves, with the unavoidable result of a very low acoustic output. However, if the outer areas of the resonator are screened off as far as the vibrational nodal circle by means of a resilient sound-absorbing material (such as foam rubber or cork), which can function as the mounting at the same time, only the central area of the resonator will radiate sound. (Alternatively, the central area may be screened off.) A drawback of this simple type of ultrasound transducer is its open construction which is not suitable for use in humid and dusty environments. A basically similar transducer is described fully in Section 6.4.

Although the transducer shown in Fig. 6.1(b) has a high efficiency it is again the open construction that makes it unsuitable for operation in humid and dusty atmospheres. However, the diaphragm types shown in Figs 6.1(c) and 6.1(d), where the resonator is edge-supported, can be given a closed construction so that they are extremely sturdy and highly resistant against dust and humidity. An additional advantage is the facility they offer in that the (mechanical) resonant frequency can be changed relatively simply by machining. The type shown in Fig. 6.1(c) still operates satisfactorily at high frequencies ( $\geq 40$  kHz), and shows good directivity and beaming characteristics (large ratio between membrane diameter and ultrasound wavelength in air). For the transducers of Figs 6.1(a) and 6.1(b) the diameter of the PXE disc is not critical. However, for the types in Figs 6.1(c) and 6.1(d), the diameter of the PXE disc should not be greater than  $0,35D$  and  $0,25D$  respectively, where  $D$  is the diameter of the metal diaphragm.

The mechanical resonant frequency  $f_{sn}$  of the flexure elements discussed so far can be approximated as:

$$f_{sn} = k_n \frac{h}{D^2}, \quad (6.1)$$

\* For the so-called 'edge-clamped' mounting method as illustrated in Figs 6.1(c) and 6.1(d), we may write:

$$f_{sn} = (\beta_n h / D^2) \{Y/\rho(1 - \sigma^2)\}^{\frac{1}{2}} \\ = (\beta_n h / D^2) v_{\text{bar}} / (1 - \sigma^2)^{\frac{1}{2}},$$

where  $n$  is the order of the flexure mode, i.e., the number of nodal circles (0, 1, 2, . . .) with  $\beta_0 = 1,88$ ,  $\beta_1/\beta_0 = 3,89$ ,  $\beta_2/\beta_0 = 8,71$ , and  $\beta_3/\beta_0 = 15,45$ . Values of the sound velocity,  $v_{\text{bar}}$ , and Poisson's ratio of lateral contraction  $\sigma$  for various metals will be found in Table 8.I.

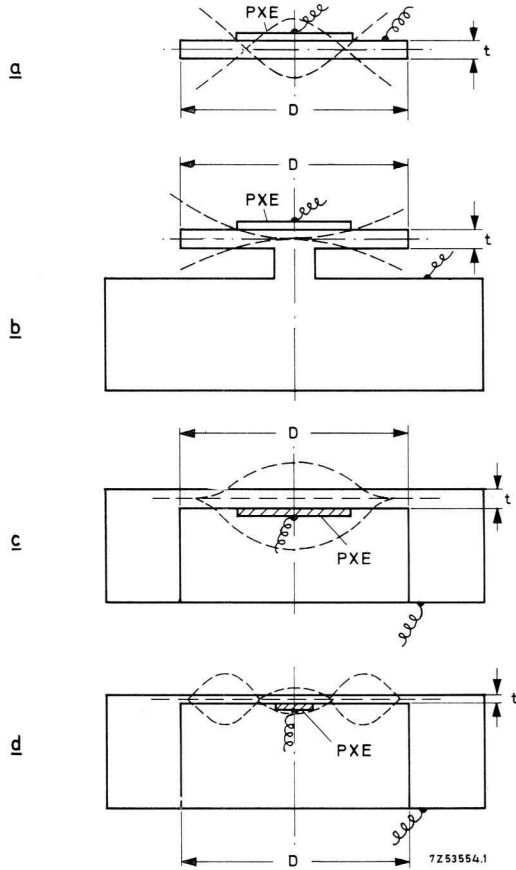


Fig. 6.1 Four different types of radially symmetric ultrasound transducers.

(a) Open construction, excursion antinode at centre.

(b) Open construction, excursion node at centre.

(c) Closed construction, fundamental resonance.

(d) Closed construction, first overtone.

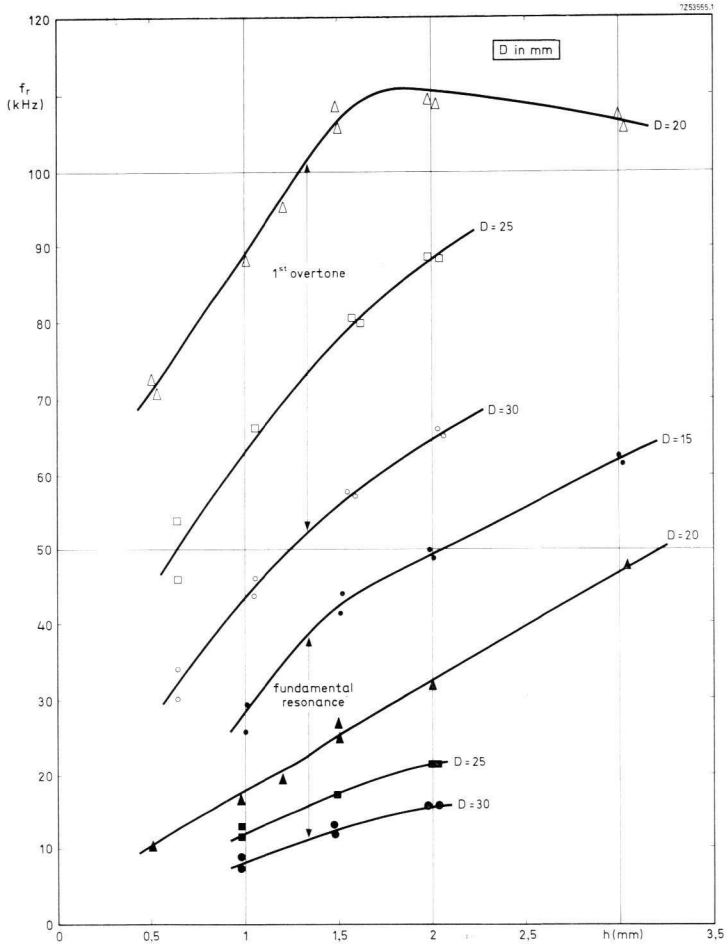


Fig. 6.2 Resonant frequency  $f_s$  of ultrasound transducers (PXE5 disc, diameter 10 mm, thickness 1 mm). The parameter  $D$  is the membrane diameter.

where  $h$  is the thickness and  $D$  is the diameter of the metal disc or diaphragm, and  $k_n$  is a material constant depending on the mounting and the mode of vibration ( $n$  indicates the order of the overtone).

For an edge-clamped aluminium or steel diaphragm without bonded PXE disc,  $k$  has the following (theoretical) values:

$$\begin{array}{ll} \text{fundamental resonance (Fig. 6.1(c)) } & k_0 = 10^4 \text{ Hz.m,} \\ \text{first overtone (Fig. 6.1(d)) } & k_1 = 4 \cdot 10^4 \text{ Hz.m.} \end{array}$$

However, the PXE disc also influences the (mechanical) resonant frequency with the result that the above values are not usually very accurate; it is best to measure the actual resonant frequency.

The curves of Fig. 6.2 show the results of a number of measurements carried out on aluminium discs of various dimensions. All discs were edge-clamped (Figs 6.1(c) and 6.1(d)), and a disc of PXE5 (10 mm diameter, 1 mm thick) was glued to the centre of each.

### 6.3.2 DIRECTIVITY AND SOUND PRESSURE

If a flexure transducer is to function as the transmitter, it is essential to know the directivity of the radiated sound. (Likewise, one needs to know the directional characteristic when it is used as a microphone.) For the so-called 'far field', i.e., distance  $> D^2/2\lambda$ , this directivity depends on the diameter  $D$  of the radiating area, the vibrational amplitude distribution over that area, and the wavelength  $\lambda$  in air (Fig. 6.3). For cases in which  $\lambda < D$ , the total angle width,  $\alpha$ , of the main sound beam directed along the axis of symmetry can be calculated quite accurately from  $D$  and  $\lambda$  alone:

$$\sin \alpha/2 \approx \lambda/D \approx \frac{v}{Df}, \quad (6.2)$$

where  $v$  is the velocity of sound in air ( $v = 344$  m/s at  $20^\circ\text{C}$ ), and  $f$  is the operating frequency. So if  $\lambda \ll D$  one gets a narrow beam and good directivity. At the same time a number of funnel-shaped lobes occur. The above relationship no longer applies if  $\lambda \geq D$ , because the directional characteristic then assumes a spherical form. Beaming can also be achieved by means of a concave acoustic reflector. In that case the diameter of the reflector must again be much greater than the wavelength.

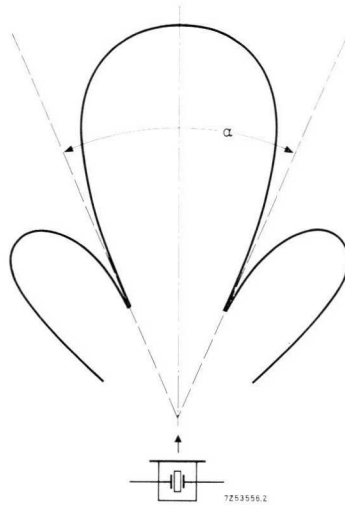


Fig. 6.3 Directional characteristic of an ultrasound transducer in the far field.

In general, a narrow sound beam is required because it reduces interference and there is less chance of undesired transducer couplings, for instance, via reflecting objects outside the main beam. On the other hand a narrow beam can be made to deviate from its original path between transmitter and receiver under the influence of turbulence. The narrower the beam and the greater the distance, the more significant is this deviation likely to be.

The ratio between the sound pressure at a given point in the ambient air and the electrical input power depend upon the overall electroacoustic efficiency of the transducer and its directional characteristic. For the transducer under discussion the sound pressure along the axis of symmetry,  $p_a$ , is given by:

$$p_a = p_0 \frac{\sqrt{P}}{l}, \tag{6.3}$$

where  $P$  is the electric input power of the transducer,  $l$  is the distance from the transducer, and  $p_0$  is a constant (sound pressure at an input power of 1 W and a distance of 1 m). It was found by experiment that overtones (Fig. 6.1(d)), which result in narrower beams, usually give better results (greater  $p_0$ ) than the fundamental resonance.

### 6.4 Design and characteristics of a 36 kHz ultrasound air transducer

Fig. 6.4 shows an ultrasound air transducer for a frequency of about 36 kHz based on a square bimorph PXE flexure element (8 mm by 8 mm and 0,6 mm thick) which is provided with a thin silver coat on either side. A specially designed metal plate at the top keeps the PXE element centred between two opposite edges, and a similar plate at the bottom (rotated through 90° with respect to the top plate) does the same with the other two opposite edges. These two metal plates also serve as the electrical contacts. The central area of the PXE element vibrates in counterphase with its edges so that, without further precaution, there will be a certain amount of cancelling of the radiated ultrasound, which will result in a very low efficiency. This is remedied by shielding the central area of the PXE element with a metal plate which prevents direct radiation from there. A secondary — and welcome — result is that phase conversion of the laterally diverted sound takes place at the same time, so that the radiation from the corners of the square element is now reinforced.

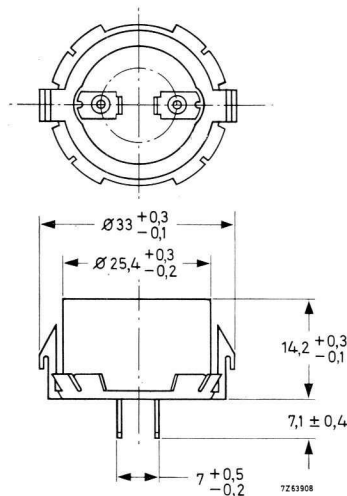


Fig. 6.4 Construction of a 36 kHz ultrasound air transducer (housing diameter about 25,5 mm, height about 15 mm).

Bimorph flexure elements based on the above principle display a greater coupling factor and a greater sensitivity than other types where the PXE element is glued to a metal diaphragm or plate (Section 6.3.1).

Fig. 6.5 shows that the ultrasound transducer has a specific resonant frequency. The electrical behaviour of the transducer can be adequately explained by means of the equivalent circuit shown in Fig. 6.6 (see also Appendix A).

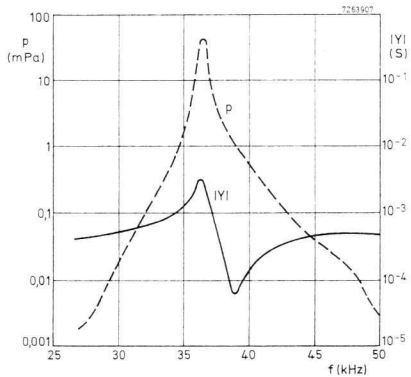


Fig. 6.5 Admittance  $|Y| = |I/V|$  and sound pressure  $p$  at a distance of 1 m, as functions of frequency for the transducer of Fig. 6.4. ( $V = 0,1 \text{ V r.m.s.}$ )

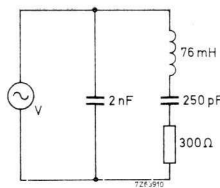


Fig. 6.6 Equivalent circuit of the transducer.

There are two characteristic frequencies:

- the series resonant frequency  $f_s = 36,5 \text{ kHz}$ , at which the admittance of the transducer reaches a maximum:

$$|Y_s| \approx 3,3 \cdot 10^{-3} \text{ S} \hat{=} |Z_s| \approx 300 \Omega \quad (|Z| = \text{impedance}),$$

- the parallel resonant frequency  $f_p = 39 \text{ kHz}$ , at which the admittance of the transducer reaches a minimum:

$$|Y_p| \approx 6 \cdot 10^{-5} \text{ S} \hat{=} |Z_p| \approx 15 \text{ k}\Omega.$$

The transducer characteristics are highly dependent on the electrical load for which we first only assign a real value  $R$ . This resistance can be regarded as the input resistance of a microphone amplifier, or the internal resistance of a transmitter generator since the characteristics of the two working conditions do not differ much. When there is effectively no electrical load ( $R \ll |Z_s|$  or  $R \gg |Z_p|$ ), the transducer has a quality factor of about 60, which means a 3 dB bandwidth of about 0,6 kHz.

Fig. 6.7 shows how the maximum response frequency  $f_M$  varies with  $R$ , the load resistance (see also eq. A.8 in Appendix A). The maximum response frequency is that frequency at which the microphone sensitivity or the sound pressure of the transmitter reaches its maximum. Fig. 6.8 shows the bandwidth in a similar manner. Note that  $f_M$  shifts from  $f_s$  to  $f_p$  as the load increases, whilst at  $R = 2 \text{ k}\Omega$  a maximum bandwidth of about 3 kHz is established. The corresponding value  $f_M$  is located about mid-way between  $f_s$  and  $f_p$ .

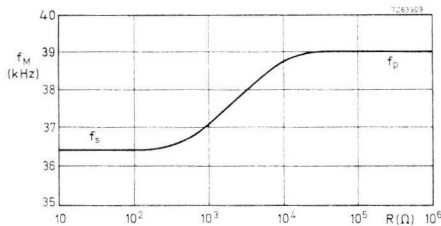


Fig. 6.7 Frequency of maximum response  $f_M$  of the transducer as a function of resistance  $R$ .

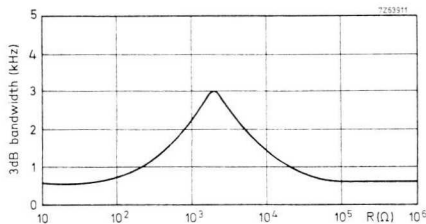


Fig. 6.8 Bandwidth of the transducer as a function of resistance  $R$ .

The voltage  $V$  and the electric output power  $P$  generated when the transducer is operated as a receiver (sound pressure 0,1 Pa) are shown in Fig. 6.9. The relationship between the electric output power and the load resistance  $R$  contains a clear indication that in the range of values of  $R$  from 100Ω to 50 kΩ efficiency remains fairly constant. The same applies when the transducer is driven as a sound transmitter.

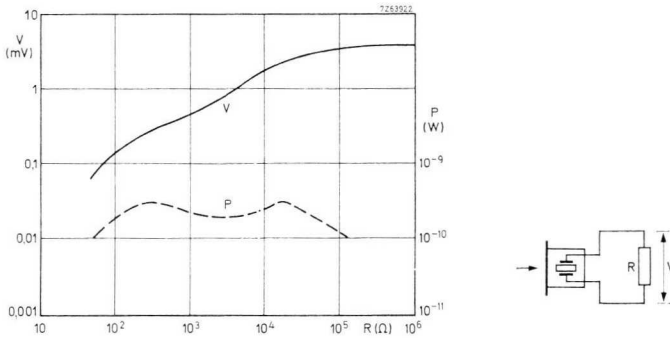


Fig. 6.9 Generated voltage  $V$  and power  $P$  of the transducer at frequency  $f_M$  operating as a receiver, as functions of load resistance, at a sound pressure of  $p = 0,1$  Pa.

Fig. 6.10 indicates the sound pressure obtained at a distance of 1 m at  $V = 0,1$  V r.m.s. It should be noted that during transmitter operation the sound pressure does not drop only by  $1/l$  (where  $l$  is distance), but that it is further damped by about 1,4 dB/m due to absorption by air (half-value distance  $\approx 4$  m). Furthermore, as the (low) power consumption changes, some other values also change. For instance, the values in Table 6.II are obtained for  $R = 0$  and  $V = 0,1$  V r.m.s. and 3 V r.m.s.

The bandwidth of the transducer can be considerably expanded if, apart from the load resistance  $R$ , an inductance of about 7 mH is connected in parallel ( $L_{par}$ ) or in series ( $L_{ser}$ ) with the transducer (Fig. 6.11). This value differs slightly from the one calculated with eqs. A.13 or A.14, because here the acoustic effect of the cover plate has been taken into account. A flat response curve is obtained by choosing a load resistance of 390Ω (series coil), or 10 kΩ (parallel coil).

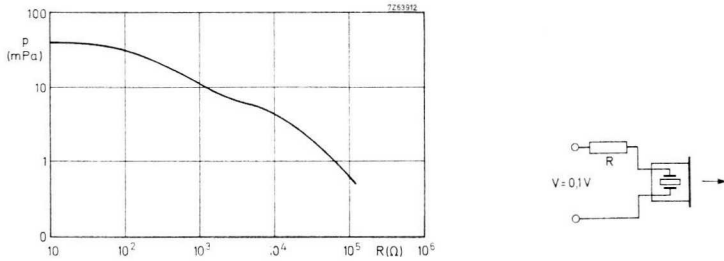


Fig. 6.10 Output sound pressure  $p$  of the transducer at frequency  $f_M$  operating as a transmitter, as a function of source resistance  $R$  ( $V = 0,1$  V r.m.s., distance 1 m).

Table 6.II. Characteristic values for a 36 kHz air transducer (transmitter) corresponding to different operating voltages.

parameter	unit	$V = 0,1$ V r.m.s.	$V = 3$ V r.m.s.
$f_s$	kHz	36,5	36
$\Delta f$ (3 dB)	kHz	0,6	1,5
$ Z_s $	$\Omega$	300	600
sound pressure $p$ (1 m distance)	Pa	0,04	0,5

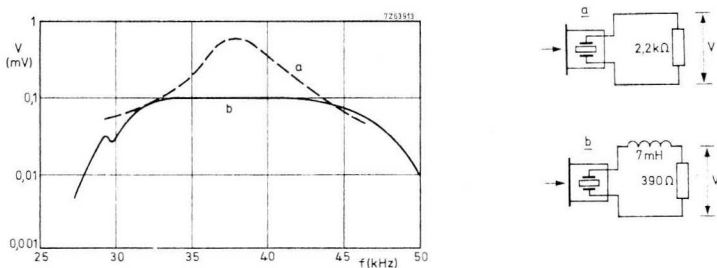


Fig. 6.11 Generated voltage  $V$  of the transducer operating as a receiver, as a function of frequency and at a sound pressure of  $p = 0,1$  Pa.

(a) With a load resistance of 2,2 k $\Omega$ .

(b) With a series inductance of 7 mH and a load resistance of 390  $\Omega$ .

Whereas the sensitivity of a transducer microphone with a series inductance ( $R = 390\Omega$ ) is about 1 mV/Pa, or 5 mV/Pa with a parallel inductance ( $R = 10\text{ k}\Omega$ ), the sound pressure at a distance of 1 m produced by a transmitter at  $V = 0,1\text{ V r.m.s.}$  is 0,007 Pa for series connection and 0,002 Pa for parallel connection. From what has been said so far it will be clear that when designing the electronic circuitry associated with these transducers, the input and output impedances must be given due consideration. Fig. 6.12 shows the directivity characteristic of a 36 kHz air transducer.

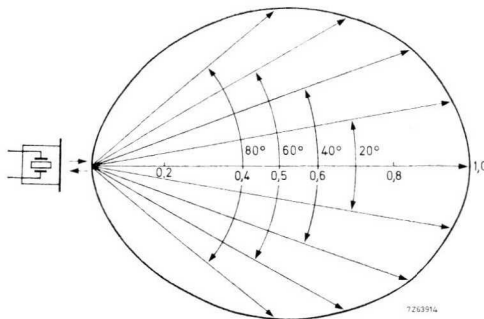


Fig. 6.12 Directional characteristic of the transducer for transmitter and receiver operation. The relative sound pressure (transmitter) and the relative sensitivity (receiver) are plotted on a linear scale.

### 6.5 Transmitter circuits for 36 kHz ultrasound air transducers

There are two different types of transmitter circuit. In a simple circuit, usually suitable for only one frequency (channel), the transducer itself is the frequency-governing element. In that case the frequency is limited to the range between the series resonant frequency and the parallel resonant frequency. Transmission of a wider frequency range, e.g., for multi-channel remote control, requires a separate oscillator whose frequency is not affected by the transducer. Both these systems will be discussed in detail in the following sections.

## 6.5.1 SINGLE-CHANNEL TRANSMITTER

Fig. 6.13 shows the circuit diagram of an oscillator with feedback transformer in which the air transducer is connected in a bridge circuit. This method ensures reliable operation at optimum frequency, even if there is a considerable spread in transducer characteristics. The bridge circuit is tuned for maximum sound pressure, which implies that the frequency is then about 36,5 kHz. At a distance of 1 m the sound pressure is then about 0,45 Pa.

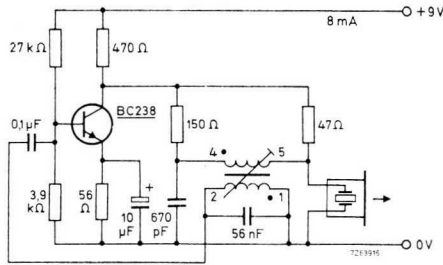


Fig. 6.13 A single-channel transmitter with feedback.

transformer 1 Lilliput coil assembly;  
 frame core ferroxcube 3B 3122 104 91460;  
 screw core ferroxcube 3B 4322 020 32250;  
 coil former 4312 021 29670;  
 inductance  $L_{1-2} \approx 180 \mu\text{H}$ ;  
 windings  $N_{1-2}$  120 turns of 0,14 mm diameter lacquered Cu wire,  
 $N_{4-5}$  60 turns of 0,14 mm diameter lacquered Cu wire.

Fig. 6.14 shows a circuit design where the oscillator operates without a coil. This arrangement produces a sound pressure of about 0,5 Pa at 36 kHz at a distance of 1 m. The operating frequency can be increased to about 39 kHz, i.e., the parallel resonant frequency of the transducer, by means of the multivibrator circuit shown in Fig. 6.15 (also without a coil). The sound pressure at a distance of 1 m is then 0,35 Pa.

The diodes in the emitter circuits of the transistors suppress the reverse voltage peaks occurring between base and emitter. These peaks are likely to exceed the maximum permissible value of 5 V for the transistor types used here, at the same time giving rise to frequency fluctuations. At low supply voltages there is no need for such diodes.

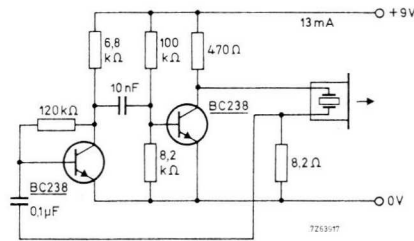


Fig. 6.14 A single-channel transmitter without coil.

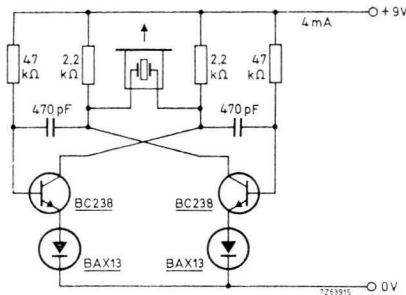


Fig. 6.15 Transmitter without coil, multivibrator circuit.

### 6.5.2 FOUR-CHANNEL TRANSMITTER

As explained in Section 6.1, four channels are required for the remote control of a slide projector. Fig. 6.16 shows a four-channel arrangement where the frequency is not governed by the transducer, but by means of a conventional *LC* circuit. The transducer described in Section 6.4 produces a sound pressure of 0,8 Pa at a distance of 1 m. The oscillator capacity can be expanded by adding more channels, however, these must fall within the range of 33 kHz to 45 kHz.

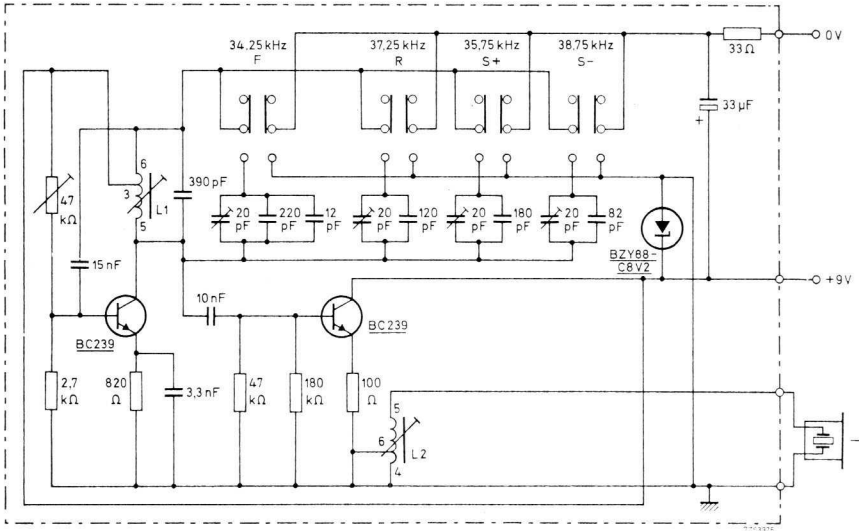


Fig. 6.16 Four-channel transmitter (for remote control of a slide projector). The functions are symbolised as follows:

$F$  = forward;  $R$  = reverse;  $S^+$  = positive focus setting,  $S^-$  = negative focus setting.

Inductances:  $L_{1, 5-3} = 35$  mH;  $L_{1, 3-6} = 79$  mH;

$L_{2, 5-6} = 5,1$  mH;  $L_{2, 6-4} = 480$   $\mu$ H.

Windings:  $N_{1, 5-3} = 1150$  turns;  $N_{1, 3-6} = 55$  turns (both of lacquered Cu wire 0,06 mm diameter),

$N_{2, 5-6} = 440$  turns;  $N_{2, 6-4} = 140$  turns (both of lacquered Cu wire 0,01 mm diameter).

## 6.6 Receiver circuits for 36 kHz ultrasound air transducers

In the following sections, three demonstration circuits are described (ultrasound beam installations and movement detector based on the Doppler effect) which are suitable for different purposes and can be adapted to any required function by making minor changes.

6.6.1 ULTRASOUND BEAM INSTALLATIONS

Fig. 6.17 shows a single or two-stage ultrasound receiver (microphone amplifier) with a microphone transducer  $W_1$ . The amplified signal is rectified, led to a direct voltage amplifier, and causes a signal lamp to light (a relay may also be used). With the second transducer,  $W_2$  (broken lines), the same circuit can be used as the ultrasound source in a beam installation operating in an acoustic feedback arrangement. In that case the single and two-stage amplifiers are capable of bridging distances of about 0,1 m and 5 m respectively. However, it is recommended that a separate transmitter be used for greater distances because one then gets shorter response times (transducer  $W_2$  is not needed). A transmitter of the type shown in Fig. 6.13, operating in conjunction with a two-stage microphone amplifier can cover a distance of about 10 m. The same arrangement can also be used for single-channel remote control.

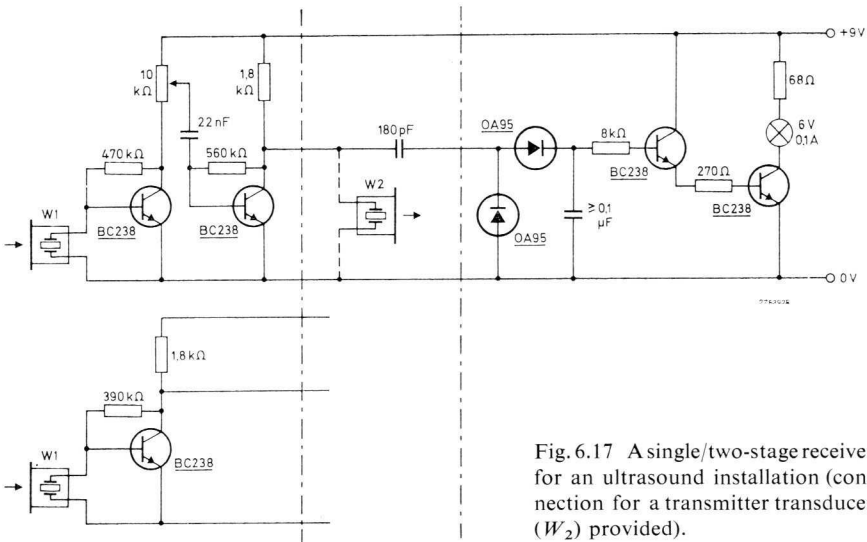


Fig. 6.17 A single/two-stage receiver for an ultrasound installation (connection for a transmitter transducer ( $W_2$ ) provided).

Greater sensitivity and consequently a greater range is obtained with the three-stage amplifier shown in Fig. 6.18. Owing to the great voltage amplification (about 100 dB), it must be ensured that no parasitic feedback can occur which



*Example*

For  $f = 36$  kHz and  $v = 1$  m/s, the frequency shift  $\Delta f$  is about 215 Hz. Interference between the ultrasound waves reflected by stationary and moving objects gives rise to a beat frequency of the same value. This change, or shift, must be sensed and indicated by the movement detector. Indication can be obtained with a frequency discriminator. The circuit in Fig. 6.19 can be used for indicating signals of frequencies ranging from 5 Hz to 1 kHz. This corresponds to a velocity range of 0,02 m/s to 5 m/s. Therefore such a circuit is eminently suitable for use in intruder alarm systems. The same principle can be used for making a remotely operated proximity switch.

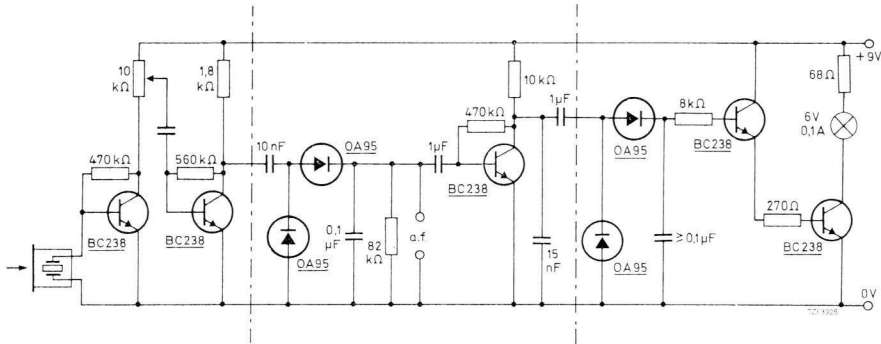


Fig. 6.19 Movement detector as used, for instance, in intruder alarm systems and proximity switches.

### 6.6.3 FOUR-CHANNEL ULTRASOUND RECEIVER

Fig. 6.20 gives the circuit of a four-channel ultrasound transducer for remote control of a slide projector which, in conjunction with the transmitter circuit shown in Fig. 6.16, has a range of almost 10 m. Several more channels can be built in.

In this receiver circuit a TAA310A\* integrated circuit is used as the i.f. amplifier for the signals picked up by the ultrasonic microphone. The TAA310A is connected in accordance with the circuit presented in our Data Handbook System.

\* The TAA310 is a similar device but the pin numbering is different.

Instead of the recommended load resistor of 1 k $\Omega$ , a transformer with a ratio of 1 : 2 is connected in parallel with a resistor of about 470 $\Omega$ , so that the circuit output can now be loaded with 100 $\Omega$ .

To prevent the gain of this circuit from being affected by the inductive components of the transformer, the impedance of the primary winding should be considerably higher than the load resistance at the lowest frequency of 30 kHz. This can best be achieved with a Macronova coil assembly set.

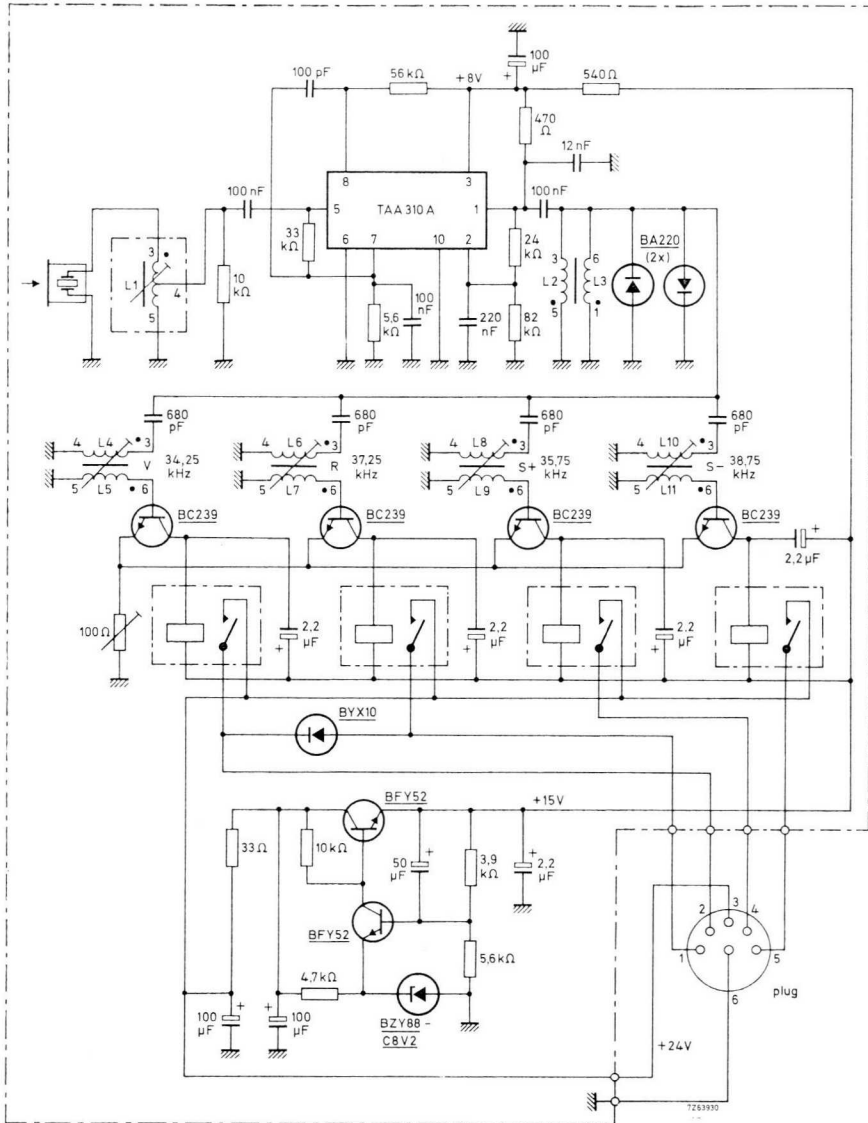
The high voltage gain of the TAA310A (about 85 dB with the 100 $\Omega$  load) would cause this circuit to oscillate if precautions were not taken. The values of some of the components of the input amplifier of the circuit shown in Fig. 6.20 would then have to be determined by experiment. However, these problems are adequately eliminated if the component values shown are used in conjunction with the arrangement shown in Fig. 6.21.

To give the microphone transducer a bandwidth of 15 kHz in the range from 30 kHz to 45 kHz, the parallel capacitance of the resonator must be compensated by an inductance, and the entire circuit must be damped by means of a resistance. There are two methods:

- a series inductance  $L \approx 7$  mH and a series resistance  $R \approx 390\Omega$  (signal taken across the series resistor),
- a parallel inductance  $L \approx 7$  mH and a parallel resistance  $R \approx 10$  k $\Omega$  (signal taken across the parallel resistor).

The first circuit corresponds to a low-impedance amplifier input and is particularly proof against parasitic oscillation of the entire circuit. The signal voltage at the series resistor is about 10 dB lower than that in the parallel connection. Hence parallel connection is preferred for the microphone circuit. An additional advantage of this method is that optimum matching between the input circuit and the input of the amplifier can be obtained by correct tapping of the inductance. The exact position of the tap (half the total number of turns) was determined by experiment.

The different transmission channels are separated by means of four tuned circuits that function as filters connected to the output of the input amplifier. In principle it is also possible to apply a larger number of such circuits if more channels are needed for other remote control functions. These circuits should be arranged at the greatest possible distance from the input inductance of the amplifier.



□

Fig. 6.20 (a) Four-channel receiver with an integrated i.f. amplifier TAA310A (for remote control of a slide projector).

(b) Winding scheme for input inductance  $L_1$ .

(c) Winding scheme for transformer  $L_2/L_3$ .

(d) Bottom view of the coil former.

input inductance  $L_1$  Lilliput coil assembly;

frame core ferroxcube 3B 3122 104 91460;

screw core ferroxcube 3B 4322 020 32250;

coil former 4312 021 29670;

housing 3122 990 94130;

$L_{1, 3-5} = 7$  mH;

winding  $N_{1, 3-5} = 480$  turns of 0,01 mm diameter lacquered Cu wire (tap at 240 turns);

transformer and oscillator circuits ( $L_2$  to  $L_{11}$ ) = 5 Macranova assemblies;

frame core ferroxcube 3D3 4322 020 37030;

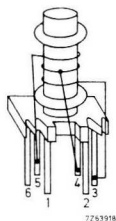
screw core ferroxcube 3D3 4312 020 32150;

coil former 4312 021 29650;

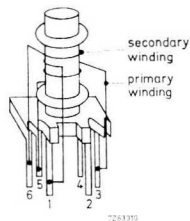
windings  $N_2 = 840$  turns } of 0,09 mm diameter  
 $N_3 = 450$  turns } lacquered Cu wire;

$N_4 = 1000$  turns }  
 $N_5 = 65$  turns } of 0,01 mm diameter  
 $N_6 = 920$  turns } lacquered Cu wire.  
 $N_7 = 56$  turns }  
 $N_8 = 960$  turns }  
 $N_9 = 60$  turns }  
 $N_{10} = 885$  turns }  
 $N_{11} = 56$  turns }

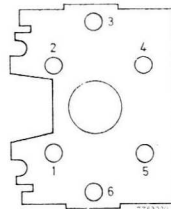
The resistance of the 12 V reed contact relay coil is about 1 k $\Omega$ .



b



c



d

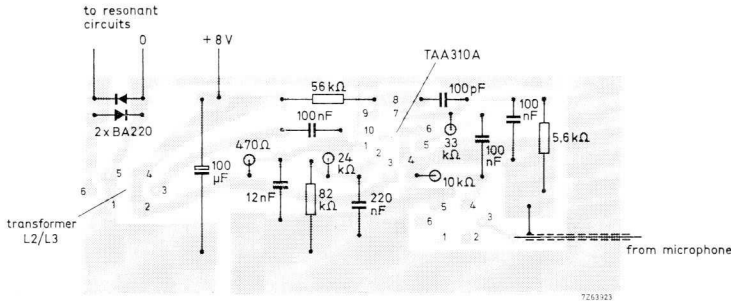


Fig. 6.21 Arrangement of the TAA310A and the components of the input amplifier on a printed circuit board corresponding to the circuit of Fig. 6.20.

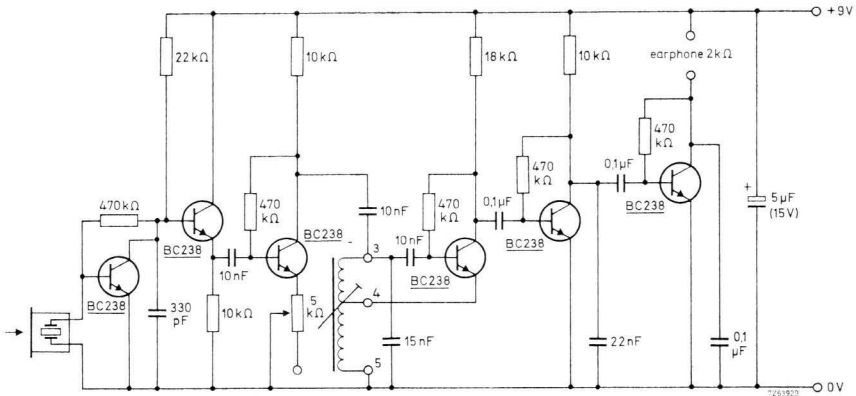


Fig. 6.22 Leak detector with oscillator.  
 Inductance  $L$  Lilliput coil assembly;  
 windings  $N_{3-4} = 23$  turns } of 0,07 mm diameter  
 $N_{4-5} = 197$  turns } lacquered Cu wire.  
 The inductance is adjusted for maximum sound output.

#### 6.6.4 LEAK DETECTOR

The circuit of an ultrasound leak detector (Fig. 6.22) contains an oscillator whose frequency is shifted by about 1 kHz to 2 kHz with respect to the received frequency. Reception of an ultrasound signal results in a difference frequency within the audible range, which produces a tone in the head-set. Since escaping gases and electric discharges are natural sources of ultrasound, an ultrasound installation is of excellent service in finding leaks in pressurized pipe systems and inflated tyres, as well as in locating discharge areas in high-tension equipment.

By using an additional sound transmitter it is also possible to detect leaks in closed non-pressurized vessels if the transmitter is placed inside. The leak detector is then used to scan the outside in search of escaping ultrasound (e.g., testing the air-tightness of motor cars).

#### 6.7 A simple 3 kHz tone generator

There are various kinds of warning system that are required to produce an acoustic signal when, for instance, an industrial machine cuts out. The sound produced by such a system must, of course, be loud enough to ensure that it will be heard in spite of the usually high ambient noise levels. Furthermore, the frequency of the sound must lie within the maximum perception range of the human ear; the preferred frequency is 3 kHz.

A piezoelectric tone generator equipped with a PXE5 flexure element is particularly suited to this type of application. *PLATE IV* shows a version where a PXE disc is glued to an aluminium diaphragm. By means of a cover and a base plate, also shown in *PLATE IV*, this unit can be made into a housing of 26 mm diameter which can accommodate the whole circuit. It is used to generate a 3 kHz tone that will be heard even above the traffic noise in a busy thoroughfare. The sound is made even more noticeable if it is interrupted at 3 Hz to 4 Hz to give an intermittent tone. A complete arrangement for producing such a sound will be discussed below.

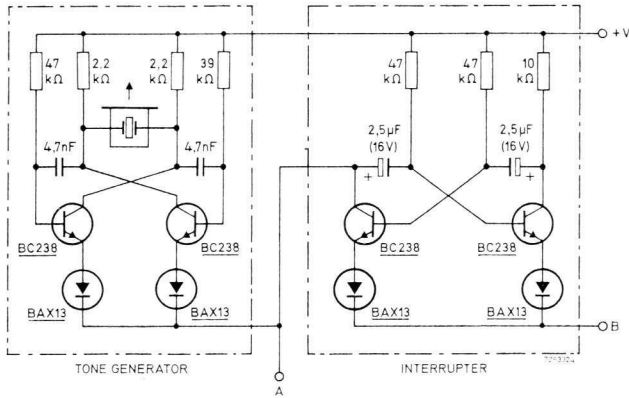


Fig. 6.23 Combined circuit of a 3 kHz tone generator and a 3.5 Hz interruptor. Terminal *A* for constant tone; terminal *B* for interrupted tone.

Fig. 6.23 shows the complete circuit diagram of an installation comprising a 3 kHz tone generator and a 3.5 Hz interrupter, both operating on the multi-vibrator principle. The main differences between this tone generator and the one shown in Fig. 6.15 are to be found in the higher capacitances and resistances required for the lower transducer frequency. The tone generator-multi-vibrator operates at the parallel resonant frequency of the transducer. The function of the diodes inserted in the emitter circuits of the transistors was explained in Section 6.5.1 (Fig. 6.15).

The sound level of the tone generator can be substantially increased by using it in conjunction with a Helmholtz resonator. Fig. 6.24 shows a cross-section of the complete assembly with the 3 kHz air transducer. The Helmholtz resonator is formed by the housing and a perforated Perspex disc in front of the resonating diaphragm. The Perspex disc used in a practical system was 3.2 mm thick and contained 12 holes of 2 mm diameter. If the total space required to accommodate the equipment must be kept as small as possible, the circuit can be mounted inside the transducer, on the bottom of the housing, as shown (see also *PLATE IV*). The complete unit will then take up little more space than the transducer alone.

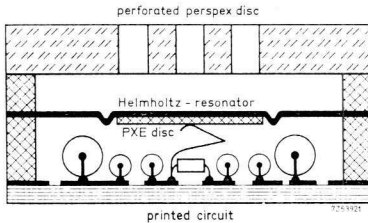


Fig. 6.24 An air transducer combined with a Helmholtz resonator.

### 6.8 Ultrasonic safety belt security system

An ultrasonic security system has recently been developed\* for ensuring that safety belts are properly used by the occupants of a car. The system described in this section employs both ultrasound and sound transducers. Salient features are its low cost and great reliability.

The principle underlying the proposal can be, for instance, that the ignition system of the engine will not function unless the driver of the car and the passenger beside him have fastened their safety belts properly. This could easily be achieved by means of a contact in the clasps of the belts, but it would still be possible to drive without using the belts; they could be led around the backs of the seats and fastened there, or simply fastened first and then sat on.

With the new safety belt control system, the upper part of each of the two belts is fitted with an ultrasound transducer (transmitter) that radiates its ultrasound towards a receiver mounted in the car body near the top of the windscreen. With this arrangement the system will detect whether the occupant of a seat is wearing his safety belt properly or not. To prevent mutual interference between the ultrasound system of the driver and that of his passenger, the systems can be operated at slightly different frequencies.

The transmitter on the belt (8 mm by 8 mm bimorph flexure element plus printed circuit board) can be accommodated in an aluminium housing of no more than 38 mm by 36 mm by 4 mm. Examples of transmitter and receiver circuits are shown in Figs 6.15 and 6.18 respectively. The warning signal can be produced by a tone generator such as the one in Fig. 6.24; the transducer itself is shown in *PLATE IV*.

\* Development in co-operation with the Ford Motor Company.

## 6.9 PXE telephone microphone

Another interesting application of PXE air transducers that has recently presented itself is the so-called PXE telephone microphone. It comprises a PXE disc and an integrated amplifier accommodated in one housing. This housing, or cartridge, can directly replace the conventional carbon microphone cartridge used so far.

A PXE telephone microphone can, for example, be a PXE diaphragm (edge-pinned mounting) formed from a PXE bimorph disc flexure element. A different construction is one where a single PXE disc is bonded to an aluminium diaphragm clamped between two rubber rings. Both constructions can be given the same dimensions as the conventional carbon microphones, including the integrated amplifier (if required, they can be made water-tight to increase immunity to humid conditions). A microphone of such design has a substantially longer life than a conventional one.

An important characteristic quantity for the PXE telephone microphone is the mechanical resonant frequency  $f_s$  of the diaphragm. The response of the PXE microphone is practically constant from the lowest frequency to the vicinity of  $f_s$ , and inversely proportional to  $f_s$ . Near  $f_s$  the response reaches a maximum to drop steeply again at still higher frequencies. On the basis of these considerations  $f_s$  is selected to lie near the upper limit of the frequency passband. The resonant frequency  $f_s$  is given approximately by eq. 6.1.

If  $f_s$  lies near to the upper limit of the passband frequency, the microphone is sufficiently sensitive. Together with the amplification and acoustic matching, this gives the PXE microphone a better frequency response than the carbon microphone.

Another advantage is that the noise level is also reduced. The high sensitivity near resonance can be compensated for by proper design of the whole microphone capsule. Furthermore, the sensitivity is independent of the attitude of the microphone, and shows no line damping effect.

The integrated amplifier must have a voltage gain of about 45 dB. If the amplifier is suitably designed, the gain will be fairly independent of the supply current and remain sufficiently high even at low currents (about 10 mA). A low supply current is of particular interest in view of future electronic telephone exchanges. Furthermore, it is of prime importance that, if carbon microphones are replaced by PXE microphones, the amplifier will function independently of

supply polarity. The amplifier can be protected against over-voltage by including two voltage regulating diodes. The overall noise figure of the complete transducer-amplifier system is lower than that of a carbon microphone.

Summarizing, the new PXE telephone microphone has the following advantages over the conventional carbon microphone:

- lower current consumption;
- sensitivity less dependent on the supply current;
- better transmission quality owing to a more favourable frequency response;
- low distortion and noise level;
- no influence of attitude on sensitivity;
- longer life;
- greater immunity to humidity,
- greater immunity to over-voltage.

## 7 Echo sounders

### 7.1 General

Nowadays small ships and boats of all types are fitted with simple but reliable echo sounding equipment, primarily for measuring the depth of water below the keel. Some types of equipment can also be used for detecting fish and, if the sound beam is radiated obliquely, underwater obstructions such as reefs and sandbanks can be detected in time to take avoiding action.

The principle behind the echo sounder is quite simple. A short pulse of ultrasound is transmitted vertically or obliquely downwards to be reflected by the sea bed, or any intervening object, and the echo is picked up by the receiver. The interval between sending and receiving pulses provides a measure of the distance covered by the ultrasound pulse and, if directed straight down, is a measure of the depth of water below the ship.

For reasons of economy one transducer is normally used for both transmitting and receiving (Fig. 7.1), these functions being switched electronically. A widely used indicator device is a time base formed by a neon lamp on the end of a rotating arm that is synchronized with the transmitter pulse rate. It responds to all received echoes, thus indicating the presence of shoals of fish as well as the sea bed. This installation can also serve as a pulse generator and will be further described as such in Section 7.7.1. Other types of equipment evaluate only the time interval up to the first strong echo, and the depth is indicated either digitally or on a dial.

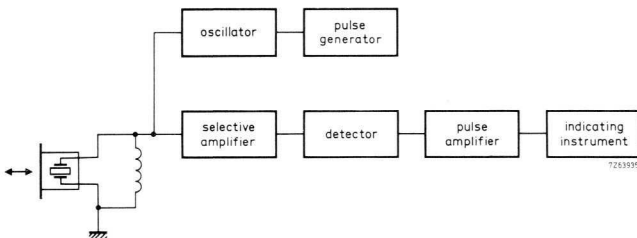


Fig. 7.1 Block diagram of an echo sounder.

## 7.2 Characteristics of echo sounding systems

### 7.2.1 MAXIMUM RANGE

The simple echo sounder systems employed in small boats are usually designed to have a maximum depth range of about 100 m. The range depends on the electronics used, the power output of the transducer and the sensitivity of the receiver. It also depends strongly on the design of the transducer.

### 7.2.2 OPERATING FREQUENCY

Ideally one wants the smallest possible transducer in an echo sounder and this suggests a high operating frequency. High frequencies are also more suitable for short pulses, which are of particular interest in shallow waters, because both minimum measuring distance and resolution depend on the duration of the ultrasound pulse. On the other hand, sound absorption in sea water increases steeply with frequency, and hence a compromise must be found.

For the equipment under consideration (maximum range 100 m) the optimum frequency lies between 150 kHz and 200 kHz. The minimum distance that can be measured is typically 30 cm; resolution should be about half of this figure.

### 7.2.3 BANDWIDTH

As the ultrasound pulses become shorter, the bandwidth of the transducer must expand. However, it should not be too broad otherwise selectivity and, consequently, the signal-to-noise ratio will suffer. The required 3 dB bandwidth is about 10 kHz to 15 kHz, corresponding to a mechanical quality factor of  $Q \approx 15$ .

### 7.2.4 DIRECTIVITY CHARACTERISTIC

The directivity characteristic of the transducer has an influence on several aspects of echo sounder performance. The range can be increased by concentrating the ultrasound into a narrower beam. At the same time smaller objects are more easily detected. However, there is the drawback that the received reflected sound intensity will fall off more sharply as the boat heels over, and the depth

indicated by the instrument will also increase due to the oblique angle of the transducer. The transducer must be so designed that it only radiates downwards, otherwise there may be interfering echoes from the boat itself or from the surface turbulence of the wake. The directivity characteristic should show the smallest possible side lobes; large side lobes tend to make the directivity of the main beam ineffective. A 6 dB beamwidth of  $10^\circ$  to  $30^\circ$  is recommended.

It should be borne in mind that the effective beamwidth of the transducer becomes smaller if the transducer has the double function of transmitting and receiving: a 6 dB transducer beamwidth entails a 12 dB beamwidth for the complete system.

### **7.3 The ultrasound transducer in echo sounding systems**

There are various types of transducer that can be used in echo sounding systems. The flexure transducers described in Section 6.3.1 are preferred for long range applications, where frequencies below 50 kHz are employed.

The higher frequencies required for medium and short range echo sounding could be produced by long cylinders vibrating in the axial 33-mode. The vibrations of the end faces resemble those of a piston and the harmonics are well separated in frequency. However, for the frequency range in question, the radiating area of such transducers is small compared with the acoustic wavelength. This results in the directivity characteristic being almost spherical. Although this can be overcome by mounting several transducers in an array to give a narrower beam, the assembly is then inconvenient and cumbersome. Alternatively, one could use a disc whose diameter is large compared with its thickness and drive this at thickness resonance. This would also give a piston-like motion with adequate directivity and a good separation of harmonics, but to achieve a true thickness resonance in this frequency range, the diameter of the disc would be inconveniently large.

A much simpler, cheaper and more compact transducer may be made by using a disc whose thickness and diameter are comparable. This results in the resonance being rather complex, because there is now coupling between vibration in the radial and thickness directions and there are several resonances occurring in the required frequency range. However, one of these has some

resemblance to a true thickness mode and gives a good directive beam. The most effective thickness-to-diameter ratio for such a transducer is about 0,4. This gives a strong 'thickness type' resonance reasonably well separated from its neighbours. The frequency of this resonance is largely governed by the thickness of the disc, but the directivity is governed by its diameter, the variation of vibration amplitude across its surface and the working frequency. The admittance graph of Fig. 7.2 illustrates the case of a transducer designed to meet the present requirements and using a PXE41 disc 31,75 mm in diameter and approximately 14,3 mm thick. The fourth resonance, with  $f_s = 151$  kHz, is of the 'thickness type' and is well suited for transducer application because the electromechanical coupling factor is relatively large and the separation from the third and fifth resonance is quite adequate. Furthermore, the strong axial component of vibration gives good acoustic coupling to water and these disc dimensions give the required directivity characteristic.

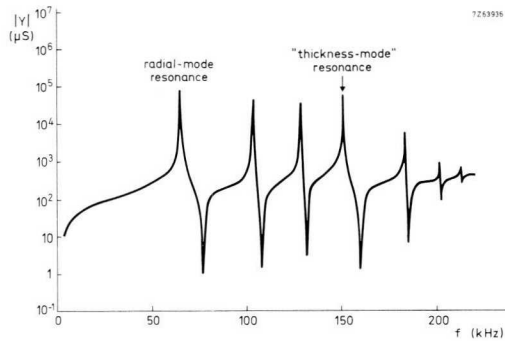


Fig. 7.2 Admittance  $Y$  of a thickness-mode resonator (PXE41 disc of 31,75 mm diameter, approx. 14,3 mm thick) as a function of frequency.

The transducer must be properly housed to ensure satisfactory functioning of the echo sounder. Fig. 7.3 shows a prototype transducer and housing. The PXE disc is mounted in a cup which is sealed with a suitable moulding compound. Since the transducer must be sensitive in the forward direction only, it would be useful if only the front face of the PXE disc were coupled to the water,

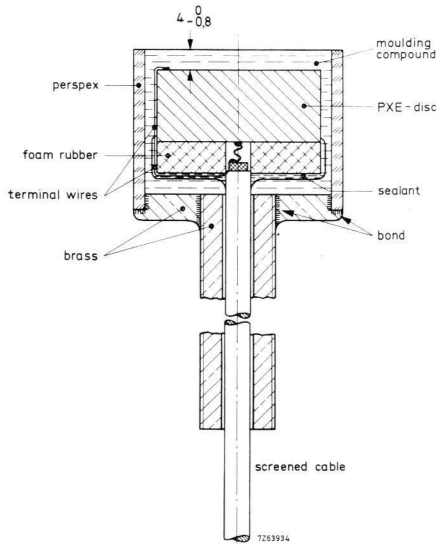


Fig. 7.3 PXE transducer for an echo sounder built into a housing (prototype: dimensions of the PXE disc, 31,75 mm diameter, 14,3 mm thick).

the other face and the cylindrical wall of the disc being isolated by air. However, it is found that such a design entails inadequate mechanical strength and that, owing to the low damping, the radial resonances can interfere with the operating resonance. In general therefore, only the back of the PXE disc is isolated, and not its cylindrical wall. An isolating medium often used is foam rubber which is acoustically equivalent to a layer of air.

The radiating face of the PXE transducer must be protected by an interface layer. Optimum results are obtained if the thickness of the protective layer equals  $\frac{1}{4}\lambda$ , where  $\lambda$  is the acoustic wavelength in the interface medium. The better acoustic matching thus obtained increases the bandwidth significantly. For best matching, the interface should have a specific acoustic impedance intermediate between those of PXE and sea water. Many synthetic materials, such as epoxy resins and other plastics, fall within this range. In most synthetic materials the propagation speed of sound is about  $2 \cdot 10^3$  m/s to  $3 \cdot 10^3$  m/s. For the required frequency range (150 kHz to 200 kHz) the optimum layer thickness is about 3 mm.

When selecting the moulding compound for the complete transducer (see Fig. 7.3) the following properties should be considered:

- low sound absorption;
- adhesive power and elasticity (protection against mechanical damage);
- tolerance of (sea) water and sunlight,
- smooth surface to reduce the growth of algae, and to facilitate cleaning.

A synthetic material is recommended for the housing for acoustic and economic reasons; metal housings involve resonance problems. However, a brass casting can be much stronger than synthetics.

#### 7.4 Electrical matching

The overall transducer impedance has a high capacitance content much of which is contributed by the long connecting lead. Good load matching and improved bandwidth are obtained by means of inductive tuning (see Appendix A).

A transducer is characterized by the following quantities:

- frequency (usually the series resonant frequency  $f_s$ );
- parallel inductance  $L_p$  (tuning);
- impedance of the tuned transducer  $|Z_s|$  at  $f_s$ ;
- 6 dB bandwidth,
- directivity characteristic.

Other important data are the minimum pulse duration that can be transmitted (which depends on the bandwidth), and the sensitivity, which is a function of the transducer parameters and the terminating impedance. The sensitivity can be derived from the response of the transducer to a fully reflected acoustic pulse at a measured distance.

With these data the behaviour of the transducer can be calculated fairly accurately. For close range ( $< 10$  m) the echo intensity depends almost solely on distance and the reflection coefficient of the sea bed. For greater distances the amount of ultrasound absorbed by the water must also be taken into account. At 151 kHz this is about 0,05 dB/m, or 10 dB when operating in a (sea) water depth of 100 m (total path length = 200 m).

## 7.5 Measurements on echo sounding transducers

### 7.5.1 IMPEDANCE AND BANDWIDTH

The compensating parallel inductance  $L_p$  must first be determined. This can be done by means of either the polar diagram (Fig. A.8, Appendix A), or by the admittance or impedance-frequency curve (Figs. A.2 and A.7, Appendix A). When properly compensated, the resonance loops in the polar diagram should be symmetrical about the real axis, and the admittance-frequency curve should be as symmetrical as possible about  $f_s$  in the vicinity of the resonance. The bandwidth and conductance at  $f_s$  are determined by further measurement.

### 7.5.2 SENSITIVITY

The sensitivity with pulse-echo operation can be expressed by the ratio between the voltage produced by the echo and the voltage applied to generate the ultrasound. Fig. 7.4 shows an arrangement for determining both sensitivity and

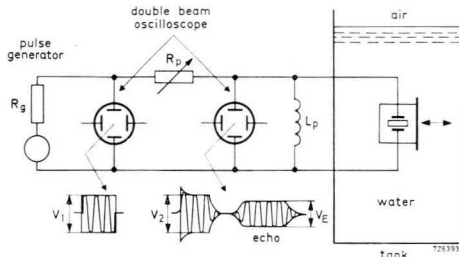


Fig. 7.4 Basic design of a sensitivity measuring instrument. Let the voltage drop across  $R_p$  be  $V_1 - V_2$  ( $R_g \ll R_p$ ). The frequency is adjusted to give the minimum value of  $V_2$  and the value of  $R_p$  is chosen so that  $V_2 = 0,5 V_1$ . The ratio  $V_E/V_2$  is a measure of sensitivity. ( $V_E$  is the echo voltage.)

pulse behaviour. The reflecting wall should be located in the far field of the transducer and the distance between wall and transducer should be greater than the minimum obtainable pulse length\*. All other reflecting surfaces, including the water surface, must be sufficiently distant to avoid spurious echoes

\* The far field of a transducer is the sound or ultrasound field at a distance greater than  $D^2/\lambda$ , where  $D$  is the transducer diameter. For a 32 mm diameter transducer working into sea water at 151 kHz, this is about 10 cm.

before the main reflected signal is received. There will then be no need to use an anechoic tank.

If such measurements are used to compare different transducers, it is best to work with power matching ( $R_p = |Z_s|$ ), although this is not always done in practice.

### 7.5.3 AUTOMATIC MEASUREMENT OF THE DIRECTIVITY CHARACTERISTICS

The arrangement of Fig. 7.4 can also be used for the simple measurement of directivity. The transducer is then simply mounted with an angle measuring device, and the 3 dB beamwidth in the pulse-echo mode may be determined directly.

The equipment described below produces a complete ultrasound directivity characteristic, and provides a particularly easy means of measuring and showing the ultrasound field produced by an echo sounder transducer. The block diagram of the equipment is shown in Fig. 7.5.

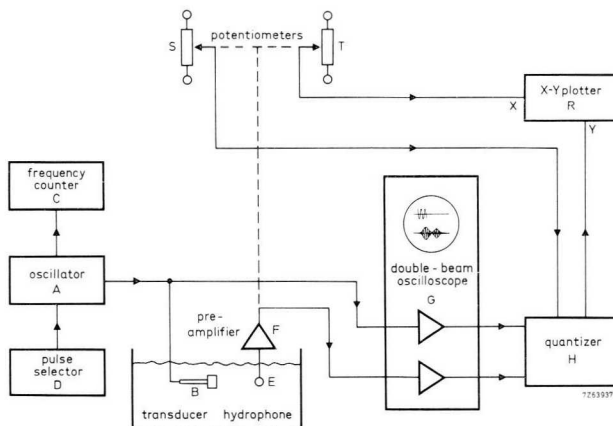


Fig. 7.5 Block diagram of an instrument for automatically recording the directivity characteristic of an ultrasound transducer.

A gated oscillator *A*, feeds the transducer under test *B* with a short tone burst at its working frequency, which is monitored by the frequency counter *C*. The oscillator is gated by the automatic pulse selector *D* which opens the oscillator's gate, counts the required number of complete cycles and then closes the gate. The time delay before this process is repeated (the repetition rate) is also adjustable; this allows all echoes to die away before another tone burst is transmitted.

The sound pressure wave generated by the transducer is detected by a small (3 mm diameter) piezoelectric hydrophone *E* and amplified by a FET pre-amplifier *F*. This received signal is displayed together with the transmitted tone burst, on a double-beam oscilloscope *G* which also acts as an amplifier to raise the signal to a level suitable for the quantizer *H*. The 5-channel latching quantizer is a parallel array of five level detectors. Each is followed by a flip-flop and a summing circuit to give an output proportional to the number of channels turned on. Each level detector can be set to trip when the signal level reaches a certain value. The flip-flops record that this level has (momentarily) been reached, and are not reset until the next transmitted tone burst. Thus the quantizer digitizes the analogue input into one of five discrete output voltage levels.

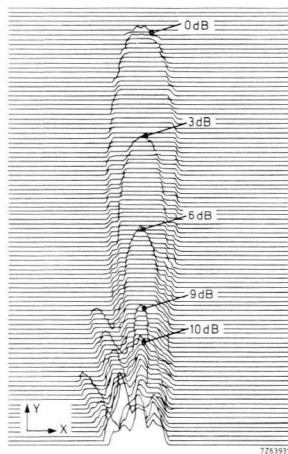


Fig. 7.6 Directivity characteristic of a transducer obtained with the equipment described in Section 7.5.3.

The hydrophone is fixed to a slider mounted on a gantry which bridges the water tank. An electric motor moves the slider back and forth by means of a chain drive. A 4-speed intermittent drive gear-box advances the gantry a short distance during part of each cycle. The pen of the XY-plotter  $R$  follows the zig-zag path of the hydrophone by means of a slide-wire potentiometer  $S$  with a wiper fixed to the slider (X-axis) and a 10-turn potentiometer  $T$  connected to one of the wheels of the gantry (Y-axis). A microswitch in the gear-box lifts the pen during the retrace while the gantry is traversing.

The quantizer output is superimposed on the Y-axis of the plotter to give a vertical pen displacement equal to the Y-axis spacing each time a quantizer trip level is exceeded. This produced the contour pattern shown in Fig. 7.6. By the appropriate setting of the quantizer trip levels, these contours can be set 3 dB apart. These lines then represent the 6 dB levels for the transducer when acting in its transmit/receive mode.

### 7.6 Performance data of a typical echo sounder transducer

The prototype transducer shown in Fig. 7.3 is equipped with a PXE41 disc 31,75 mm in diameter and 14,3 mm high. The technical data on the complete transducer are:

- |   |   |
|---|---|
| - operating frequency $f_s$                         | 151 kHz   |
| - capacitance of PXE disc (at 1 kHz)                | 640 pF  |
| - compensation inductance $L_p$                     | to tune with total<br>capacitance of disc plus cable<br>(see Section 7.5.1) |
| - impedance $ Z_s $ at $f_s$ (with $L_p$ )          | 1,3 k $\Omega$  |
| - 6 dB bandwidth (without load resistor)            | 15 kHz  |
| - 6 dB beamwidth - normal characteristic            | $\approx 19^\circ$  |
| - pulse-echo operation                              | $\approx 13^\circ$ } Fig. 7.7   |
| - sensitivity (reflection distance = 27 cm)         | $V_E/V_2 = 0,07$ (Fig. 7.4)   |
| - minimum pulse duration for the same<br>conditions | $80 \mu s \hat{=} 12 \text{ cm}$  |

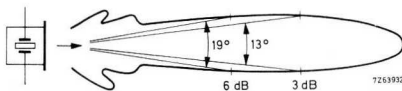


Fig. 7.7 Directivity characteristic of the transducer shown in Fig. 7.3.

### 7.7 Transmitter and receiver circuits for echo sounding systems

Apart from the transceiver transducer, simple echo sounding systems usually comprise three main parts:

- pulse generator and transmitter stage;
- receiver stage,
- indicating device.

The following sections deal with circuit designs for the first two parts which function satisfactorily under laboratory conditions, but can be improved by optimization and adapted to the indicating device. Since there are so many types of these devices, they cannot be discussed in detail here. The circuit designs are based on the following requirements:

- |                        |                    |
|------------------------|--------------------|
| - supply voltage       | 9 V                |
| - pulse power          | $\approx 1$ W      |
| - receiver sensitivity | $\approx 0,1$ mV   |
| - frequency range      | 150 kHz to 180 kHz |

With these requirements fulfilled, the circuits can be used for echo sounding over a range of about 50 m.

#### 7.7.1 TRANSMITTER STAGE

Fig. 7.8 shows the circuit diagram of the transmitter stage. It comprises a pulse generator, an oscillator and a power amplifier. The pulse generator  $TR_1$ - $TR_2$  is a multivibrator supplying pulses of about 250  $\mu$ s at intervals of about 17 ms. This corresponds to a pulse length of 40 cm in water and, depending on the pulse interval, a maximum range of about 12 m.

As it is difficult to increase the trigger ratio of 1 : 70 any further, longer ranges can only be realized at the expense of longer pulse intervals and, consequently, longer pulses; the result is reduced resolution. In that case the resistors and capacitors in the multivibrator must be given higher values.

For these reasons, it is usually better to use a different method of pulse generation. For instance, the pulses can be generated by means of a permanent magnet mounted on a rotating arm moving over a fixed coil. A neon lamp is

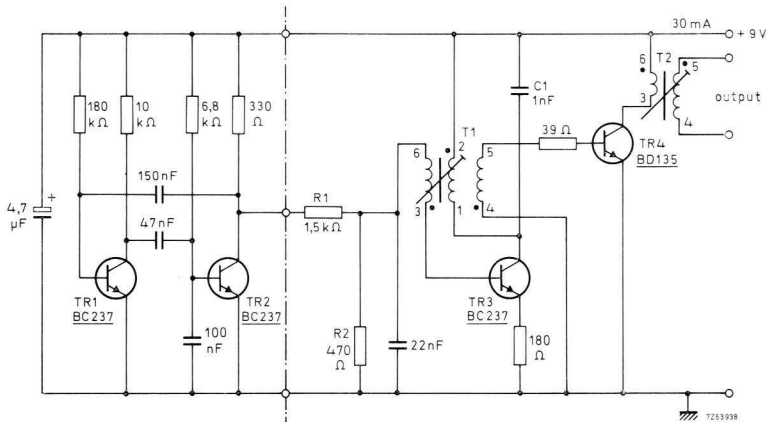


Fig. 7.8 Transmitter stage for an echo sounder.

Transformer: 2 Lilliput coil assemblies (for type numbers see Fig. 6.13);

windings:

$N_1, 3-6$	30 turns	}	of 0,08 mm diameter lacquered Cu wire;
$N_1, 2-1$	200 turns		
$N_1, 4-5$	70 turns		
$N_2, 6-3$	22 turns	}	of 12 by 0,03 mm diameter stranded Cu wire.
$N_2, 5-4$	177 turns		

mounted on the same arm and serves as the indicator which lights up each time the receiver stage detects a pulse. The position of the neon lamp when this takes place is a measure of the delay between the transmitted and received pulses, and thus a measure of the distance of the reflecting object.

It is also possible to generate the next transmitted pulse immediately after an echo pulse is received (the so-called 'sing-around' method). The repetition frequency is then a measure of range. In this case the multivibrator is eliminated and a voltage of about 3 V across  $R_1$  or 1,5 V across  $R_2$  is required to trigger the oscillator  $T_1$  and  $TR_3$ .

The oscillator has been designed to operate at 160 kHz and can be used for the frequency range of 150 kHz to 180 kHz by inductance adjustment. The frequency range itself can be shifted by altering  $C_1$  or  $T_1$ .

The power of the output stage is 1 W to 1,5 W if the output transformer  $T_2$  is properly matched to the sound transducer. This matching depends on the transformation ratio of  $T_2$  and the impedance  $|Z_s|$  of the transducer. At the same time the transformer provides the compensating inductance  $L_p$ , which is roughly determined by the number of turns  $N_{2, 5-4}$ . The values given in the caption of Fig. 7.8 are related to  $|Z_s|$  at 1,3 k $\Omega$  and  $L_p$  at 0,8 mH. The same circuit can be used in conjunction with the transducer described in Section 7.6. For other requirements the numbers of turns of  $T_2$  are calculated as:

$$N_{2, 5-4} = 198\sqrt{L_p} \quad (L_p \text{ in mH});$$

$$N_{2, 6-3} = N_{2, 5-4} \sqrt{20/|Z_s|} \quad (|Z_s| \text{ in } \Omega).$$

The inductances of  $T_1$  can be varied  $\pm 25\%$ .

### 7.7.2 RECEIVER STAGE

Fig. 7.9 shows the circuit diagram of a receiver amplifier consisting of two h.f. amplifier stages,  $TR_1$  and  $TR_5$ , a detector  $D_3$ , a pulse amplifier stage  $TR_6$  and a circuit with which the gain of the first stage can be made time variable  $TR_2$ - $TR_3$ - $TR_4$ .

Such a time-dependent gain control is of particular importance if the echo is not displayed by an analogue indicator, such as a rotating lamp, but by a time interval measuring system. Without further precaution, the echo sounder would be more susceptible to spurious echoes from sea weed and shoals of fish. These echoes are relatively weak, but they may resemble in strength, though not in time delay, echoes from greater depths. With time-dependent amplification it is easier to separate and recognize the different echoes.

The gain control functions as follows. A positive pulse on the base of  $TR_4$ , synchronized with the transmitter pulse, causes  $C_2$  to charge and this leads to a reduction in the gain of stage  $TR_1$ . Capacitor  $C_2$  now discharges and the gain rises accordingly until the next positive pulse is received, when the whole process is repeated. By suitable adjustment of  $R_3$ , the amplitude of the received echoes at the output of the stage can be made more or less independent of water depth, but it still depends on the reflection coefficient. This helps one to distinguish between echoes from the sea bed and from intervening objects. A trigger pulse



synchronized with the transmitter pulse can be obtained from the collector of  $TR_2$  in the circuit shown in Fig. 7.8. If a negative pulse is available, the base of  $TR_3$  can be driven directly ( $TR_4$  and  $R_4$  are then not needed). After setting up the stage, the maximum sensitivity is about 0,1 mV at input 1.

The gain control circuit is not absolutely necessary for analogue display: the control circuit ( $TR_2$ - $TR_3$ - $TR_4$ ) can be separated at the three points *a* indicated in Fig. 7.9. It is then recommended that a 4,7 k $\Omega$  potentiometer be connected between the emitter of  $TR_1$  and  $R_2$ - $C_1$  for gain control.

Diodes  $D_1$  and  $D_2$  are included to limit the direct transmitter signal, which of course also appears at input 1. Thus it is not necessary to switch the transducer electronically between transmitter and receiver. Potentiometer  $R_6$  serves to adjust the threshold voltage of  $TR_6$ . Both *LC* circuits are designed for 160 kHz (150 kHz to 180 kHz), and can be tuned to other frequencies by making minor changes (other capacitance values, for example).

The 6 dB bandwidth of the h.f. amplifier is about 20 kHz, so that only pulses of a duration of at least 70  $\mu$ s will be fully amplified. The *RC* circuit of  $R_5$ - $C_3$  ensures that only the leading edge of pulses exceeding about 150  $\mu$ s will produce an output signal.

## 8 PXE high intensity transducers

### 8.1 General

Most high intensity ultrasound applications, such as ultrasonic cleaning, require half wavelength transducers with resonant frequencies between 18 kHz and 45 kHz. The physical dimension in the main excursion direction of a single-piece PXE4 transducer with sound velocity of approximately 3200 m/s would range accordingly from 9 cm to 3,5 cm. Furthermore, the power specifications would usually necessitate such large lateral dimensions that the ultimate size of the single-piece ceramic blocks would present enormous manufacturing problems. Finally, such blocks might be relatively inefficient, because the *whole* transducer volume would dissipate vibrational energy at a rate inversely proportional to the mechanical quality factor of the piezoelectric ceramic, which usually lies below that of metals.

The alternating driving force of the PXE ceramic is only really efficient in the centre of the half-wavelength transducer where the stress amplitude  $T_c$  reaches a maximum, the two end portions acting mainly as inert masses. Consequently, these end portions may conveniently be replaced by less expensive non-piezoelectric (usually metallic) portions with much higher mechanical quality factors. This construction is known as a composite, or sandwich, transducer (see Section 8.2).

With high intensity transducers the overall electroacoustic efficiency  $\eta$  is of particular interest. In cases of practical importance  $\eta$  is given, to a good approximation, by

$$\eta \approx 1 - \frac{1}{k_{eff}^2 Q_e Q_L} - \frac{Q_L}{Q_{m0}}, \quad (8.1)$$

dielectric                      mechanical  
losses                              losses

assuming  $k_{eff} \sqrt{Q_e Q_{m0}} \gg 1$  and  $Q_L \leq 0,1 Q_{m0}$ . In eq. 8.1  $Q_{m0}$  is the mechanical quality factor of the transducer without an acoustic load, and  $Q_e$  is the electrical quality factor, which is the reciprocal of the dielectric loss factor  $\tan \delta$ . The term  $Q_L$  is the mechanical quality factor due to the acoustic load alone.

It is the transducer  $Q$  which would be measured if  $Q_e = Q_{m0} = \infty$ , and in this case  $\eta$  would always be 1 (for any  $Q_L$ ). With a small acoustic load  $Q_L$  is high, and vice versa. When

$$Q_L = \frac{1}{k_{eff}} \sqrt{\frac{Q_{m0}}{Q_e}} = Q_{L \text{ opt}}, \quad (8.2)$$

$\eta$  reaches a maximum:

$$\eta_{\max} = 1 - \frac{2}{k_{eff} \sqrt{Q_e Q_{m0}}}. \quad (8.3)$$

If  $Q_L$  is small compared with  $Q_{L \text{ opt}}$ , the second term of eq. 8.1 (mechanical losses) can be ignored: in the opposite case the first term can, possibly, be ignored. It should also be borne in mind that the dielectric and mechanical losses depend on the electric field strength and the mechanical excursion, respectively. At high drive levels  $Q_e$  and  $Q_{m0}$  can no longer be treated as constants, and they are often much lower than the low signal values.

## 8.2 Advantages of composite transducers

The overall mechanical quality factor  $Q_{m0}$  (no-load condition) of composite transducers is somewhat higher than that of single-piece transducers and, owing to better heat removal, the temperature in the ceramic components is lower. Therefore, as eq. 8.1 indicates, the overall electroacoustic efficiency  $\eta$  can be made higher.

Another reason why the efficiency of composite transducers is so high is that their piezoelectric coupling coefficient  $k_{eff}$  is not necessarily much lower than that of single-piece transducers. This is illustrated in Fig. 8.1 where the end portions 1 and 2, with lengths  $l_1 = l_2$ , have the same acoustic properties and cross-sectional area as the central ceramic portions. In such a case the excursion amplitudes  $u$  of the end faces 1 and 2 are equal ( $u_1 = u_2$ ) as are their velocity amplitudes  $\omega_s u$ . Consequently, the maximum attainable velocity amplitudes  $(\omega_s u)_{\max}$  at the end faces are related to the permissible stress amplitude in the central nodal plane  $T_{c \text{ max}}$  according to the relation:

$$(\omega_s u_1)_{\max} = (\omega_s u_2)_{\max} = \frac{T_{c \text{ max}}}{Q_{mc} v_c} \text{ (m/s)}, \quad (8.4)$$

where  $Q_{mc}$  is the density of the ceramic material and  $v_c$  is the sound velocity in this material.

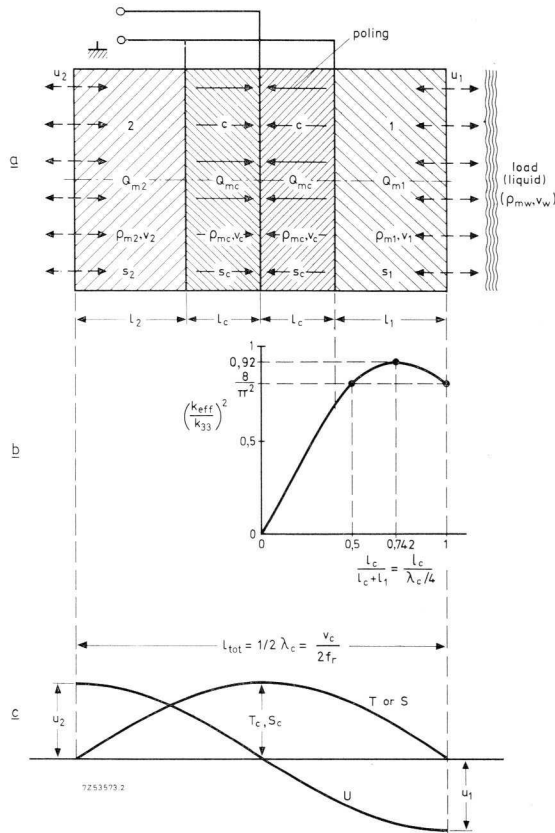


Fig. 8.1 (a) A composite half-wavelength cylindrical transducer consisting of four portions with equal cross-sectional areas  $A$  and equal acoustic properties. The curves (b) and (c) are valid only if  $s_2 = s_c = s_1$ ;  $Q_{m1} = Q_{mc} = Q_{m2}$ ;  $v_2 = v_c = v_1$ , and  $l_2 = l_1$ . The numbers 1 and 2 refer to the end portions,  $c$  to the ceramic middle portion.

If end face 1 is loaded with a liquid  $w$  (density  $\rho_{mw}$  and sound velocity  $v_w$ ), and is assumed to launch perfectly planar waves into the liquid, eq. 8.4 is also valid for the particle velocity amplitude inside the liquid near radiating face 1, so that the maximum attainable ultrasound intensity in the liquid  $I_{w \max}$  may be evaluated by inserting eq. 8.4 into the basic equation:

$$I_{w \max} = \frac{1}{2}(\omega_s u_1)^2_{\max} \rho_{mw} v_w \quad (\text{W/m}^2). \quad (8.5)$$

If the end portions 1 and 2 have equal length and acoustic characteristics, the important fractional bandwidths ( $B_F$ ) of such a simple composite transducer are:

$$\text{coil tuned} \quad B_{F \text{ em}} \approx \frac{k_{eff}}{(1 - k_{eff}^2)^{\frac{1}{2}}}; \quad (8.6)$$

$$\text{single load} \quad B_{F \text{ m}} = \frac{1}{Q_{m0}} + \frac{2\rho_{mw}v_w}{\pi\rho_{mc}v_c}, \quad (8.7)$$

$$\text{double load} \quad B_{F \text{ m}} = \frac{1}{Q_{m0}} + \frac{2}{\pi} \cdot \frac{(\rho_{mw}v_w)_1 + (\rho_{mw}v_w)_2}{\rho_{mc}v_c}. \quad (8.8)$$

In many cases the industrial application, or the laboratory experiment, requires much higher values of  $I_{w \max}$  and  $B_{Fm}$  than those offered by the simple composite half-wavelength transducers discussed so far. In the next section we discuss how these parameters can be improved in such transducers.

### 8.3 Improving radiation intensity and bandwidth by means of different end sections

If an arbitrary material is used for each end portion while the bond plane between the ceramic central portions is maintained as the nodal plane where the stress amplitude reaches a maximum of  $T_c \leq T_{c \max}$ , the simple amplitude and frequency relations of Section 8.2 and Fig. 8.1 are no longer valid. The new equations can be conveniently expressed in terms of two numerical parameters  $q_i$  and  $G_i$  ( $i$  is either end portion 1 or 2):

$$q_i = \frac{\rho_{mc}v_c A_c}{\rho_{mi}v_i A_i}, \quad (8.9)$$

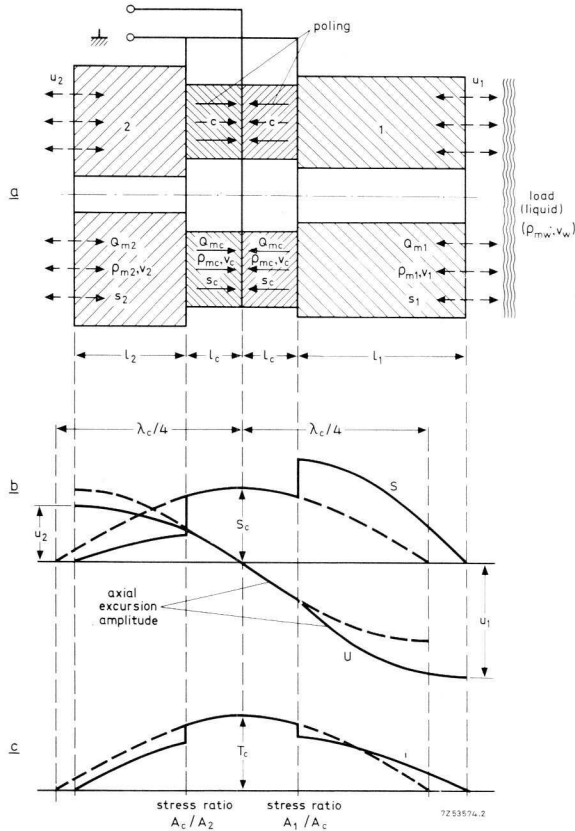


Fig. 8.2 (a) A composite half-wavelength transducer consisting of four portions. The cross-sectional areas  $A$  of the two ceramic middle portions are equal, but differ from the areas of either end portion. The same applies to the acoustic properties. The curves (b) and (c) are valid only if  $Q_{m2}v_2 > Q_{mc}v_c > Q_{m1}v_1$ ;  $s_2 < s_c < s_1$  and  $A_2 > A_c < A_1$  (when using the materials steel-PXE4-magnesium, for instance).

where  $q_i$  is the ratio of the characteristic acoustic impedances ( $Qv$  multiplied by cross-sectional area  $A$ ) of the central and end portions, with cross-sectional areas  $A_c$  and  $A_i$  respectively. In practice,  $A_i \geq A_c$  (Fig. 8.2), and

$$G_i = q_i^2 - (q_i^2 - 1) \sin^2 \frac{\omega_s l_c}{v_c}, \quad (8.10)$$

where  $G_i$  is the coefficient of gain in ultrasound intensity at the end faces relative to a homogeneous transducer (Fig. 8.1), or for the gain in excursion squared, the stress amplitude at the centre,  $T_c$ , remaining constant.

Both  $q_i$  and  $G_i$  are unity for the simple composite transducer discussed so far, but they are greater (less) than unity for up (down) transforming end portions. Obviously  $G_i$  ranges between  $q_i^2$  and unity, and increases as the specific acoustic impedance  $\rho_{mi}v_i$  decreases.

Using the above variables and assuming a load on both end faces one may write (cf. eqs. 8.4, 8.5 and 8.8):

$$I_{wi \max} = \frac{1}{2} G_i \left( \frac{T_c \max}{\rho_{mc} v_c} \right)^2 (\rho_{mw} v_w)_i \quad (\text{W/m}^2) \quad (8.11)$$

$$B_{Fm} \approx \frac{1}{Q_{m0}} + \frac{2}{\pi} \cdot \frac{G_1 (\rho_{mw} v_w)_1 + G_2 (\rho_{mw} v_w)_2}{\rho_{mc} v_c} \quad (8.12)$$

The following resonant condition should be satisfied:

$$\tan \frac{\omega_s l_i}{v_i} \cdot \tan \frac{\omega_s l_c}{v_c} = q_i \quad (8.13)$$

Here both angles  $\omega l/v$  have values between 0 and  $\pi/2$  radians and can be conveniently represented in a diagram using  $q_i$  as a parameter. An even clearer diagram is obtained if the angles are multiplied by  $2/\pi$ , so that fractional lengths act as an ordinate and an abscissa, viz:

$$\frac{2}{\pi} \cdot \frac{\omega_s l_i}{v_i} = \frac{l_i}{\lambda_i/4}, \text{ and } \frac{2}{\pi} \cdot \frac{\omega_s l_c}{v_c} = \frac{l_c}{\lambda_c/4} \quad (8.14)$$

A family of  $l_i/(\lambda_i/4)$  versus  $l_c/(\lambda_c/4)$  curves for  $q_i$  values in the useful range of 0,4 to 4,0 is shown in Fig. 8.3(a). All the corresponding  $G_i$  versus  $l_c/(\lambda_c/4)$  curves are drawn in Fig. 8.3(b).

These curves are very useful to the engineer for working out the first concept of a high intensity transducer as they provide a short-cut through the detailed calculations required for final design. It should be borne in mind that such detailed calculations require an appropriate choice of the material constants  $v_i$  and  $v_c$  (or  $\lambda_i$  and  $\lambda_c$ ). For instance, if diameter  $D$  of a mechanical transmission

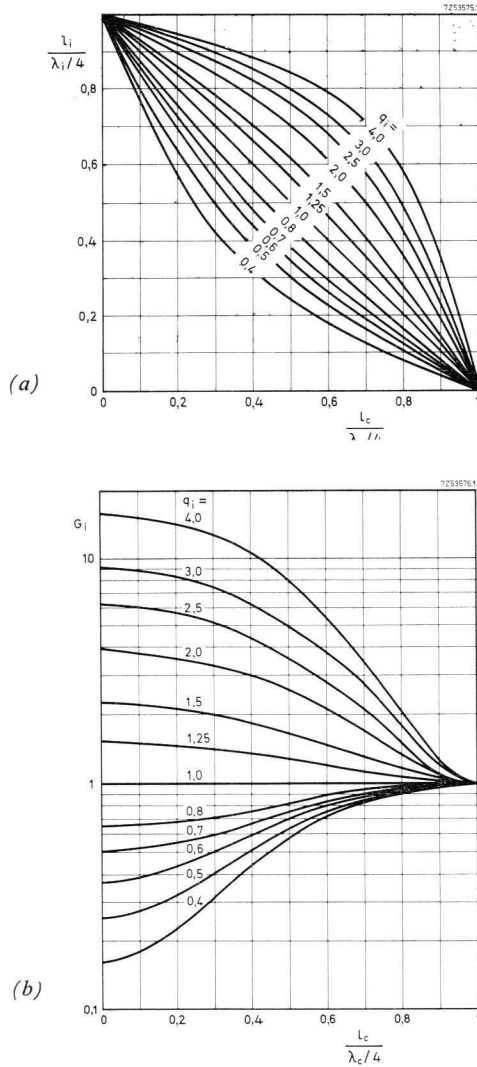


Fig. 8.3 (a) Required length  $l_i$  of the end portion of material  $i$  as a function of the operating frequency ( $\omega_s \approx 1/\lambda_c$ ) for a given pair of central ceramic driving rings (discs) of axial thickness  $l_c$ .

(b) Ultrasound intensity gain  $G_i$  as a function of the operating frequency ( $\omega_s \approx 1/\lambda_c$ ) for a given pair of ceramic driving rings (discs) of axial thickness  $l_c$ .

line increases to such an extent that the  $D$ -to- $\lambda/4$  ratio changes from unity to two, the effective phase velocity of extensional waves of the first mode already falls considerably below:

$$v_{\text{bar}} = \frac{1}{sQ_m}, \quad (8.15)$$

commonly called the 'thin wire value'.

The correction needed on the value of  $v_{\text{bar}}$  depends on the value of Poisson's ratio of lateral contraction  $\sigma$ . Fig. 8.4 represents the phase velocity of extensional waves in cylindrical bars in terms of  $v_{\text{bar}}$  for materials with  $\sigma = 0,29$ .

Table 8.I contains numerical data on  $v_{\text{bar}}$  and other important properties of some materials that are of prime importance for high intensity transducers, either for high intensity end 1 ( $G_1 > 1$ ) or for end 2 whose intensity is usually

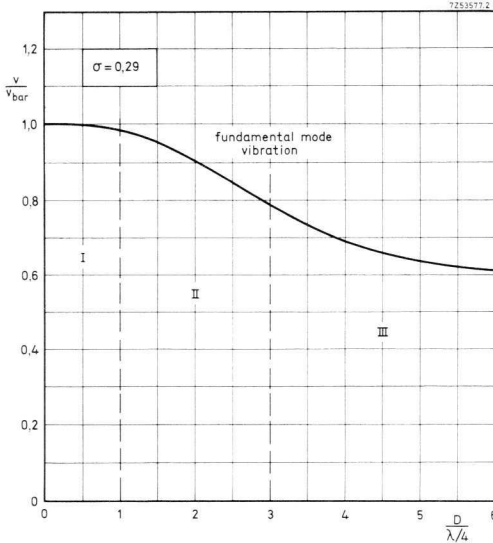


Fig. 8.4 Normalized phase velocity of extensional waves in round bars (diameter  $D$ ) for materials with a Poisson ratio  $\sigma = 0,29$ . In region I the excursion of the whole radiating faces is almost uniform. In region II the radiating faces show no circle of zero axial amplitude (nodal circle), but in region III there is one such circle.

Table 8.1. Physical properties of materials for high-intensity transducers.

quantity	unit	materials for the moderate-intensity end portion 2		ceramic central portion c			materials for the high-intensity end portion 1			
		tool steel	aluminum bronze (1)	naval brass (2)	PXE4	PXE41	PXE42	titanium alloy (3)	duralumin (4)	magnesium alloy (5)
$\rho_m$	$10^3 \text{ kg/m}^3$	7,85	8,50	8,37	7,50	7,90	7,80	4,42	2,79	1,74
$\nu_{bar}$	m/s	52,50	40,70	33,20	32,20 (6)	29,15 (6)	28,50 (6)	4900	5130	4800
$\rho_m \nu_{bar}$	$10^6 \text{ kg/m}^2\text{s}$	41,2	34,6	27,8	24,0	23,0	22,3	21,7	14,3	8,35
s	$10^{-12} \text{ m}^2/\text{N}$	4,6	7,0	10,8	13,5 (7)	14,6 (7)	15,5 (7)	9,4	13,5	23,8
$\sigma$		0,29		0,35	$\approx 0,30$ (8)	$\approx 0,30$ (8)	$\approx 0,30$ (8)	0,36	0,34	0,28
$\Delta l/\Delta T$	$10^{-6}/^\circ\text{C}$	14	19	19	2,5	1,5	1,7	9	23	26
$Q_m^{(9)}$		$\approx 1400$	$\approx 17000$	$\approx 3000$	$\approx 500$ (10)	$\approx 1000$ (10)	$\approx 750$ (10)	$\geq 2400$	$\approx 50000$	
$T_f$	$10^6 \text{ Pa}$	550	370	150				720	190	123
$S_f$	$10^{-3}$	2,52	2,59	1,69				6,80	2,57	2,93

(1) Langley-Hidurax Special.

(2) Naval brass BS 251 (right-hand-side data).

(3) Titanium ICI 318A with composition 90% Ti, 6% Al, and 4% V.

(4) Duralumin BS L 65 fully heat treated.

(5) Magnesium alloy AZ61 with composition 93% Mg, 6% Al, and 1% Zn.

(6)  $\nu_3^E = 2N_3^E$ .

(7)  $s_{33}^E$ .

(8)  $\sigma_{31}$ .

(9) Mechanical quality factors at approximately half the fatigue strength; the symbol  $\approx$  stands for lower intensities. See also Section 8.4.

(10)  $Q_m^E$ .

reduced ( $G_2 < 1$ ) to have it radiate much less power when submerged together with active end 1. The fatigue strength  $T_f$  and the maximum strain  $S_f$  are also given. These are particularly important data if a bolt of one of the indicated metals is used for pre-stressing the transducer.

Combining the numerical data of Table 8.I and the graphical data of Figs. 8.2, 8.3 and 8.4, one readily comes to the following conclusions:

- The combination of steel-PXE-magnesium is very favourable; the cheaper combination of steel-PXE-aluminium (duralumin) is also favourable but to a lesser extent. Aluminium (and magnesium) end portions can be upgraded by drilling holes or cutting slots in them.
- PXE has a relatively low sound velocity. Consequently, the ratio of diameter-to-quarter-wavelength readily exceeds unity in 40 kHz to 50 kHz applications of the available PXE discs or rings. It is necessary, therefore, to take a correction factor into account when determining the actual sound velocity, see Fig. 8.4, for instance.
- When the diameter of a half-wave resonator is comparable to, or greater than, its length then 'lateral' or radial mode resonances are possible which may (depending on the diameter-to-thickness ratio) be close to, or lower, in frequency than the fundamental thickness mode. Thus it is generally best to have  $D < \lambda/2$  where possible with this type of transducer.

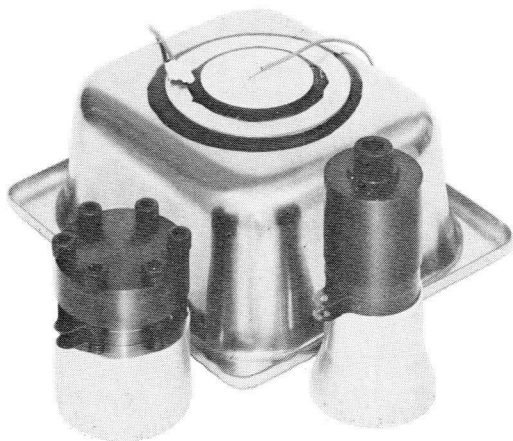


Fig. 8.5 Some high-intensity ultrasound transducers for cleaning applications. (See also Figs. 8.8, 8.9 and 8.10.)

- According to Fig. 8.3(b) the highest intensity gain  $G_1$  and the highest  $G_1/G_2$  ratio (which may be of interest in totally immersed transducers) are obtained if the wavelength in the ceramic material is greater than 20 or 30 times the thickness of the ceramic disc or ring. In other words, the lowest possible resonant frequency should be chosen. However, there are two factors opposing the use of extremely low operating frequencies for a given pair of PXE discs (diameter  $D_c$ , axial length  $l_c = 6,35$  mm).

1. The effective piezoelectric coupling factor becomes too low. Although the low-intensity end portion with  $q_i < 1$  slightly improves coupling, the high-intensity end portion with  $q_i > 1$  reduces coupling, so that the total coupling does not differ much from that of a composite transducer with  $q_i = 1$  (see Figs. 8.6(a) and 8.1(b)). According to these curves we may write:

$$k_{eff} \leq 0,5k_{33} \text{ for } \lambda_c \geq 25l_c,$$

i.e., for  $f_s \leq 20$  kHz (for discs with  $l_c = 6,35$  mm).

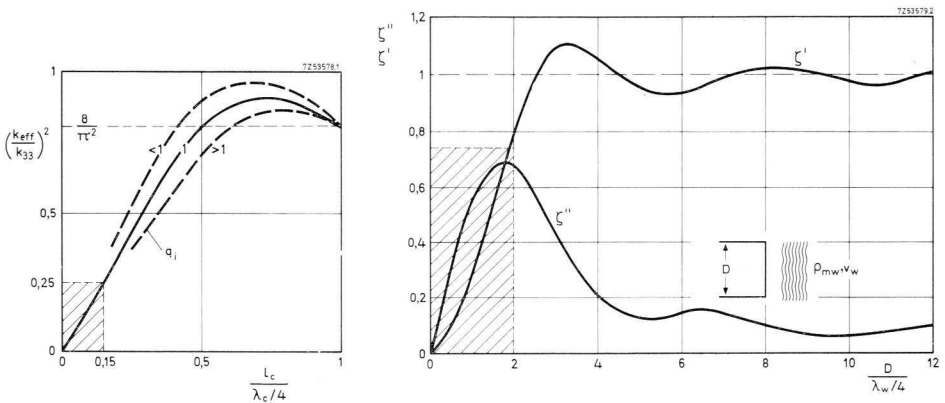


Fig. 8.6 (a) Relationship between the effective coupling coefficient and the thickness  $l_c$  of the PXE rings or discs (for determining the minimum required length  $l_c$ ). The shaded area shows the range in which  $k_{eff} \leq 0,5 k_{33}$ ,  $f_s \leq 20$  kHz for  $l_c = 6,35$  mm.

(b) Relationship between the factors  $\zeta'$  and  $\zeta''$  ( $\zeta = \zeta' + j\zeta''$ ) and the diameters  $D_1$  and  $D_2$  of the radiating faces 1 and 2. The shaded area shows the range in which the real part of the radiation coefficient becomes unacceptably low.

2. The ultrasound intensity in the liquid  $w$  near radiating surface 1 is no longer given by eqs. 8.5 and 8.11 which only hold for planar waves in the liquid. At low frequencies the radiated waves are no longer planar. If this effect is to be taken into account, the right-hand terms of eqs. 8.5 and 8.11 must be multiplied by the real part of a radiation coefficient. This coefficient is plotted in Fig. 8.6(b) as a function of the diameter-to-wavelength ratio (in water). It is clear that at low frequencies radiation drops more than linearly with the frequency, which is indeed a severe limitation. A moderate fall in  $\zeta'$  may be welcomed however, as it is accompanied by less beaming. Therefore allowing a minimum  $\zeta'$  of approximately 0,75, the minimum diameter of the radiating face would be approximately half a wavelength in the liquid load.

A considerable effective mass is added to the transducer in the form of the liquid load, so that the transducer is considerably mismatched (see curve  $\zeta''$  in Fig. 8.6(b)). This mismatching can usually be allowed for in the electronic design. Thus, in the case of a single pair of PXE rings 6,35 mm thick and with  $D_c = 38,1$  mm, and an aluminium or magnesium end portion with a diameter  $D_1$  only slightly larger, the minimum operating frequency is 20 kHz. The same minimum frequency is also derived from coupling factor considerations. For frequencies below 20 kHz, the effective coupling factor can be improved by using more than one pair of rings.

#### 8.4 Performance of non-pre-stressed composite transducers

It has been mentioned in Sections 8.2 and 8.3 that the maximum radiation intensity is proportional to the square of  $T_{c \max}$ . This symbol stands for the maximum permissible dynamic tensile stress amplitude, hence, for a safety factor  $\beta$  times the fatigue strength  $T_f$  of the material present at or near the nodal plane where the stress amplitude reaches a maximum (see Fig. 8.7(a)). Consequently, the fatigue strength of both the piezoelectric ceramic ( $T_{fc}$ ) and the bond material ( $T_{fb}$ ) should be considered:

$$\beta \cdot T_{fc} \geq T_{c \max} \leq \beta \cdot T_{fb}$$

Approximate data on fatigue strength under conditions of negligibly small thermal stresses are given in Table 8.II.

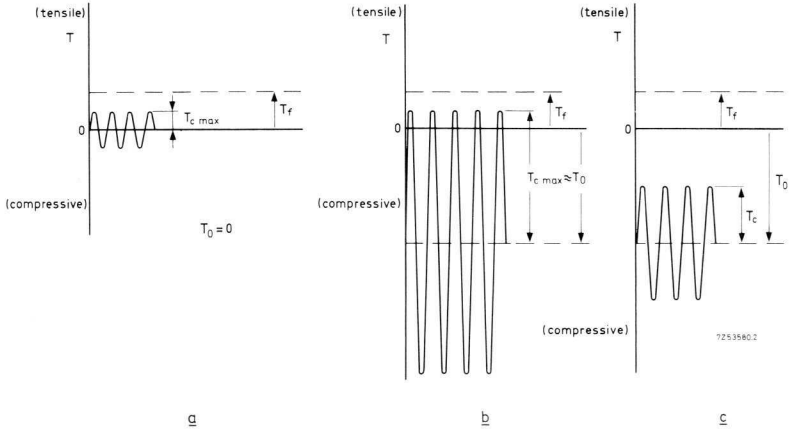


Fig. 8.7 Fatigue strength  $T_f$ , pre-stress  $T_0$  and maximum permissible stress amplitude  $T_{c \max}$  in the centre of the transducer.

- (a) without pre-stress,  $T_{c \max}$  small ( $T_c$  limited by fatigue strength of ceramic or bonds);  
 (b) with pre-stress,  $T_{c \max} \approx T_0$  ( $T_c$  limited by fatigue strength of bolts),  
 (c) with pre-stress,  $T_{c \max} < T_0$  ( $T_c$  limited by losses).

Table 8.II. Fatigue strength amplitudes at ultrasonic frequencies.

material		fatigue strength $10^6 \text{ Pa}$ ( $\approx 10 \text{ kg/cm}^2$ )
piezoelectric ceramic (PXE4)		25
hot-set epoxy cement (Araldite)	fresh	40
	aged*	25
cold-set epoxy cement (Araldite)	fresh	25
	aged*	15

\* Shelf-aging under normal humid conditions. Aging in dry atmosphere would not reduce the fatigue strength significantly.

Sometimes the critical stress amplitudes, or fatigue strengths tabulated in Table 8.II, are not very reliable as they may be drastically reduced by static thermal stresses resulting from the considerable differential thermal expansion of the cemented parts. When cementing aluminium or magnesium to PXE4 (according to Table 8.II), a differential thermal strain of 20 or more p.p.m./°C is to be expected, so that the curing of epoxy cement at, say, 150 °C, would lead to differential thermal radial stresses of approximately  $50 \cdot 10^6$  Pa to  $150 \cdot 10^6$  Pa. In other words, the surface layer of a large ceramic disc would be severely pre-stressed in the radial direction with the correct sign but in an uncontrolled, inhomogeneous way. Considering such ill-defined conditions, which also exist when the transducer is dissipating considerable energy at high intensities, and allowing for a safety factor  $\beta = 0,5$ , the resulting critical stress amplitude in the frequency range 20 kHz to 50 kHz would be no more than:

$$T_{c \max} \approx 4 \cdot 10^6 \text{ Pa (or } 10 \text{ kg/cm}^2\text{)}.$$

Substituting this into eq. 8.5, and assuming a watery load  $\rho_{mw}v_w = 1,485 \cdot 10^6$  kg/m<sup>2</sup>s, we find for the attainable intensity:

$$I_{wi \max} \approx 2G_i \text{ (W/cm}^2\text{)}.$$

The gain factor for normal proportions may be derived from Table 8.II and Fig. 8.3(b) and this gives

$$I_{wi \max} \approx 10 \text{ W/cm}^2$$

(magnesium end portion with a gain  $G$  of approximately 5),

$$I_{wi \max} \approx 4 \text{ W/cm}^2$$

(duralumin end with a gain  $G$  of approximately 2).

### 8.5 Pre-stressed composite transducers (with applications)

As already explained, it has been found useful to assemble high-power ultrasound transducers from thin rings or discs of PXE material with metal end pieces to match. For many types of transducer used for ultrasonic cleaning, the

power requirements are often so severe that the tensile strength of the ceramic material cannot take the high mechanical stress involved. This can be remedied by mechanically pre-stressing such transducers in the axial direction by means of one or more bolts, the useful amount of pre-stress  $T_0$  being about  $25 \cdot 10^6$  Pa ( $\approx 250$  kg/cm<sup>2</sup>). Under these conditions  $T_0$  replaces  $T_{c \max}$  in the intensity equation (eq. 8.11), as is illustrated in Fig. 8.7(b). In continuous operation one is usually limited in practice to lower stresses by overheating due to electrical and mechanical losses so that, in this case, the situation is as in Fig. 8.7(c). A compromise between efficiency and intensity must be accepted.

Mechanical pre-stress causes significant (more or less) reversible changes of all the dielectric, electromechanical and mechanical properties of piezoelectric ceramics with high coupling coefficients. Too high a pre-stress may cause the bolt to break and could also cause considerable irreversible changes in the properties of the ceramic material (depolarization). Thus repeated application and removal of the same mechanical pre-stress could cause the relationship between capacitance and stress, or between coupling factor and stress, to vary in an irreproducible manner. However, provided that the pre-stress is kept below about  $30 \cdot 10^6$  Pa, the variations are reasonably reproducible. Too low a pre-stress reduces efficiency because there is an increase in mechanical loss at the various interfaces.

#### 8.5.1 CONSTRUCTION OF TWO HIGH INTENSITY TRANSDUCERS

Figs 8.8 and 8.9 show two designs of high intensity transducers that have been thoroughly tested. Both of them can be built around PXE4 or PXE41. The most important data are presented in Table 8.III. The design shown in Fig. 8.8 consists of two PXE rings (in the centre) clamped between two end portions by means of a bolt. The bolt is insulated from the centre electrode by means of a thin PVC sleeve. A transducer thus constructed has a slightly higher efficiency than the one where the centre bolt is replaced by six or eight bolts around the circumference of the transducer (Fig. 8.9) because the centre bolt construction allows a more uniform and radially symmetric application of pre-stress to the PXE. However, the centre bolt assembly with its conical front portion may be more costly to produce, and its greater length may be a disadvantage where space is important.

If the transducer is bonded to the cleaning tank (usually of stainless steel), the temperature necessary to harden the glue may be high enough to impair the properties of the PXE rings or discs. It is, therefore, often recommended that the front block of the transducer is first bonded to the tank wall, and that assembly is completed after the bonding agent has had sufficient time to harden and cool. If the torque required for tightening the bolt is not taken up by a holding tool applied to the coupling portion, there is a risk that the bonded joint to the tank will be broken. The main advantage of the transducer of Fig. 8.9 (with bolts around the circumference) lies in its compactness, as well as in the possibility of first bonding the front portion to the tank and then assembling the transducer. The bolts can be tightened without overloading the bond because the torque for any one of the bolts is substantially lower than required for the one large bolt in the transducer of Fig. 8.8. A special holding tool is then not needed.

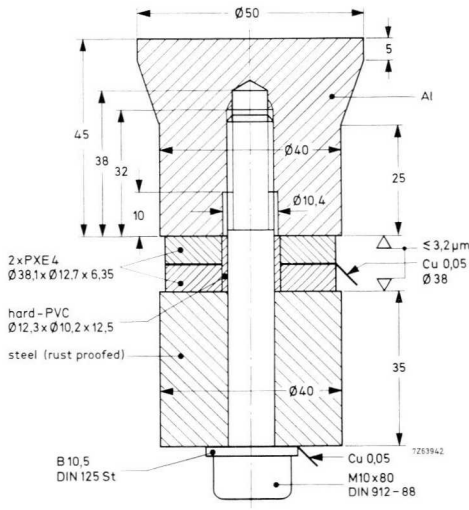


Fig. 8.8 Composite mechanically pre-stressed transducer with a low-intensity and a high-intensity end. The pre-stress is provided by means of a high-tensile centre bolt.

The PXE components used for the transducers shown in Figs 8.8 and 8.9 consist of two rings (outside diameter 38,1 mm, inside diameter 12,7 mm and 6,35 mm thick) or two discs (38,1 mm diameter and 6,35 mm thick) of PXE4 or PXE41. The electrodes are of copper-beryllium alloy (250  $\mu\text{m}$  gauge), which has a high fatigue strength ([2], page 973). The soldering tags must be damped with a pliable substance (e.g., silicone rubber) to prevent breakage due to fatigue, particularly if other materials, such as sheet copper, are used. The steel cylinders (often of free cutting steel) should be protected against corrosion; chemically protected or cadmium-plated steel or, even better, stainless steel can be used. The front portion radiating ultrasound can be made of duralumin or free cutting alloy (e.g., Al, Cu, Mg, Pb alloy according to [2], page 1109).

When assembling the transducer it is important that the right amount of pre-stress is applied (e.g.,  $25 \cdot 10^6$  Pa). There are various methods of measuring the stress, the most reliable way being to measure the charge generated in the PXE under short-circuit conditions. A capacitor  $C$  of, say, 10  $\mu\text{F}$  (not an electrolytic one) is connected to the electrical terminals and to a d.c. voltmeter

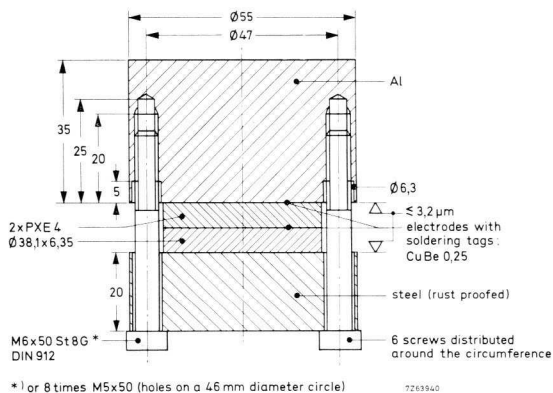


Fig. 8.9 Composite mechanically pre-stressed transducer with a low-intensity and a high-intensity end. The pre-stress is provided by means of bolts positioned around the circumference.

whose internal resistance should be at least  $10 \text{ M}\Omega$ . This meter measures the charge generated during the tightening of the bolts. If the total area of the PXE rings is, for instance,  $2 \cdot 10^{-3} \text{ m}^2$ , and the piezoelectric charge constant  $d_{33} = 290 \cdot 10^{-12} \text{ C/N}$  (PXE4), the charge after pre-stressing amounts to  $14,5 \mu\text{C}$ . Together with a capacitor value of  $10 \mu\text{F}$ , this results in a voltage of  $1,45 \text{ V}$ , which can easily be measured. With  $R_i \approx 10 \text{ M}\Omega$ , a time constant of about  $100 \text{ s}$  is obtained and therefore the bolt must be tightened as quickly as possible (within a few seconds). This will not be necessary if  $R_i \gg 10 \text{ M}\Omega$ . A simpler method than charge measurement, though less accurate, is to use a torque spanner. (A torque spanner is always necessary for tightening multi-bolt transducers to ensure that the stress is applied uniformly.) Since the torque required for a certain amount of pre-stress depends to a large extent on the finish of the transducer parts, this method is particularly recommended for series production where the respective components are always the same. The torque must first be calibrated in some way, for instance, by charge measurement. To ensure a uniform pre-stress distribution in multi-bolt transducers, the bolts positioned diagonally across from each other must be tightened in turn, increasing the torque progressively by small increments until the required value is reached all round.

Before the transducer is bonded to the tank, the contact areas must be cleaned with an abrasive cloth or by sand blasting, followed by chemical degreasing in trichlorethylene or acetone. A suitable glue is, for instance, epoxy resin AV141 (see Appendix B), setting time about  $120 \text{ min}$  at  $140^\circ\text{C}$ . It is recommended that the bonding layer be reinforced with a copper gauze (e.g., mesh  $0,5 \text{ mm}$ , wire diameter  $0,3 \text{ mm}$ ). As explained when comparing the pros and cons of the two transducer types, the PXE can be protected against high temperatures by bonding the coupling portion of the transducer to the tank wall before final assembly. If a single (centre) bolt transducer is used, the bonding layer would have to take the whole torque, involving the risk of fracture. Hence this method can only be used if the bonding layer is protected from the shear stress by a tool that takes up the torque.

The forces taken up by the bolt, or bolts, to obtain a pre-stress of  $25 \cdot 10^6 \text{ Pa}$  can be considerable; for PXE rings or discs of  $38 \text{ mm}$  diameter they amount to about  $25 \text{ kN}$  to  $30 \text{ kN}$ . When an a.c. voltage is applied to the transducer, the bolts will have to take up additional large alternating forces of course. Table 8.I shows that titanium alloy combines the highest fatigue strength with extremely

low losses (even at large excursions), and is therefore the best material for the bolts. The threaded end of the bolt and the thread in the metal end piece must be perfect, although they are positioned in the vicinity of a nodal point. Repeated assembly and dismantling reduces the torque required, therefore the torque values presented in Table 8.III serve only as a guide.

Table 8.III. Technical data for two mechanically pre-stressed high-intensity transducers.<sup>(1)</sup>

parameter	unit	construction and dimensions			
		Fig. 8.8		Fig. 8.9	
		PXE4	PXE41	PXE4	PXE41
series resonant frequency $f_s$ in air	kHz	22	22	26	25,5
parallel resonant frequency $f_p$ in air	kHz	23,5	23,5	27	27
impedance $ Z(f_s) ^{(2)(3)}$	k $\Omega$	1,7	2,5	1,2	1,3
mechanical quality factor $Q$		8	8	12	12
capacitance (1 kHz)	nF	5,5	3,5	6	4
inductance for parallel tuning	mH	12	16	7	10
torque	10 N·m	$\approx 5$	$\approx 5$	$\approx 0,6$ for 8 M5 $\times$ 50 mm $\approx 0,8$ for 6 M6 $\times$ 50 mm	
mechanical pre-stress generated charge	$\mu$ C	$\approx 16$	$\approx 17$	$\approx 17$	$\approx 19$

<sup>(1)</sup> These data were measured 24 h after the transducers were pre-stressed. The rings and discs used are not necessarily typical. Aging, operation and bonding to a tank may well result in greater deviations (see Section 8.5.2).

<sup>(2)</sup> Loaded with water (immersed about 5 mm).

<sup>(3)</sup> With parallel inductance;  $Z$  decreases as the sonic power increases.

### 8.5.2 HIGH INTENSITY TRANSDUCERS IN OPERATION

Water load, tank wall, and bonding layer have the effect of reducing the transducer frequency slightly (the water load alone causes a frequency decrease of about 0,5 kHz in a centre-bolt transducer). The characteristic frequency of the tank and the water load usually give rise to several additional resonances. With a properly designed generator circuit the transducer will always operate close to its own resonant frequency.

Since the transducer capacitance  $C_0$  might involve a high reactive current, it is useful to compensate this capacitance with an inductance  $L$  (see Appendix A), usually connected in shunt across the transducer, but series connection is also possible. The required inductance is calculated as:

$$L = \frac{1}{4\pi^2 f^2 C_0}, \quad (8.16)$$

where  $f$  is the operating frequency.

The impedance of a transducer thus compensated is almost real at the operating frequency. However, the tank and water resonances can again cause deviations. Cavitation occurring at high powers causes a reduction in impedance which becomes all the more pronounced when the radiating plane of the transducer is brought into direct contact with the water. The change of impedance due to cavitation is much reduced when the transducer is bonded to the tank wall and radiates through it into the water.

The maximum permissible operating power depends to a large extent on the operating conditions (temperature, coupling to the tank, type of tank and its contents, and so forth). Reliable performance is ensured at an (electrical) input power of 50 W; at higher powers one must take careful consideration of heat loss and the stresses and strains involved. The overall efficiency is also governed by the operating conditions, but is usually better than 90%.

## 8.6 Disc transducers (bonded to a cleaning tank)

### 8.6.1 CONSTRUCTION OF A PXE DISC TRANSDUCER

Pre-stressed composite transducers are not absolutely necessary for effective ultrasonic cleaning, good results are also obtained with PXE disc transducers bonded direct to the tank wall. The transducer itself consists of a PXE disc alone (PXE41), or a PXE disc and a metal disc bonded together. In the latter case the metal disc is positioned against the tank wall. Fig. 8.10 shows such an arrangement.

When bonding a PXE disc direct to the tank, it should be borne in mind that, apart from involving considerable losses, a thick bond impedes heat removal.

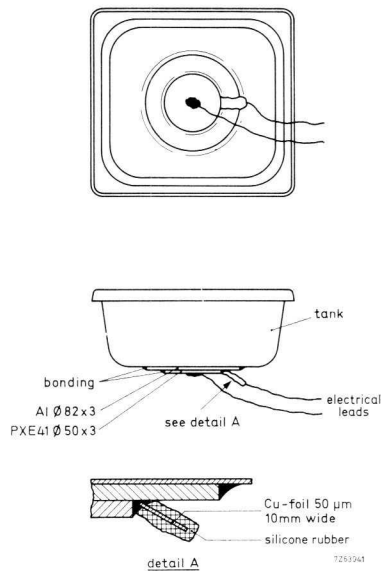


Fig. 8.10 Disc resonator bonded to an aluminium disc and the cleaning tank. The connecting foil and stranded wire are protected from fatigue by an acoustic damping material (e.g., silicone paste, Silastic 731 RTV).

It is, therefore essential that the bond be as thin as possible. On the other hand one must bear in mind the danger of fracture; heavy objects dropping into the tank are likely to fracture the disc. Obviously a compromise must be made. A bond of defined thickness can best be made by reinforcing it with a fibre-glass or metal gauze about 0,5 mm thick. The thickness of the PXE disc cannot be chosen independently of the thickness of the tank wall. Stainless steel tanks with the usual wall thickness of 1 mm used in conjunction with 3 mm thick discs provide a satisfactory compromise as regards mechanical strength and efficiency.

If a metal plate is placed between the PXE disc and the tank (Fig. 8.10), this has the advantage of protecting the PXE and reduces losses. The metal disc may be aluminium or steel. Size for size, aluminium gives a greater electro-mechanical coupling factor than steel (and a better matching).

The PXE disc and the metal disc are usually of the same thickness, their diameters being chosen so that they also have the same radial mode resonant frequency. For optimum results a PXE disc of, say 50 mm diameter, requires a steel or aluminium disc of about 82 mm diameter.

With both transducer types it is advantageous to use a tank without sharp corners which tend to impede the spreading out of the ultrasound. The connections to the free electrode must be made with a soldered stranded wire, and contact to the bonded electrode is made with a compression bonded or soldered metal foil (beryllium copper, for instance).

To ensure reliable operation, all free ends of the stranded wire and the foil must be acoustically damped with a suitable damping agent (such as silicone rubber). A low-loss bonding agent recommended for bonding the disc is Eccobond 45 + 50% Catalyst 15 (see Appendix B), hardening time is 4 hours at 50 °C.

The PXE disc bonded to the tank vibrates in the radial mode with an impedance of a few hundred ohms and radiates power mainly through the tank wall into the bath. On the other hand transducers bonded to the tank with a metal plate in between involve various resonances between 40 kHz and 60 kHz and have impedances of several kilohms. The radial vibrations of the transducer apply shear forces to the tank wall causing the wall to vibrate in flexure mode and thus radiating power into the liquid. Due to mechanical feedback the transducer is caused to vibrate in a superimposed flexure mode.

Since the tank wall has in fact become part of the transducer, both form and thickness of the tank have a great influence on the overall characteristics of the equipment. Optimum results can be obtained only if the tank data are taken into account, which calls for a great deal of experimental work. The transducer data, such as operating frequency, impedance, and maximum efficiency, can be determined only after samples have been made.

#### 8.6.2 OPERATING FREQUENCY AND POWER

Ultrasonic cleaning tanks equipped with PXE disc transducers and constructed as shown in Fig. 8.10 operate at about 50 kHz, which is somewhat higher than the radial mode frequency of the freely suspended disc (radial vibration  $f_s \approx 45$  kHz for a disc of 50 mm diameter). The transducer can be safely driven at an electrical input power of 50 W and it exhibits no irreversible changes, but between 100 W and 150 W the transducer begins to show signs of permanent damage.

## 9 PXE delay line transducers

### 9.1 General

There are several systems which require electrical signals to be delayed for periods of up to several milliseconds without a substantial loss of information contained in the signal. Electrical transmission lines with either lumped or distributed components give rise to considerable attenuation and distortion, and involve rather large physical dimensions.

Modern acoustic delay systems operate with an electromechanical transducer which converts the electrical signal into an acoustic signal that is converted back into an electrical signal after having travelled over an appropriate distance through an acoustic delay medium, which may be either solid or liquid. In the case of analogue signals it is important for the energy conversion in the transducer to be linear and reversible to ensure satisfactory restoration of the delayed electrical signal.

In this method the delay time depends almost entirely on the transit time of the acoustic wave, and to a negligible extent on that of the electrical signal. The velocity of sound in liquids and solids is about 1 km/s to 5 km/s, whereas the velocity of electromagnetic waves in dielectrics is about  $10^5$  times as high. Compact mechanical structures are therefore quite suitable to provide delay times of a few milliseconds.

Although ultrasonic delay lines are basically information storage devices, they are quite valuable for many other applications. They are practically indispensable items when long delays or high fidelity, or both are required. Bandwidths of no less than 80% of the carrier frequency are quite common; so are delays of several milliseconds.

An ultrasonic line must satisfy the following basic requirements: long (and sometimes variable) delay with precise control, accurate preservation of pulse or modulation envelope shape (wide bandwidth and linear performance), a minimum of spurious signals, very moderate attenuation, compactness and stability under varying ambient conditions of temperature, humidity and vibration.

The field of application for ultrasonic delay systems is still expanding. Such systems are now widely employed in telecommunications (radar), in computers (wire lines and solid lines in digital, analogue and high-speed, multi-purpose

computers), and in domestic applications like colour television (PAL and SECAM systems). A new application field is found in video recording (drop-out compensator).

## 9.2 Solid delay lines

A solid ultrasonic delay line consists of a block of material through which the signal is propagated as an acoustic wave launched and received by electro-acoustic transducers. These transducers are piezoelectric plates bonded to one face of the delay medium and, sometimes, to a backing material. The theory of solid ultrasonic delay lines is therefore concerned with:

- transducers for launching and receiving the ultrasound signal;
- propagation of acoustic waves through the solid delay medium;
- the geometrical design of the solid body and the path taken by the ultrasound beam,
- bonding techniques for producing reliable, extremely thin intermediate layers.

With the high coupling coefficient of PXE it is possible to design delay lines having a rather broad bandwidth and a relatively low attenuation. However, let us first consider the much simpler case when the piezoelectric coupling is low and when the materials of the transducer, bonds, and delay medium all have the same specific acoustic impedance, i.e., product of density and sound velocity. If a voltage  $V_1$  is applied to one transducer of such a line (Fig. 9.1),

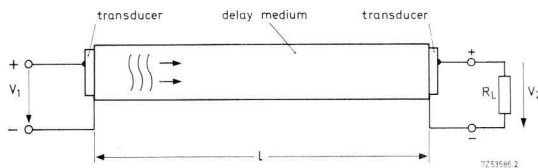


Fig. 9.1 Basic construction of a delay line.

and the other transducer is connected to a matched load resistance  $R_L$ , the voltage  $V_2$  developed across  $R_L$  can be calculated from the formula:

$$\frac{V_2}{V_1} = \frac{4k^2 Q_e}{\pi} \cos^4 \left( \frac{\pi}{2} \cdot \frac{f - f_s}{f_s} \right) \exp \left\{ -j2\pi f \left( \tau + \frac{1}{2f_s} \right) \right\}, \quad (9.1)$$

where  $f$  is the signal frequency;  $f_s$  is the fundamental series resonant frequency of the transducer;  $Q_e (= 2\pi f_s R_L C_0)$  is the electrical quality factor of the terminating circuit;  $C_0$  is the clamped capacitance of each transducer, and  $\tau$  is the delay time in the medium between the transducers, including the bonds.

Eq. 9.1 is the transfer function of the transducer pair if the piezoelectric coupling is rather low, say,  $k \leq 0.2$ . Transmission and beam divergence or diffraction losses in the medium are not included, and electrical terminating networks actually involve additional losses.

For this low  $k$  transducer pair the transfer function is a smooth bell-shaped curve centred on  $f_s$  with a 3 dB bandwidth of  $0.52f_s$ .

### 9.3 High coupling PXE transducers

For high coupling ceramic transducers the situation is much more complicated. High  $k$  PXE transducers are often used without backing, and coupled to a delay block made of fused silica or isopaustic glass (i.e., with a temperature independent propagation time), the specific acoustic impedance of which is about 40% lower than that of PXE. Under these conditions the line output can be improved with an electrical 'matching' network consisting of a simple parallel coil  $L_{par}$  giving an electrical resonant frequency  $f_e$  according to:

$$f_e = \frac{1}{2\pi} \sqrt{\frac{1}{L_{par} C_0}}. \quad (9.2)$$

With, for instance,  $f_e/f_s = 0.7, 1.0$  or  $1.4$ , and a load resistance  $R_L$  given by  $Q_e = 2\pi f_s R_L C_0 = 2$ , a PXE transducer pair with a piezoelectric coupling coefficient  $k \approx 0.6$  then gives the three transfer functions drawn in Fig. 9.2. Similar curves are shown in Fig. 9.3 for  $Q_e = 5$ , so that the influence of load resistance  $R_L$  on the shape of the transfer function becomes apparent. The conclusion is that the passband of the transducer pair, and hence the total delay line, can be tilted and shifted by an appropriate choice of  $Q_e$  and  $f_e$  ( $R_L$  and  $L_{par}$ ).

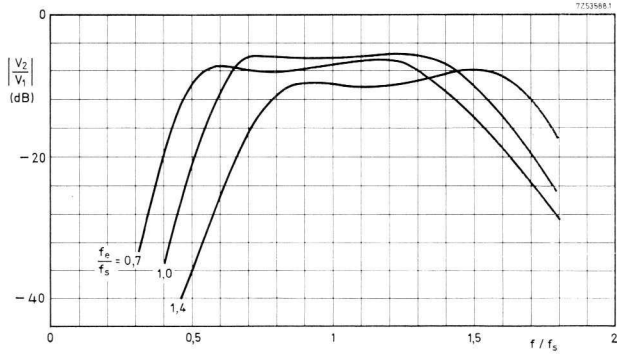


Fig. 9.2 Transfer function of an electrically tuned PXE shear-wave transducer pair coupled to a quartz or potassium lead silicate glass via a thin bonding layer. The frequency is normalized to the acoustic series resonant frequency  $f_s$ ,  $k = 0,6$ ,  $Q = 2$ ,  $f_e$  is the electrical resonant frequency as given by eq. 9.2.

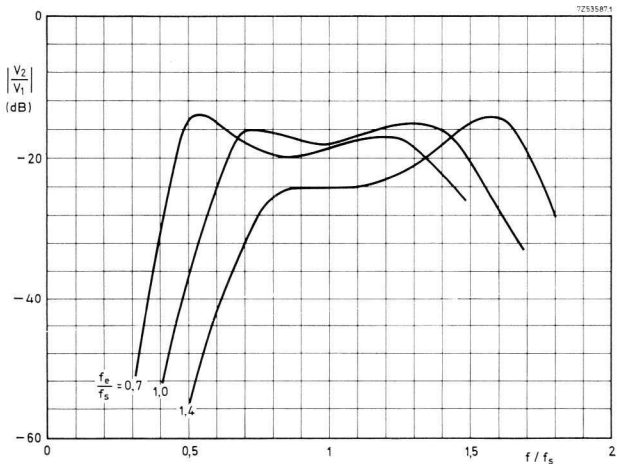


Fig. 9.3 As for Fig. 9.2, but now  $Q = 5$ .

### 9.4 Modes of vibration

As shear waves are propagated more slowly than compressional waves they are usually preferred where small dimensions are required. The ratio of the velocities of propagation of these two modes is given by the following expression:

$$\frac{V_c}{V_{sh}} = \sqrt{\frac{2(1-\sigma)}{1-2\sigma}}, \quad (9.3)$$

where  $\sigma$  is Poisson's ratio for the delay medium. This velocity ratio is approximately 1,6 and 1,7 for materials with  $\sigma = 0,17$  (fused silica) and  $\sigma = 0,225$  (isopaustic potassium lead silicate glasses) respectively.

Fig. 9.4 shows the deformation, with magnitude exaggerated, of a transducer operating in the shear resonant mode. In a shear transducer the poling direction must be perpendicular to the direction of the alternating electric field, and so parallel to the electrode surfaces, as shown in Fig. 9.4 (see also Appendix E).

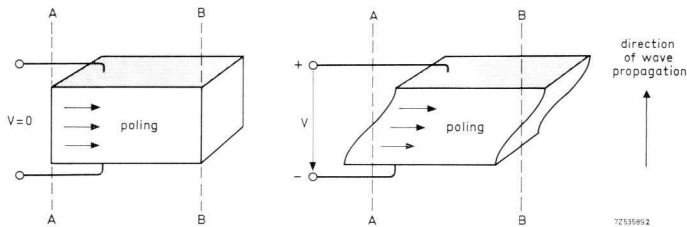


Fig. 9.4 PXE transducer operating in the shear mode.

### 9.5 Directivity of transducers

Most delay line transducers have a large aperture (20 or more wavelengths wide), and are therefore highly directional. This permits the use of ray paths intricately folded by repeated reflection to obtain a long delay in a small volume of material. The side lobes of the radiation pattern can give rise to spurious

signals which follow 'stray' paths to arrive with unwanted delays. These can be minimized by careful geometrical design, accurate machining, and by coating the delay medium at appropriate points with absorbent materials such as epoxy resins or solder.

For a planar rectangular radiator with side lengths  $a$  and  $b$  which produces a shear stress amplitude  $p_0$  in the semi-infinite medium with which it is in contact, the shear stress amplitude  $p$  of the radiated wave (of wavelength  $\lambda$ ) at a distant point whose radius vector  $r$  forms angles  $(\pi/2) - \alpha$  and  $(\pi/2) - \beta$  with the  $a$  and  $b$  directions of the radiator, is given by the relation:

$$p = p_0 \cdot \frac{ab}{r\lambda} \cdot \frac{\sin \{(\pi a/\lambda) \cdot \sin \alpha\}}{(\pi a/\lambda) \cdot \sin \alpha} \cdot \frac{\sin \{(\pi b/\lambda) \cdot \sin \beta\}}{(\pi b/\lambda) \cdot \sin \beta} \cdot \exp \{-j2\pi f(t - r/v)\}. \quad (9.4)$$

Evidently zeros are found at  $\alpha_n \approx \pm n\lambda/a$  and  $\beta_m \approx \pm m\lambda/b$ , where  $n$  and  $m$  are positive integers.

In this distant region, the so-called far field or Fraunhofer region, the wave-front is approximately spherical, and the amplitude varies along the axis inversely with the distance from the radiator. However, the expression is only valid for a distant point in a long and very thick delay block in which the beam can spread freely. In fact the conditions are significantly different where long lines are concerned. Dimension  $b$  of the transducer is usually almost equal to the vertical thickness of the plate of delay material, so the wave-front cannot spread vertically, and a partially guided wave is produced. The beam spread still occurs in the plan view and such a delay plate has a cylindrical wavefront with the following shear stress distribution:

$$p = p_0 \cdot \frac{a}{\sqrt{r\lambda}} \cdot \frac{\sin \{(\pi a/\lambda) \cdot \sin \alpha\}}{(\pi a/\lambda) \cdot \sin \alpha} \cdot \exp \{-j2\pi f(t - r/v)\}. \quad (9.5)$$

In practice many delay lines do not work with a relatively large transducer separation  $l$ . In other words they do not operate in the far field, but somewhere in the transition region between the far field and the near field, or Fresnel region. This near field extends from the transmitting transducer over a distance  $l_n$  ( $l_n = l_{near}$ ) along its axis which is expressed by the following relations:

for the  $a$  direction:

$$l_n \approx a^2/2\lambda = fa^2/2v; \tag{9.6}$$

for the  $b$  direction:

$$l_n \approx b^2/2\lambda = fb^2/2v. \tag{9.7}$$

Details are shown in Fig. 9.5, which also illustrates the average shear stress  $p_{av}$  integrated in phase and amplitude over area  $ab$  of a receiving transducer at a distance  $l$  from a similar transmitting transducer.

Optimizing the ratio of main delayed signal amplitude to worst spurious delayed signal amplitude (often called the ‘third time around’ signal) usually leads to the following preferred dimensions:

$$l_n \approx (0,7 \text{ to } 1,0) l = (0,7 \text{ to } 1,0) \tau v, \tag{9.8}$$

hence

$$a \approx b \approx v \sqrt{1,7\tau/f}. \tag{9.9}$$

The velocity of shear waves in special isopaustic glass is about  $2500 \text{ m/s} = 2,5 \text{ mm}/\mu\text{s}$ .

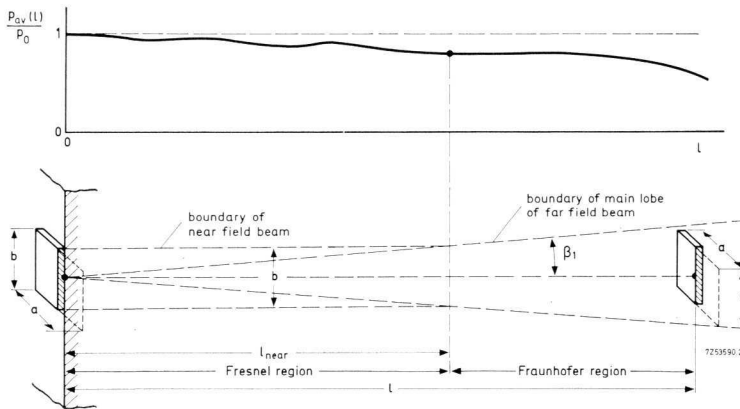


Fig. 9.5 Near field and far field beam pattern.

### 9.6 Bonds for shear wave transducers

The vibrating transducer must be acoustically coupled to the delay medium to transfer the vibration from the one medium to the other. This coupling entails more difficulty with solid lines than it does with liquid lines which operate in the compressional mode and where in most cases the liquid will readily wet the transducer surface, thus establishing excellent acoustic contact.

The bond must transmit shear waves, that is to say, it must be either a solid or a very viscous liquid. Its thickness must be closely controlled either to be very small as compared with the acoustic wavelength in the bond material or to be precisely  $\lambda/4$  or  $\lambda/2$ . A widely used method of bonding is making soldered joints to metal electrodes on both transducer and delay line medium by means of low melting point solders (see Appendix B).

### 9.7 PXE materials for shear wave transducers

The recommended materials in the PXE series for delay line transducers are PXE7 and PXE11. The relevant data are given in Table 9.I. PXE11 is the best choice of material for high frequency applications (10 MHz to 100 MHz), as its propagation velocity is about 1,5 times that of PXE7. For a given frequency therefore, a PXE11 transducer is in fact 1,6 times the thickness of a PXE7 transducer, so that higher frequencies can be used. Moreover, PXE11 offers the advantage of a 40% lower dielectric constant, which eases the electrical termination problem at high frequencies. These considerations are reflected in  $M$ , the piezoelectric figure of merit. The only drawback of PXE11 is that owing to a very special production technique (continuous hot pressing) it is comparatively expensive. The rather low crystallographic transition temperature should also be taken into account (see Table 9.I).

Table 9.1. Properties of materials used for shear wave transducers.

property	symbol	unit	PXE7	PXE11
coupling coefficient	$k_{15}$		0,66	0,65
wave propagation velocity:				
twice frequency constant				
$N_{15}^E$ closed circuit	$v_5^E = 2hf_s$	m/s	1940	3000
twice frequency constant				
$N_{15}^D$ open circuit	$v_5^D = 2hf_p$	m/s	2400	3690
relative permittivity:				
free	$\epsilon_{11}^T/\epsilon_0$		1000	600
clamped	$\epsilon_{11}^S/\epsilon_0$		590	350
piezoelectric figure of merit:				
	$M_5^{E,T} = \frac{k_{15} v_5^E}{\epsilon_{11}^T/\epsilon_0}$	m/s	1,28	3,25
$M = \frac{kv}{\epsilon/\epsilon_0} \approx k Z ^{(1)}$				
	$M_5^{D,S} = \frac{k_{15} v_5^D}{\epsilon_{11}^S/\epsilon_0}$	m/s	2,68	6,87
aging of the permittivity	$\frac{\Delta\epsilon_{11}/\epsilon_{11}}{\log t_2/t_1} \cdot 100$	%/decade	- 2,5	
Curie temperature	$\vartheta_C$	°C	320	400
transition temperature <sup>(2)</sup>		°C		180

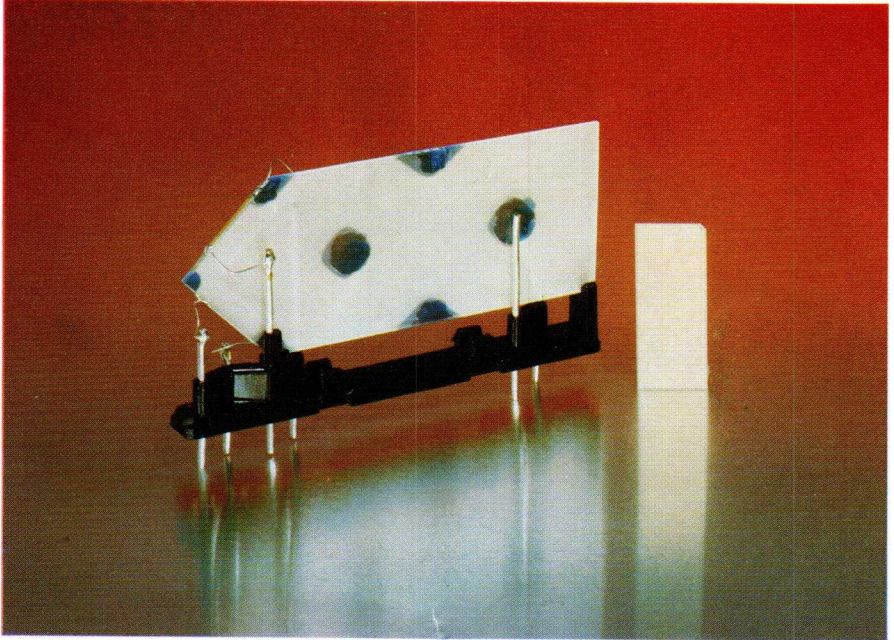
<sup>(1)</sup>  $|Z|$  = specific acoustic impedance.

<sup>(2)</sup> In PXE11 there is a transition from the ferroelectric orthorhombic to the ferroelectric tetragonal phase at 180 °C. If the material passes through this temperature in either direction then it must be repoled.

## 9.8 Description of an actual delay line

A brief description of the design of a type DL50 delay line used in PAL colour television receivers may serve to illustrate the use of PXE7 in low frequency delay lines.

*PLATE V*



*Delay line type DL50 with plastic housing removed.*



Compared to older types of delay line, the DL50 is very small and light. These improvements result from making the delay line in the form of a thin plate, and giving it oblique end faces resulting in multiple reflection.

Fig. 9.6 shows the dimensions and form of the glass plate used for the DL50 delay line and the path followed by the ultrasound waves. The PXE transducers are bonded to the oblique end faces. *PLATE V* shows the delay line stripped of its plastic encapsulation. The thickness of the glass plate is about the same as the wavelength of the ultrasound, therefore it forms a waveguide in the thickness dimension so that the wave-front is cylindrical. Consequently beam losses caused by spread are less than in older types of delay line in which the wave-front is spherical.

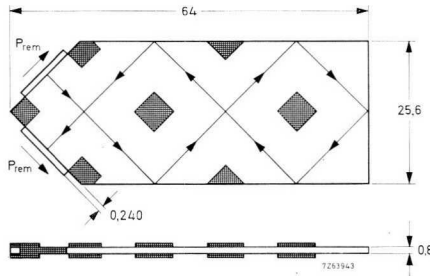


Fig. 9.6 Operating principle of the delay line type DL50.

If the dimensions of the glass plate perpendicular to its thickness are to be kept small, the sound wave must be reflected several times within the delay line. In the DL50 delay line the ultrasound is reflected five times. Repeated reflection means more undesired stray waves, but these can easily be suppressed in this type of delay line. The regions of the two large faces of the glass plate which are not on the path of the useful main beam are provided with a damping medium (see Fig. 9.6 and *PLATE V*). Only stray waves incident on these areas are heavily damped (e.g., 35 dB at frequencies between 3,9 MHz and 4,7 MHz).

The delay medium in use is a potassium lead silicate glass which has the advantage that by careful selection of its composition the delay time can be made almost temperature independent (isopaustic) over a sufficiently wide temperature range. The thermal expansion is compensated by a corresponding variation in propagation speed of the ultrasound wave.

The poling direction  $P_{rem}$  of the PXE7 transducer is parallel to the longitudinal axis (the long side) of the transducer (Fig. 9.6), which results in a shear wave polarized in the same direction, and causes the ultrasound wave to be propagated perpendicularly to the longitudinal axis, i.e., in the thickness direction of the PXE transducer. The glass particles within the range of the ultrasound wave will then move in a direction parallel to the glass plate surfaces, but perpendicular to the direction in which the sound wave is propagated. This polarization of the shear wave in the glass will result in a total reflection only if the angle of incidence is larger than  $36^\circ$  (the limit angle). This requirement, which sets a limit to the form and dimensions of the delay line, is fulfilled in the type DL50 delay line for all reflections.

Under no-load conditions (in free air) the series resonant frequency of the PXE7 transducer used for the delay line is about 4,2 MHz, for which the thickness  $h$  of the transducer is calculated as:

$$h = \frac{N_s^E}{f_s} = \frac{970}{4,2 \cdot 10^6} = 230 \text{ } \mu\text{m.}$$

The transducers have no acoustic feedback and are electrically tuned to about the carrier frequency (mid-band frequency) by means of parallel coils. They are terminated with a resistance  $R_L = 390 \text{ } \Omega$ , which yields a quality factor of about 2,5. The resulting 3 dB bandwidth ranges from 3,4 MHz to 5,2 MHz.

## Appendix A Dynamic behaviour of PXE transducers

A piezoelectric transducer operating at or near its series resonant frequency (defined below) can be characterized by the simple equivalent circuit of Fig. A.1.\*

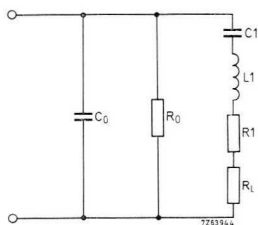


Fig. A.1 Equivalent circuit of a piezoelectric transducer.

$C_0$  = capacitance of the transducer far below resonance minus capacitance  $C_1$ ;

$R_0$  = parallel resistance representing dielectric losses of the transducer  $(2\pi f_s C_0 \tan \delta)^{-1}$ ;

$R_1$  = resistance representing mechanical losses;

$R_L$  = load resistance representing radiated energy, in vacuum,  $R_L = 0$ ;

$C_1$  = capacitance of the mechanical circuit,

$L_1$  = inductance of the mechanical circuit.

If the moduli of the electrical admittance  $|Y|$  and impedance  $|Z|$  are plotted against the frequency, we obtain the curves shown in Fig. A.2. The frequency  $f_m$  at which the admittance reaches a maximum lies close to\*\* the series resonant frequency:

$$f_s = \frac{1}{2\pi} \sqrt{\frac{1}{L_1 C_1}}, \quad (\text{A.1})$$

which is the frequency at which the impedance in the equivalent circuit becomes zero if  $R_1$  is ignored.

\* The internal loss resistance (parallel with  $C_0$ ) caused by the dielectric losses of the transducer can often be ignored and is, therefore, not shown in Fig. 6.6, Chapter 6.

\*\* As an example, if we take the values given in Fig. 6.6, the deviation  $\Delta f$  will be no more than about 43 Hz, so that  $\Delta f/f_s \approx 1.2 \cdot 10^{-3}$ .

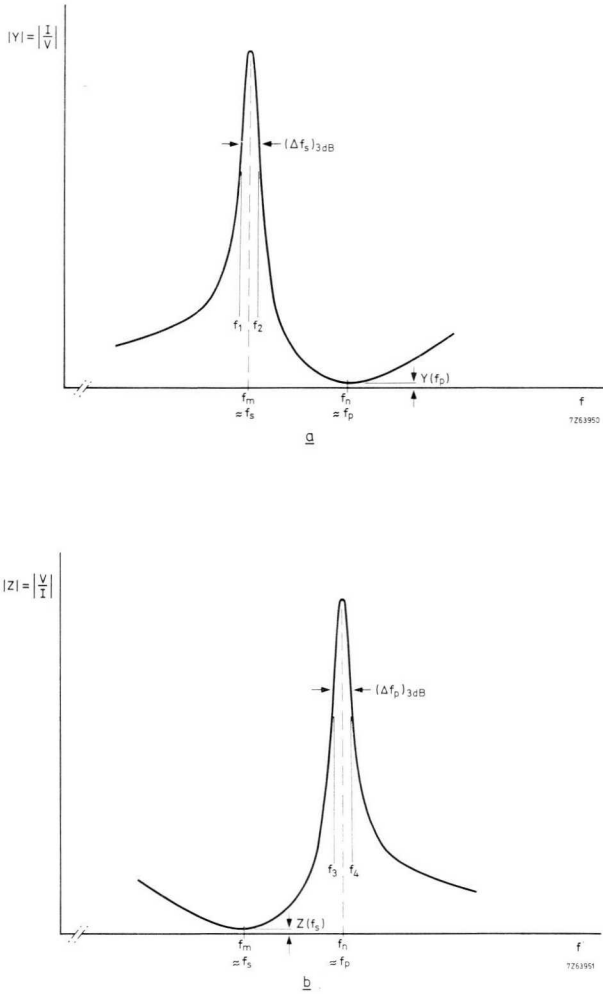
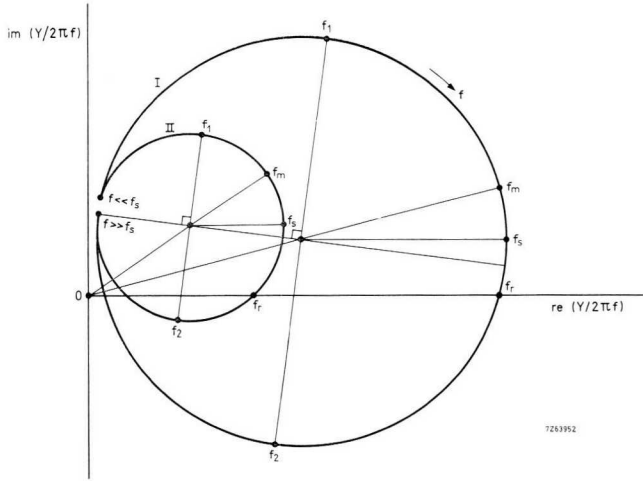
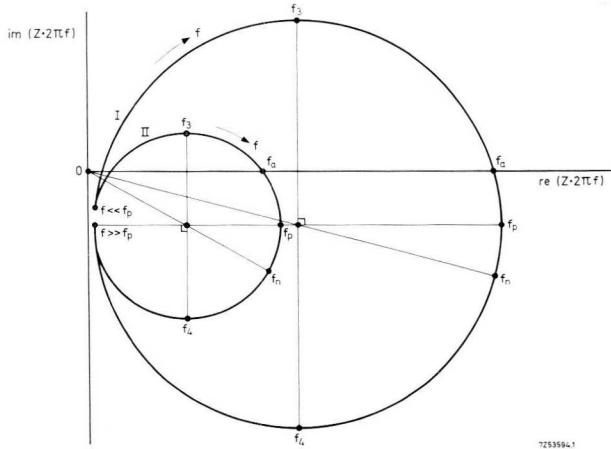


Fig. A.2 Admittance (a) and impedance (b) as functions of frequency. The series resonant frequency  $f_s$  lies close to the minimum impedance frequency  $f_m$ ; the parallel resonant frequency  $f_p$  lies close to the maximum impedance frequency  $f_n$ . Below  $f_m$  and above  $f_n$  the transducer behaves capacitively, between  $f_m$  and  $f_n$  it behaves inductively.



a



b

Fig. A.3 Circle diagrams corresponding to the resonance curves in Fig. A.2. Admittance (a) and impedance (b) divided and multiplied respectively by  $2\pi f$ . Circles I hold for low damping and circles II for high damping.

The frequency  $f_n$  at which the admittance reaches a minimum lies close to the parallel resonant frequency:

$$f_p = \frac{1}{2\pi} \sqrt{\frac{C_0 + C_1}{L_1 C_0 C_1}}, \tag{A.2}$$

which is the frequency at which the impedance in the equivalent circuit becomes infinite if  $R_1$  is ignored and  $R_0$  is infinite.

The corresponding circle diagrams are given in Fig. A.3. In these diagrams  $Y/2\pi f$  and  $Z \cdot 2\pi f$  are plotted instead of just  $Y$  or  $Z$  because, in the case of transducers with high  $k$  values (as with PXE materials), the plots are then easier to understand. The circles I hold for low damping, the circles II for high damping. The curves of Fig. A.3 can be measured with the circuits shown in Fig. A.4. The curves of Fig. A.2 can be measured if appropriate resistors are substituted for  $C_1$  and  $C_{II}$ . This is a simple method of finding the 3 dB bandwidth at  $f_s$  or  $f_p$ . The mechanical quality factor  $Q_m$  can be derived in turn from the 3 dB bandwidth:

$$Q_m^E = \frac{f_s}{(\Delta f_s)_{3 \text{ dB}}} = \frac{f_s}{f_2 - f_1}, \tag{A.3}$$

and

$$Q_m^D = \frac{f_p}{(\Delta f_p)_{3 \text{ dB}}} = \frac{f_p}{f_4 - f_3}, \tag{A.4}$$

(valid only when  $k^2 Q_m > 10$ ).

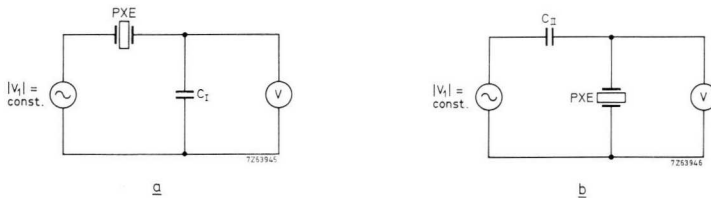


Fig. A.4 Circuits for measuring admittance and impedance.

(a) Transducer voltage constant. Requirement:  $|V| \leq 0,1 |V_1|$  at  $f_s$ ;  $C_I \geq 10 k_{eff}^2 Q_m^E C_0$ .  
 (b) Transducer current constant. Requirement:  $|V| \leq 0,1 |V_1|$  at  $f_p$ ;  $C_{II} \leq 0,1 C_0 / (k_{eff}^2 Q_m^D)$   
 $C_I$  and  $C_{II}$  can be replaced by real resistances.

It can be shown that  $(\Delta f_p)_{3 \text{ dB}} < (\Delta f_s)_{3 \text{ dB}}$ , whilst the difference between the two bandwidths increases with  $k_{eff}$ . Since on the other hand  $f_p > f_s$ , it is always true that  $Q_m^D > Q_m^E$ .

The effective coupling coefficient  $k_{eff}$  (see Appendix D) can be derived from the series and parallel resonant frequencies of the transducer under no-load conditions:

$$\frac{k_{eff}^2}{1 - k_{eff}^2} = \frac{f_p^2 - f_s^2}{f_s^2} = \frac{C_1}{C_0}, \quad (\text{A.5})$$

or

$$k_{eff}^2 = \frac{f_p^2 - f_s^2}{f_p^2}. \quad (\text{A.6})$$

As an approximation, when  $k_{eff} \ll 1$ , we may write:

$$k_{eff}^2 \approx 2 \frac{f_p - f_s}{f_s} = 2 \frac{\Delta f}{f_s}. \quad (\text{A.7})$$

The complete equivalent circuits of transducers which operate as sound receivers (microphones) or sound transmitters, are given in Fig. A.5. These types of operation are alike as regards their characteristic properties.

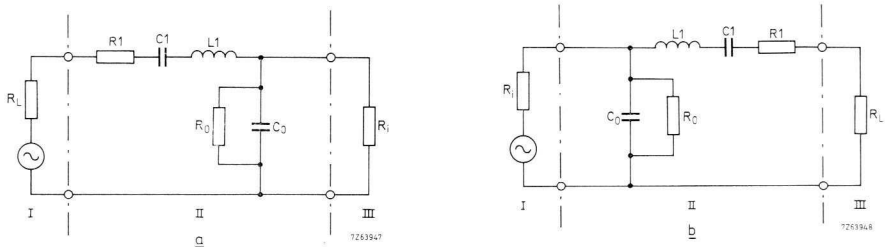


Fig. A.5 (a) Equivalent circuit of an ultrasound receiver:

I = Acoustic a.c. source (with internal resistance);

II = PXE transducer,

III = Input impedance of the amplifier.

(b) Equivalent circuit of an ultrasound transmitter:

I = Electric a.c. source (with internal resistance);

II = PXE transducer,

III = Acoustic load.

Apart from  $f_s$  and  $f_p$  there is the maximum response frequency  $f_M$  of the transducer, at which the modulus of its transfer function is a maximum. This is the frequency at which a microphone has maximum sensitivity, and at which a transmitter gives maximum sound output. The frequency  $f_M$ , the bandwidth and the output power are influenced by the external resistance  $R_i$ , which can be either the input impedance of a microphone amplifier or the internal impedance of a transmitter generator.

When  $k_{eff} \ll 1$  (which is so in most practical cases) we have the following relationships:

$$f_M = f_s + \frac{f_p - f_s}{1 + \frac{1}{Q^2}}, \quad (\text{A.8})$$

where  $Q = \omega_s C_0 R_i$ , ( $R_i \ll R_0$ );

$$f_M = f_s \text{ for } Q \ll 1 \quad (\text{A.9})$$

(short circuit conditions,  $R_i$  small),

$$f_M = f_p \text{ for } Q \gg 1 \quad (\text{A.10})$$

(no-load conditions,  $R_i$  large). At  $Q = 1$ ,  $f_M$  lies half way between  $f_s$  and  $f_p$ .

The approximate bandwidth can be calculated from:

$$\begin{aligned} (\Delta f_M)_{3 \text{ dB}} &= (\Delta f_s)_{3 \text{ dB}} \left( 1 + \frac{Q Q_m^E k_{eff}^2}{1 + Q^2} \right) \\ &= \frac{f_s}{Q_m^E} \left( 1 + \frac{Q Q_m^E k_{eff}^2}{1 + Q^2} \right). \end{aligned} \quad (\text{A.11})$$

Near to  $f_p$  this formula is less accurate (compare with eq. A.4).

A maximum bandwidth is obtained at  $Q = 1$  with:

$$(\Delta f_M)_{3 \text{ dB}} = (\Delta f_s)_{3 \text{ dB}} \left( 1 + \frac{Q_m^E k_{eff}^2}{2} \right). \quad (\text{A.12})$$

Optimum power matching is also obtained when  $Q = 1$  with  $k_{eff}^2 Q_m^E \leq 2$ . (Matching can be considerably improved by means of additional inductance particularly if  $k_{eff}^2 Q_m^E \ll 2$ .) If  $k_{eff}^2 Q_m^E > 2$ , optimum matching may be

achieved at two different values of  $R_i$ . Matching to minimum impedance at  $f_s$  is then with  $R_i \approx |Z(f_s)| \approx R_1 + R_L$ , or to maximum impedance at  $f_p$  with  $R_i \approx |Z(f_p)| \approx \{1/\omega_p^2 C_0^2 (R_1 + R_L)\}$ .

As mentioned above it is often advantageous to tune the transducer with an inductance. This can be done with a parallel inductance ( $L_{par}$ ) as well as with a series inductance ( $L_{ser}$ ). Thus two coupled resonant circuits result: a mechanical one formed by  $L_1$ ,  $C_1$ , and  $R_1$ , and an electrical one formed by  $L_{par}$  (or  $L_{ser}$ ),  $C_0$ , and  $R_i$  (the resistance of the a.c. generator or the microphone amplifier). The coupled circuits display passbands similar to those of band filters. The inductances are approximately:

$$L_{par} = \frac{1}{\omega_s^2 C_0}, \quad (\text{A.13})$$

$$L_{ser} = \frac{1}{\omega_p^2 C_0}. \quad (\text{A.14})$$

Fig. A.6 shows the equivalent circuits for tuned transducers (parallel and series tuning). Fig. A.7 shows how the impedance varies with frequency. Curve I applies to a transducer without an acoustic load. At medium or heavy loads the curve assumes the form of curves II and III respectively. The impedance of the parallel-tuned transducer is real at  $f_s$ , that of the series-tuned transducer is real at  $f_p$ . The frequency response can be electrically or mechanically controlled by varying the electrical or mechanical terminating resistance. This does not affect  $f_s$  and  $f_p$  noticeably, or the maximum obtainable bandwidth  $B$ , which is about equal to the distance between the respective minima and maxima of  $f_s$  and  $f_p$  under no-load conditions.

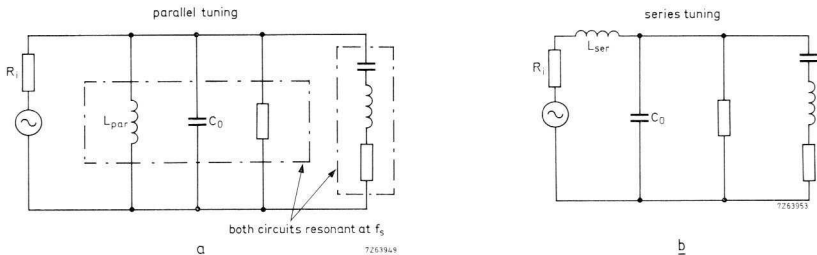


Fig. A.6 Equivalent circuits of tuned transducers.

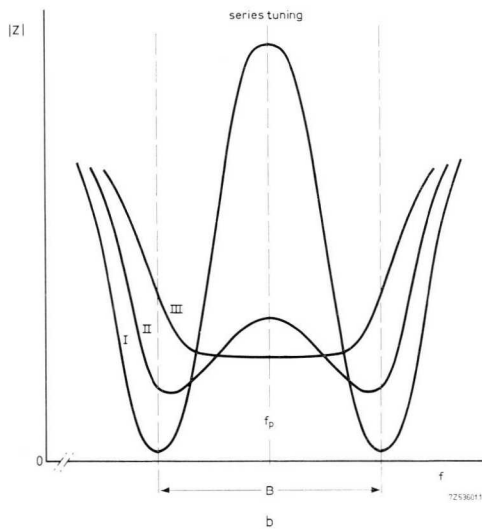
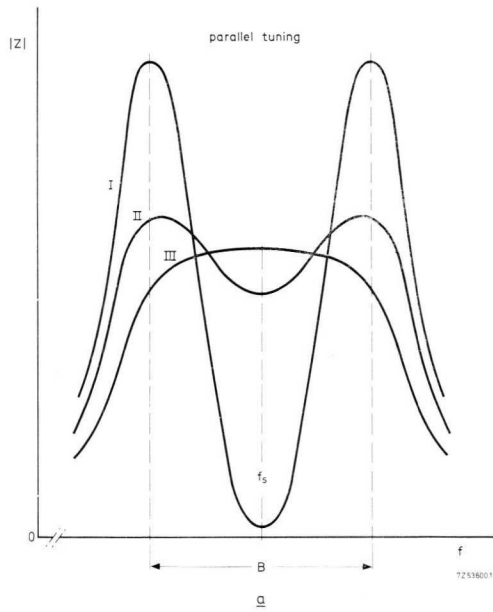


Fig. A.7 Impedance as a function of frequency at parallel and at series tuning.

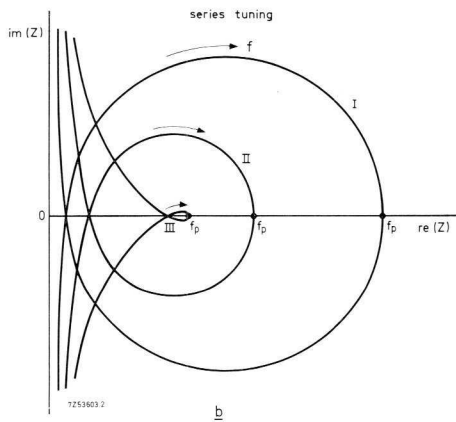
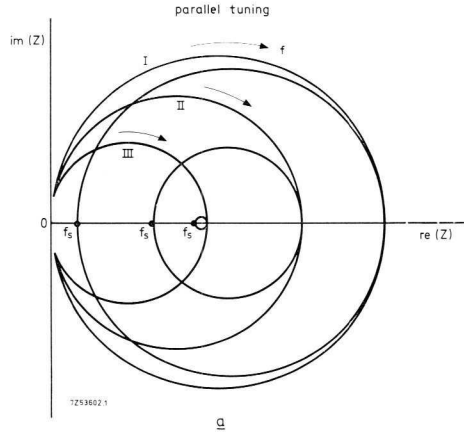


Fig. A.8 Impedance circle diagrams corresponding to Fig. A.7.

The bandwidth obtainable by electrical tuning is about equal to the product of the actual coupling coefficient and the series or parallel resonant frequency (compare with eq. 8.6),

$$B \approx k_{eff} f_{s,p}. \quad (\text{A.15})$$

Fig. A.8 shows the corresponding circle diagrams.

The terminating resistance  $R_i$  for a fairly flat frequency response curve for a parallel inductance arrangement with a sufficiently high transducer quality factor ( $Q_m^E > Q$ ) can be calculated from:

$$Q = \sqrt{\frac{1 - k_{eff}^2}{2k_{eff}^2}}, \quad (\text{A.16})$$

or

$$R_i \approx \frac{0,7}{\omega_s C_0 k_{eff}} \quad (\text{for } k_{eff}^2 \ll 1). \quad (\text{A.17})$$

For a series inductance arrangement the formula is:

$$R_i \approx \frac{k_{eff}}{0,7 \omega_p C_0}. \quad (\text{A.18})$$

## Appendix B Bonding techniques

### B.1 Gluing

Before the glue is applied to the electrodes of a PXE element, they should be thoroughly cleaned, preferably with a degreasing agent such as trichlorethylene. If the glued PXE electrode must be in good electrical contact with the adjacent metal surfaces, conductive glues are often used, e.g., epoxy glue E-solder E3021 (Epoxy Products Europe), which has a setting time of about 3 hours at 60 °C.

A disadvantage of this conductive glue is that its mechanical damping is highly temperature dependent, and that the temperature limit of the glued joint is no more than 50 °C. However, conductive joints can also be made with non-conductive glues. The transducer is glued under pressure, the metal surfaces having been first slightly roughened. A compressive force of a few kg/cm<sup>2</sup> is sufficient to make the glue film so thin that electrical contact is ensured by the roughness of the adjacent surfaces.

#### B.1.1 RECOMMENDED GLUES

##### 1. *Araldite AV8* (Ciba, one-component glue)

Setting time is about four hours at 150 °C to 160 °C. To prevent the depolarization of the PXE material, higher temperatures should be avoided (see Section B.2). The glue displays a very low mechanical damping and properties almost independent of temperature up to more than 70 °C.

##### 2. *Araldite AW142* (Ciba, one-component glue)

A slightly flexible, quick-setting, variety of Araldite AV8. The setting time is about 1 hour at 120 °C.

##### 3. *Araldite D* (Ciba, two-component glue)

Setting time is about 24 hours at 20 °C, however, it is better to let the glue set for 30 minutes at 100 °C, or 10 minutes at 130 °C. Damping is slightly greater than that of the glues mentioned under 1 and 2, and the properties are only sufficiently independent of temperature below 50 °C.

### B.1.2 GLUES FOR POWER TRANSDUCERS

1. For bonding the coupling portions of assembled composite 'sandwich' transducers to the tank (Section 8.5), Araldite AV141 (Ciba, one-component glue) is recommended. Setting time is about 2 hours at 140 °C. It is advantageous to 'reinforce' the bonding layer with a copper gauze (mesh about 0,5 mm, wire diameter about 0,3 mm).
2. For bonding a disc type resonator (Section 8.6), Eccobond 45 + 50% Catalyst 15 (Emerson & Cuming) with a setting time of about 4 hours at 50 °C, is recommended.

## B.2 Soldering

The electrodes on our piezoelectric transducer elements are usually made of silver. A strong joint between the silver and the ceramic body is made by firing a silver paste on to the ceramic surface. The thickness of the resulting silver layer is about 25 microns and can be used for soldering purposes if the following rules are observed.

### B.2.1 SOLDERING WIRES ONTO A TRANSDUCER ELECTRODE

The electrode surface should be free from grease and dust. Suggested soldering prescription:

- soldering iron: Oryx type 6A, with non-coated copper tip;
- soldering iron temperature: 250 °C to 300 °C;
- solder: Sn/Pb 60/40;
- soldering time: 5 s ± 2 s;
- flux: 502 (750 g of resin, 250 g of isopropylalcohol and 2,5 g of DMA as an activator),
- standard wire diameter: 0,2 mm.

All flux remnants should be carefully removed.

The soldering time should be kept as short as possible; otherwise the solder will dissolve the silver layer (to an extent depending on temperature and time), and polarization might be partly destroyed. Dissolving of the silver layer can be avoided by using a silver-saturated solder, but a higher soldering temperature is then required.

### B.2.2 SOLDERING MAJOR FACES OF TRANSDUCER PLATES

Before making a soldered joint between two PXE plates, or between a PXE plate and a solid body, the plates should be heated to a temperature above the melting point of the solder. It is recommended that a low melting point solder be used such as 52% Bi, 32% Pb and 16% Sn (Newton alloy, melting point about 95 °C), to prevent thermal depolarization of the PXE material. Some thermal depolarization figures are given below. The temperatures given are those at which, after an exposure time of about 1 hour, the  $k_p$  of the PXE is reduced by 10% (20% in the case of the temperatures in parentheses).

PXE4 - 160 °C (190 °C);  
PXE5 - 170 °C (210 °C),  
PXE41 - 200 °C (280 °C).

## Appendix C Temperature graphs

The graphs in this appendix concern grades PXE4, PXE5, PXE6, PXE7, PXE21, PXE22 and PXE41. They show how temperature affects different quantities which are of interest to designers of PXE transducers.

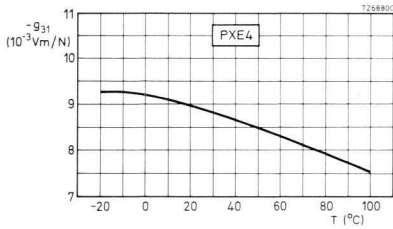


Fig. C.1(a)  $-g_{31}$  as a function of temperature for PXE4.

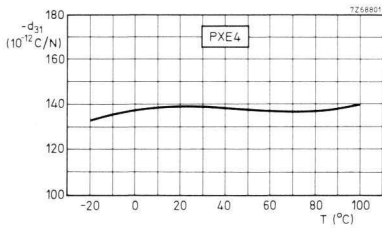


Fig. C.1(b)  $-d_{31}$  as a function of temperature for PXE4.

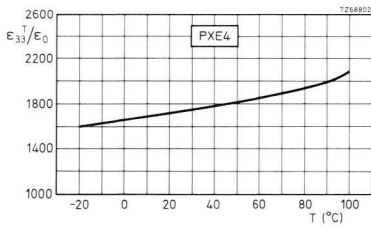


Fig. C.1(c)  $\epsilon_{33}^T/\epsilon_0$  as a function of temperature for PXE4.

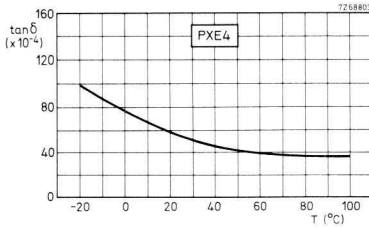


Fig. C.1(d)  $\tan \delta$  as a function of temperature for PXE4.

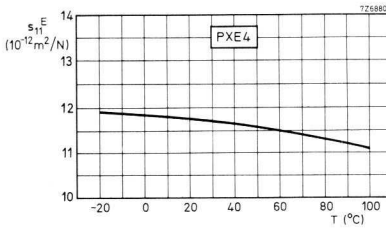


Fig. C.1(e)  $s_{11}^E$  as a function of temperature for PXE4.

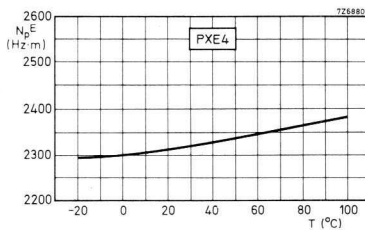


Fig. C.1(f)  $N_p^E$  as a function of temperature for PXE4.

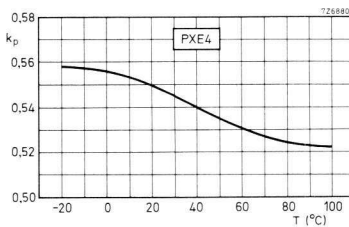


Fig. C.1(g)  $k_p$  as a function of temperature for PXE4.

Fig. C.1(a)-(g) The temperature dependence of various PXE4 parameters.

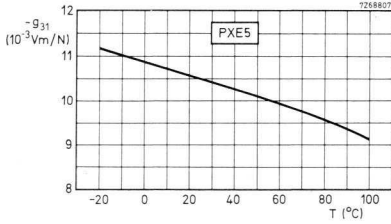


Fig. C.2(a)  $-g_{31}$  as a function of temperature for PXE5.

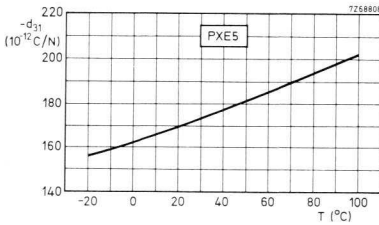


Fig. C.2(b)  $-d_{31}$  as a function of temperature for PXE5.

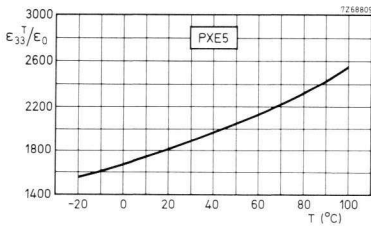


Fig. C.2(c)  $\epsilon_{33}^T/\epsilon_0$  as a function of temperature for PXE5.

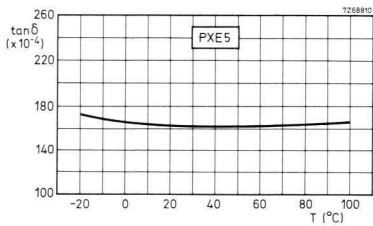


Fig. C.2(d)  $\tan \delta$  as a function of temperature for PXE5.

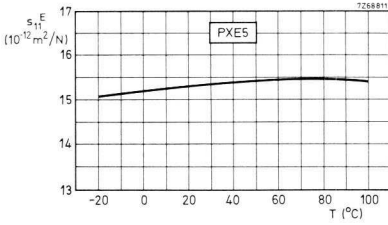


Fig. C.2(e)  $s_{11}^E$  as a function of temperature for PXE5.

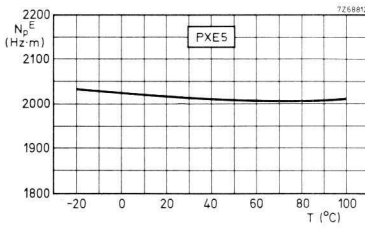


Fig. C.2(f)  $N_p^E$  as a function of temperature for PXE5.

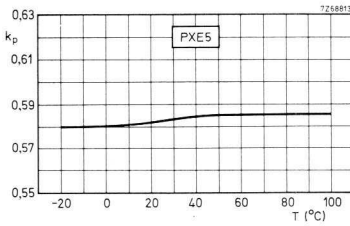


Fig. C.2(g)  $k_p$  as a function of temperature for PXE5.

Fig. C.2(a)-(g) The temperature dependence of various PXE5 parameters.

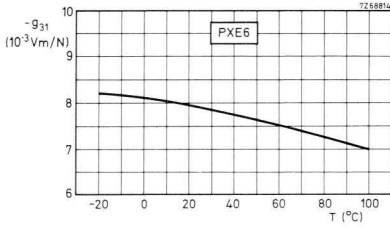


Fig. C.3(a)  $-g_{31}$  as a function of temperature for PXE6.

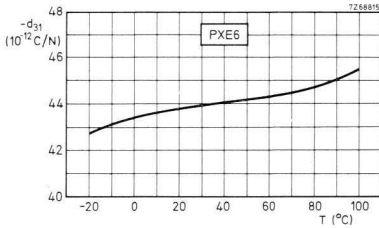


Fig. C.3(b)  $-d_{31}$  as a function of temperature for PXE6.

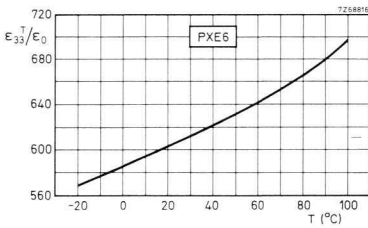


Fig. C.3(c)  $\epsilon_{33}^T/\epsilon_0$  as a function of temperature for PXE6.

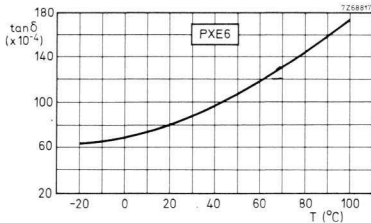


Fig. C.3(d)  $\tan \delta$  as a function of temperature for PXE6.

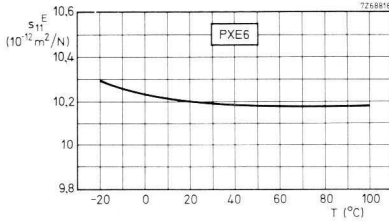


Fig. C.3(e)  $s_{11}^E$  as a function of temperature for PXE6.

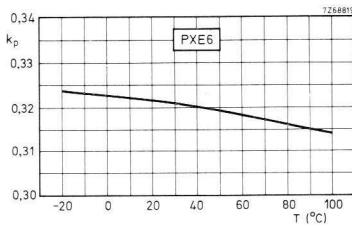


Fig. C.3(f)  $k_p$  as a function of temperature for PXE6.

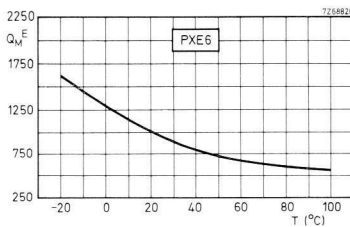


Fig. C.3(g)  $Q_M^E$  as a function of temperature for PXE6.

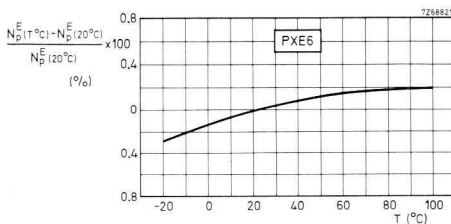


Fig. C.3(h)  $N_p^E(T^\circ\text{C}) - N_p^E(20^\circ\text{C}) / N_p^E(20^\circ\text{C}) \times 100\%$  as a function of temperature for PXE6.

Fig. C.3(a)-(h) The temperature dependence of various PXE6 parameters.

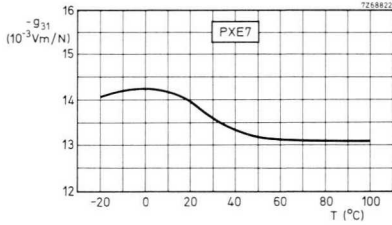


Fig. C.4(a)  $-g_{31}$  as a function of temperature for PXE7.

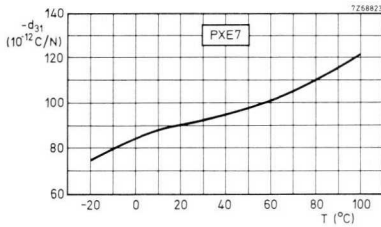


Fig. C.4(b)  $-d_{31}$  as a function of temperature for PXE7.

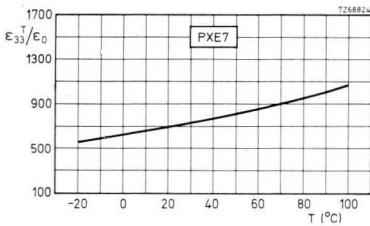


Fig. C.4(c)  $\epsilon_{33}^T/\epsilon_0$  as a function of temperature for PXE7.

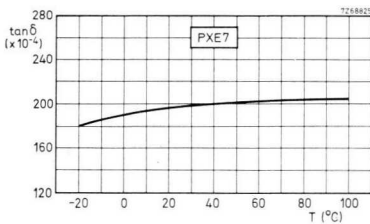


Fig. C.4(d)  $\tan \delta$  as a function of temperature for PXE7.

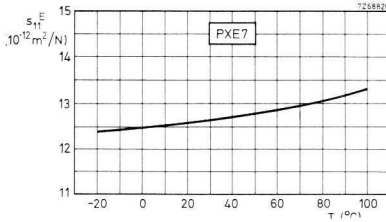


Fig. C.4(e)  $s_{11}^E$  as a function of temperature for PXE7.

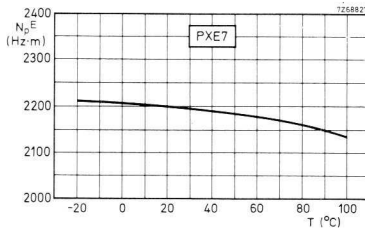


Fig. C.4(f)  $N_p^E$  as a function of temperature for PXE7.

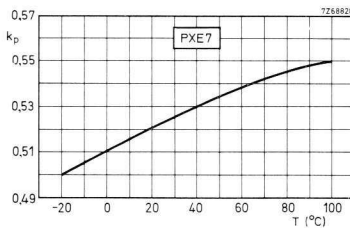


Fig. C.4(g)  $k_p$  as a function of temperature for PXE7.

Fig. C.4(a)-(g) The temperature dependence of various PXE7 parameters.

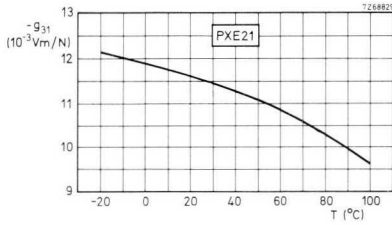


Fig. C.5(a)  $-g_{31}$  as a function of temperature for PXE21.

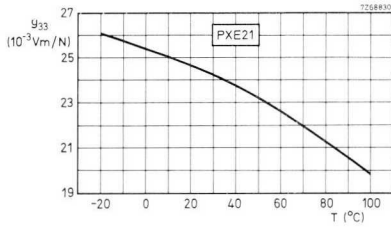


Fig. C.5(b)  $g_{33}$  as a function of temperature for PXE21.

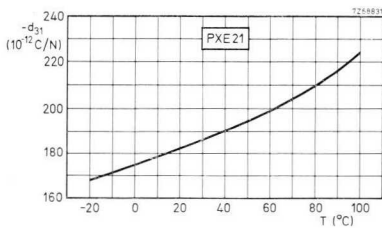


Fig. C.5(c)  $-d_{31}$  as a function of temperature for PXE21.

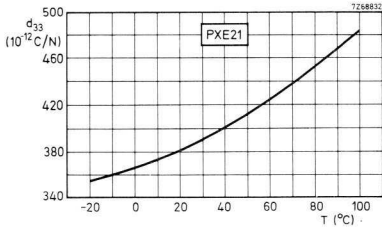


Fig. C.5(d)  $d_{33}$  as a function of temperature for PXE21.

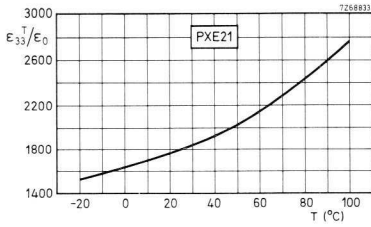


Fig. C.5(e)  $g_{33}^T/\epsilon_0$  as a function of temperature for PXE21.

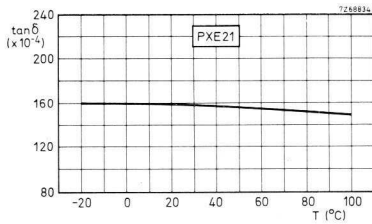


Fig. C.5(f)  $\tan \delta$  as a function of temperature for PXE21.

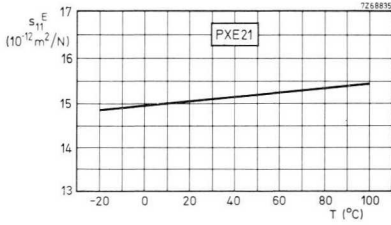


Fig. C.5(g)  $s_{11}^E$  as a function of temperature for PXE21.

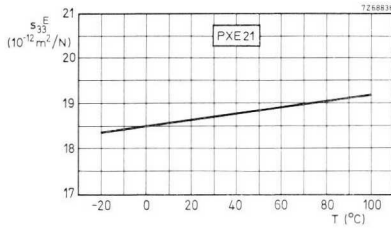


Fig. C.5(h)  $s_{33}^E$  as a function of temperature for PXE21.

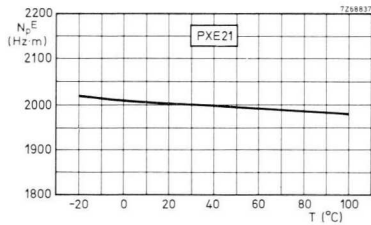


Fig. C.5(i)  $N_p^E$  as a function of temperature for PXE21.

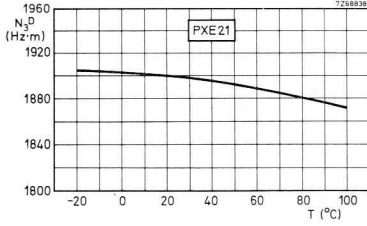


Fig. C.5(j)  $N_3^D$  as a function of temperature for PXE21.

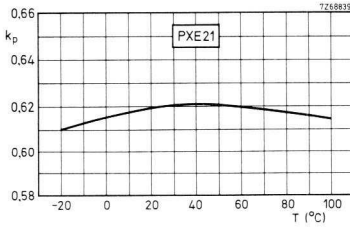


Fig. C.5(k)  $k_p$  as a function of temperature for PXE21.

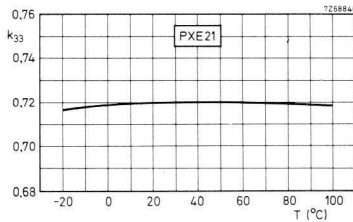


Fig. C.5(l)  $k_{33}$  as a function of temperature for PXE21.

Fig.C.5(a)-(l) The temperature dependence of various PXE21 parameters.

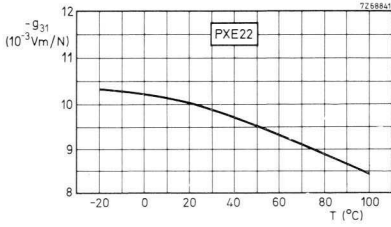


Fig. C.6(a)  $-g_{31}$  as a function of temperature for PXE22.

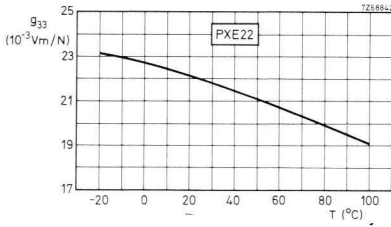


Fig. C.6(b)  $g_{33}$  as a function of temperature for PXE22.

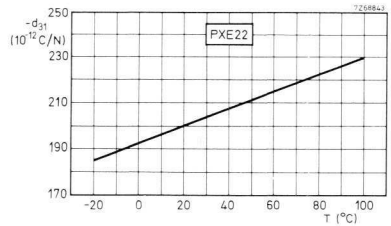


Fig. C.6(c)  $-d_{31}$  as a function of temperature for PXE22.

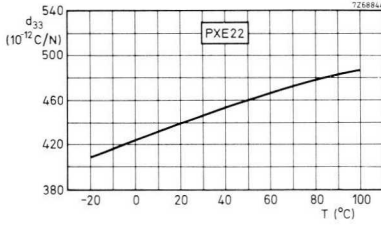


Fig. C.6(d)  $d_{33}$  as a function of temperature for PXE22.

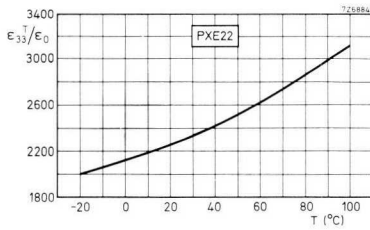


Fig. C.6(e)  $\epsilon_{33}^T/\epsilon_0$  as a function of temperature for PXE22.

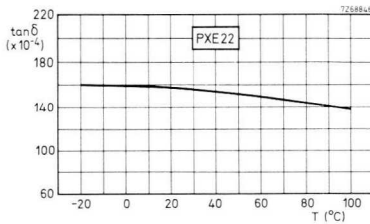


Fig. C.6(f)  $\tan \delta$  as a function of temperature for PXE22.

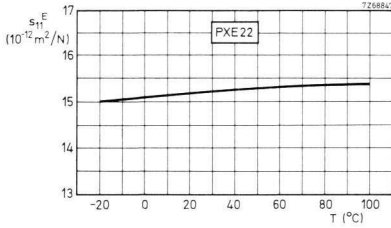


Fig. C.6(g)  $s_{11}^E$  as a function of temperature for PXE22.

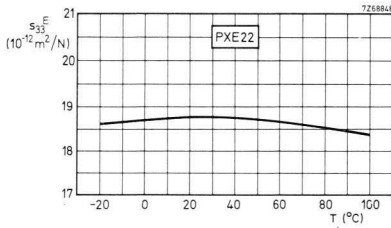


Fig. C.6(h)  $s_{33}^E$  as a function of temperature for PXE22.

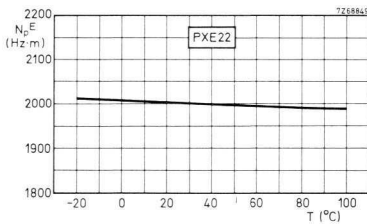


Fig. C.6(i)  $N_p^E$  as a function of temperature for PXE22.

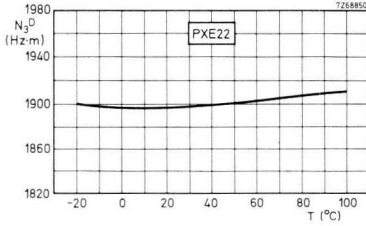


Fig. C.6(j)  $N_3^D$  as a function of temperature for PXE22.

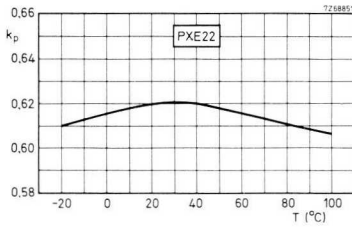


Fig. C.6(k)  $k_p$  as a function of temperature for PXE22.

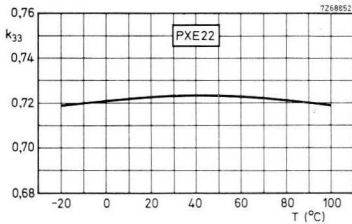


Fig. C.6(l)  $k_{33}$  as a function of temperature for PXE22.

Fig. C.6(a)-(l) The temperature dependence of various PXE22 parameters.

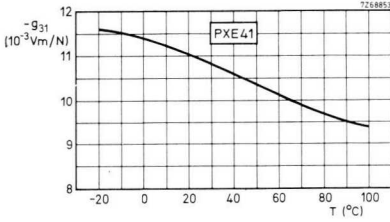


Fig. C.7(a)  $-g_{31}$  as a function of temperature for PXE41.

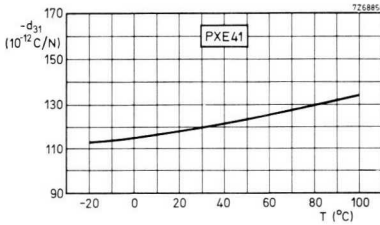


Fig. C.7(b)  $-d_{31}$  as a function of temperature for PXE41.

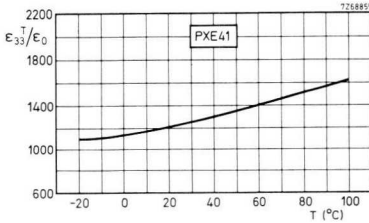


Fig. C.7(c)  $\epsilon_{33}^T/\epsilon_0$  as a function of temperature for PXE41.

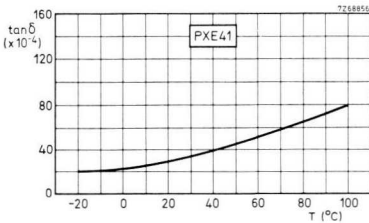


Fig. C.7(d)  $\tan \delta$  as a function of temperature for PXE41.

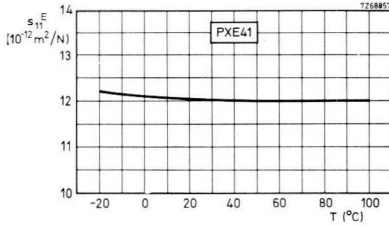


Fig. C.7(e)  $s_{11}^E$  as a function of temperature for PXE41.

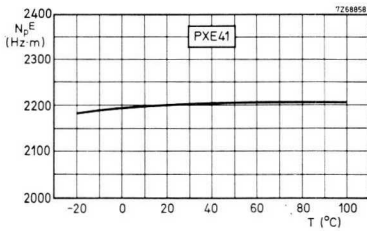


Fig. C.7(f)  $N_p^E$  as a function of temperature for PXE41.

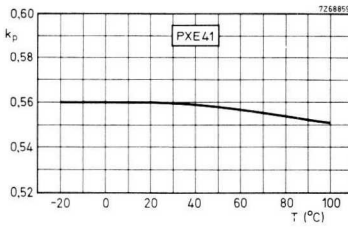


Fig. C.7(g)  $k_p$  as a function of temperature for PXE41.

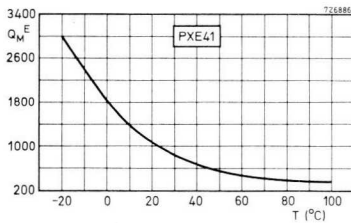


Fig. C.7(h)  $Q_M^E$  as a function of temperature for PXE41.

Fig. C.7(a)-(h) The temperature dependence of various PXE41 parameters.

## Appendix D Coupling coefficient chart

The graph of Fig. D.1 shows the relationship between the various material coupling coefficients and the relative frequency interval between  $f_s$  and  $f_p$  for the relevant fundamental resonance. The curves are related to three different modes of vibration.

(a) Thin-walled ring resonators in uniform radial vibration:

$k_u$  as a function of  $\Delta f/f_s$ .

(b) Half-wavelength resonators:

wave propagation perpendicular to the a.c. field:

$k_{\lambda/2\perp}$  as a function of  $\Delta f/f_s$ ;

wave propagation parallel to the a.c. field:

$k_{\lambda/2\parallel}$  as a function of  $\Delta f/f_p$ .

(c) Planar (radial) thin disc resonators:

$k_p$  as a function of  $\Delta f/f_s$ .

The effective coupling coefficient of an arbitrary type of resonator (including types (a), (b) and (c)), either at the fundamental resonance or at any overtone, can also be read off immediately because  $k_{eff}$  is given by the same mathematical relation as the coupling coefficient of a thin ring resonator (type (a))

$$\frac{k_{eff}^2}{1 - k_{eff}^2} = \frac{f_p^2 - f_s^2}{f_s^2}; \quad (D.1)$$

$k_{eff}$  as a function of  $\Delta f/f_s$ .

In the case of a thin ring the simple expression holds that

$$k_{eff} = k_u, \quad (D.2)$$

whereas, for resonators of the types (b) and (c), consisting of one piece and provided with full electrodes, we have that

$$k_{eff} \approx 0,9k.$$

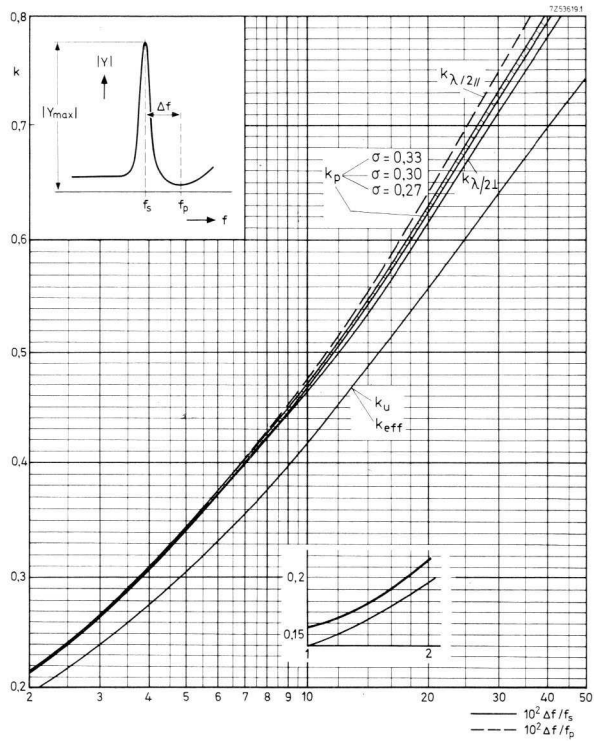


Fig. D.1 Various coupling coefficients as functions of the relative frequency interval between series and parallel resonant frequency.

*Equations pertaining to Fig. D.1*

The relationships given below are only valid when the resonance is sufficiently strong for the following condition to be met:

$$\left| \frac{Y_{\max}}{Y_u} \right| \frac{f_u}{f_s} \geq 10.$$

The term  $Y_u$  is the admittance at a frequency  $f_u$ , far below  $f_s$ .

$$\left. \begin{aligned} \frac{k^2_{mn\ e f f}}{1 - k^2_{mn\ e f f}} \\ \frac{k^2_{mn\ u}}{1 - k^2_{mn\ u}} \end{aligned} \right\} = 2 \frac{\Delta f}{f_s} \left( 1 + \frac{1}{2} \cdot \frac{\Delta f}{f_s} \right) \equiv \frac{f_p^2 - f_s^2}{f_s^2}; \tag{D.3}$$

$$\frac{k^2_{mn\ \lambda/2\perp}}{1 - k^2_{mn\ \lambda/2\perp}} = \frac{\pi}{2} \left( 1 + \frac{\Delta f}{f_s} \right) \tan \left( \frac{\pi}{2} \cdot \frac{\Delta f}{f_s} \right) \tag{D.4}$$

(if the waves are propagated perpendicularly to the a.c. field);

$$k^2_{mn\ \lambda/2\parallel} = \frac{\pi}{2} \left( 1 - \frac{\Delta f}{f_p} \right) \tan \left( \frac{\pi}{2} \cdot \frac{\Delta f}{f_p} \right) \tag{D.5}$$

(if the wave propagation and the a.c. field have the same direction, e.g., for  $k_{33\ \lambda/2}$  and  $k^2_{t\ \lambda/2}$ );

$$\frac{k_p^2}{1 - k_p^2} = \frac{1 - \sigma_{12}^E}{1 + \sigma_{12}^E} - \frac{R_1}{1 + \sigma_{12}^E} \frac{J_0 \left\{ R_1 \left( 1 + \frac{\Delta f}{f_s} \right) \right\}}{J_1 \left\{ R_1 \left( 1 + \frac{\Delta f}{f_s} \right) \right\}}, \tag{D.6}$$

where  $J_0$  and  $J_1$  represent the zero-order and first-order primary Bessel functions.

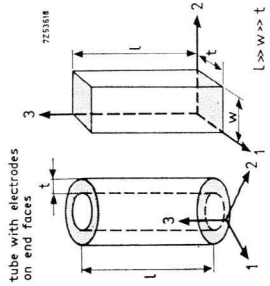
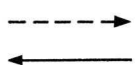
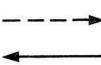
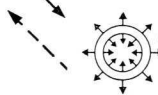
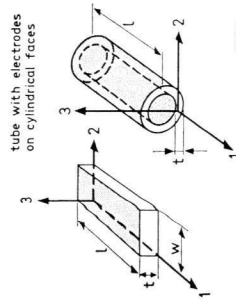
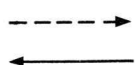
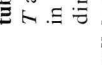
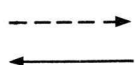
The term  $R_1 = \omega_1 r/c$  is the lowest positive root of the equation

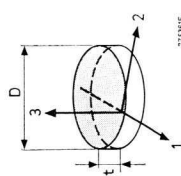
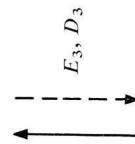
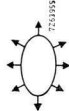
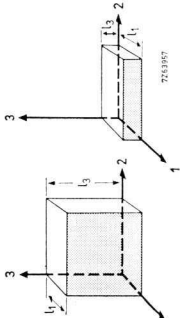
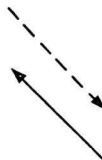
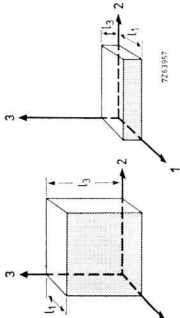
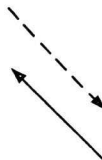
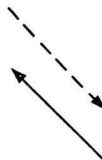
$$(1 - \sigma_{12}^E) J_1(R) = R J_0(R).$$

In the equations of the previous sentence,  $r$  is the radius of the disc,  $c$  is the velocity of sound in the plane of the disc with zero a.c. field, and  $\sigma_{12}^E$  is Poisson's ratio for the material of the disc, in the plane of the disc at zero field, i.e.,  $\sigma_{12}^E = S_{12}^E/S_{11}^E$ . For example,  $R_1 = 2,05$  for  $\sigma_{12}^E = 0,30$ .

## **Appendix E**

Survey of seven important modes of vibration and their associated coupling coefficients  $k$  and frequency constants  $N$ . In literature, symbol  $N_3$  (frequency constant for the length mode with parallel excitation) has often been used for denoting the frequency constant for the thickness mode with parallel excitation indicated as  $N_t$  here.

resonant element with electrodes	biasing polarization	a.c. field and polarization	main component of a.c. stress and strain	conditions satisfied	pertinent coupling factor and frequency constant vibrational mode
 <p>tube with electrodes on end faces</p> <p>7253896</p>		 <p><math>E_3, D_3</math></p>	 <p><math>T_3, S_3</math></p> <p>(axial direction in tube)</p> <p>parallelepiped</p>  <p><math>T_1, S_1</math></p> <p>tube <math>T</math> and <math>S</math> in radial direction</p>	$S_1 = S_2 = 0$ $T_1 = T_2 = 0$	$(k_{33})T_1 T_2 = k_{33}$ $(N_1^E)T_1 T_2 = N_3 = f_1 l$ <p>length mode with parallel excitation</p>
 <p>tube with electrodes on cylindrical faces</p> <p>7253906</p>		 <p><math>E_3, D_3</math></p>	 <p><math>T_3, S_3</math></p> <p>tube <math>T</math> and <math>S</math> in radial direction</p> <p>parallelepiped</p>  <p><math>T_1, S_1</math></p> <p>(axial direction in tube)</p>	$S_1 = S_2 = 0$ $T_1 = T_3 = 0$	$(k_{33})S_1 S_2 = k_t$ $(N_3^E)S_1 S_2 = N_t = f_1 t$ <p>thickness mode with parallel excitation</p>
		 <p><math>E_3, D_3</math></p>		$S_2 = S_3 = 0$ $T_2 = T_3 = 0$	$(k_{31})T_2 T_3 = k_{31}$ $(N_1^E)T_2 T_3 = N_1 = f_1 l$ <p>length mode with transverse excitation</p>

			 <p><math>T_1, S_1</math></p> <p>(radial direction) (also <math>T_2, S_2</math> in circular direction)</p>	<p><math>S_3 = 0</math> <math>T_3 = 0</math></p>	<p><math>k_{31} \sqrt{2(1-\sigma)} = k_p</math> <math>N_p^E = N_p = P_p D</math> planar mode with transverse excitation</p>
			<p>shear in 31-plane</p> <p><math>T_5, S_5</math></p>	<p><math>S_1 = S_2 = 0</math> <math>T_1 = T_2 = 0</math></p>	<p><math>(k_{33})S_1 S_2 = k_t</math> <math>(N_3^E)S_1 S_2 = N_t = f_r t</math> thickness mode with parallel excitation</p>
			<p>propagation of shear waves in 1-direction if <math>l_1 = t \ll l_3</math>, in 3-direction if <math>l_3 = t \ll l_1</math></p>	<p><math>k_5</math> <math>N_5^E = N_5 = f_r t</math> thickness shear mode thickness <math>t</math> being <math>l_1</math> or <math>l_3</math> whichever is smaller</p>	

## Appendix F S.I. units

It is strongly recommended that all calculations relating to piezoelectricity are done in S.I. units. This system is, in general, the most convenient one to use and, when one is concerned with electromechanical interaction, its use is virtually essential if confusion is to be avoided. A description of the basic features of the system is given below, together with many of the relevant units for piezoelectric calculations and conversion factors for other commonly used units. The units for the piezoelectric parameters are not given here, they are discussed fully in Chapter 2.

The international system of units (S.I.) uses six base units as shown in Table F.I.

Table F.I. Base units.

base unit	symbol	quantity
metre	m	length
kilogramme	kg	mass
second	s	time
ampere	A	electric current
kelvin	K	thermodynamic temperature
candela	cd	luminous intensity

Note:  $K = ^\circ C + 273,15$ .

Decimal multiples and sub-multiples of the S.I. units are formed by means of the prefixes given below.

$10^{12}$ = tera = T	$10^{-1}$ = deci = d
$10^9$ = giga = G	$10^{-2}$ = centi = c
$10^6$ = mega = M	$10^{-3}$ = milli = m
$10^3$ = kilo = k	$10^{-6}$ = micro = $\mu$
$10^2$ = hecto = h	$10^{-9}$ = nano = n
10 = deca = da	$10^{-12}$ = pico = p
	$10^{-15}$ = femto = f
	$10^{-18}$ = atto = a

Examples: the meganewton ( $\text{MN} = 10^6 \text{ N}$ ) and the  
 micrometre ( $\mu\text{m} = 10^{-6} \text{ m}$ )  
 the kilowatt ( $\text{kW} = 10^3 \text{ W}$ ) and the  
 nanosecond ( $\text{ns} = 10^{-9} \text{ s}$ ).

In principle any one of these prefixes may be used with any unit although the prefixes hecto, deca, deci and centi should be avoided where possible.

The decimal sign is a comma on the line.

Where there are more than four figures to right or left of the decimal sign, a full space should divide each group of 3 figures counting from the position of the decimal sign.

e.g. 25 000

but 2500

If the magnitude of the number is less than unity, the decimal sign is preceded by a zero, e.g., 0,5  $\text{m}^2$ .

When a compound unit is formed by multiplication of two or more units it is only necessary to use a dot between unit symbols where ambiguity would otherwise occur.

Examples: Nm and not N.m

m.N (metre-newton) and not mN (millinewton).

Tables F.II and F.III give information on the units of the basic quantities referred to in this book. The second columns show units together with convenient multiples and sub-multiples recommended for general use. *For calculations only the units printed in bold type should be used.* The third columns give conversion factors for other commonly used units.

Table F.II. Miscellaneous and mechanical units.

parameter	unit	remarks and conversion factors	
length	<b>m</b>	km (metre)	
		mm	
		$\mu\text{m}$	
		nm	
time	<b>s</b>	h (hour) min (minute) (second) ms $\mu\text{s}$ ns	
	<b>m/s</b>	1 ft/s = 0,3048 m/s*	
		1 mph = 1,609 34 km/h	
	mass	<b>kg</b>	t (tonne) (kilogramme) g mg $\mu\text{g}$
			1 t = 1000 kg
		1 ton = 1,016 05 t	
		1 lb = 0,453 592 37 kg*	
frequency		MHz kHz	
	<b>Hz</b>	(hertz)	
mass density	<b>kg / m<sup>3</sup></b>	1 lb/ft <sup>3</sup> = 16,0185 kg/m <sup>3</sup>	
		g/cm <sup>3</sup>	
force	<b>N</b>	MN kN (newton) mN	
		1 N = 1 kg.m/s <sup>2</sup>	
		1 tonf = 9,964 02 kN	
		1 lbf = 4,448 22 N	
		1 kgf = 9,806 65 N*	
	1 dyn = 0,01 mN		

Table F.II (continued)

parameter	unit	remarks and conversion factors
moment of force (bending moment) torque	MNm	1 lbfft = 1,355 82 Nm
	kNm	1 lbfin = 112,985 mNm
	<b>Nm</b>	
	mNm	
	$\mu$ Nm	
stress tensile strength modulus of elasticity	MPa	1 Pa = 1 N/m <sup>2</sup>
	kPa	1 lbf/in <sup>2</sup> = 6894,76 Pa
	<b>Pa</b> (pascal)	1 tonf/in <sup>2</sup> = 15,4443 MPa
		1 kgf/mm <sup>2</sup> = 9,806 65 MPa
pressure	MPa	1 in <i>H<sub>2</sub>O</i> = 249,089 Pa
	kPa	1 in <i>Hg</i> = 3,386 39 kPa
	<b>Pa</b> (pascal)	1 lbf/in <sup>2</sup> = 6,894 76 kPa
	mPa	1 bar = 100 kPa
		1 torr = 133,322 Pa
work energy heat, quantity of heat	kJ	1 J = 1 Nm = 1 Ws
	<b>J</b> (joule)	1 Btu = 1,055 06 kJ
	mJ	1 ftlbf = 1,355 82 J
	$\mu$ J	1 therm = 105,506 MJ
		1 cal <sub>IT</sub> = 4,1868 J*
power	kW	1 W = 1 J/s = 1 Nm/s
	<b>W</b> (watt)	1 hp = 745,700 W
	mW	1 ftlbf/s = 1,355 82 W
	$\mu$ W	
customary temperature	$^{\circ}\text{C}$ (degree Celsius)	$^{\circ}\text{F} = (9/5 ^{\circ}\text{C}) + 32$
thermal conductivity	<b>W/(m<math>^{\circ}\text{C}</math>)</b>	1 Btu in/ft <sup>2</sup> h $^{\circ}\text{F}$ = 0,144 228 W/(m $^{\circ}\text{C}$ )

\* Exact conversion.

Table F.III. Electrical units.

parameter	unit	remarks and conversion factors
current	<b>A</b> (ampere)	
	mA	
	$\mu$ A	
	nA	
	pA	
electric charge	<b>C</b> (coulomb)	1 C = 1 As
	mC	
	$\mu$ C	
electric potential	kV	1 V = 1 W/A
	<b>V</b> (volt)	
	mV	
	$\mu$ V	
electric field strength	<b>V/m</b>	
	kV/mm	
	V/mm	
capacitance	<b>F</b> (farad)	1 F = 1 As/V
	$\mu$ F	
	nF	
	pF	
inductance	<b>H</b> (henry)	1 H = 1 Vs/A
	mH	
	$\mu$ H	
resistance impedance reactance	G $\Omega$	1 $\Omega$ = 1 V/A
	M $\Omega$	
	k $\Omega$	
	<b><math>\Omega</math></b> (ohm)	
	m $\Omega$	
	$\mu\Omega$	
conductance admittance susceptance	kS	1 S = 1 A/V = 1/ $\Omega$
	<b>S</b> (siemens)	1 $\overline{\Omega}$ (mho) = 1 S
	mS	
	$\mu$ S	

## REFERENCES

- [<sup>1</sup>] IRE Standards on Piezoelectric Crystals: Measurements of Piezoelectric Ceramics, 1961. Proc. IRE 49 (1961), pp. 1161-1169.
- [<sup>2</sup>] Hütte - Theoretische Grundlagen -, 28. Auflage, Verlag Wilhelm Ernst und Sohn, Berlin 1955.

## Index

The more important or useful references are given in a **bold** type face.

Accelerometers, 17, 43.

Acoustic

- delay lines, 146.
- impedance. *See* Impedance.
- matching. *See* Matching.
- shock waves, 26.

Adhesives. *See* Bonding techniques.

Aging. *See* Stability.

Air transducers, **78** et seq.

All-ceramic filters. *See* Filters.

Anharmonic vibration, 51, 65, 76, 87, 110.

Anti-resonant frequency  $f_p$ . *See* Resonant frequency (parallel).

**Bandwidth, 157** et seq.

- of a ceramic resonator, 64 et seq.
- of a high intensity sandwich transducer, 126.
- of an echo sounder transducer, 109, 114, 117.
- of an ultrasound air transducer, 89.
- of a shear mode transducer, 148.

Beaming. *See* Directivity.

Bandwidth. *See* Directivity.

Bilaminar cantilever. *See* Flexure elements.

Bimorph. *See* Flexure elements.

Bonding techniques (for piezoelectric transducers), 169.

- adhesives or glues, 169.
- solders, 170.

Cantilever mounting of flexure elements. *See* Flexure elements

Ceramic resonators, 21, **64** et seq.

Choppers (optical). *See* Light beam deflectors and choppers.

Cigarette lighters (ignition of). *See* Ignition systems.

Cleaning bath transducers. *See* High intensity transducers.

Compliance  $s$ , **8** et seq.

Composite transducers. *See* High intensity transducers.

Cookers, gas ignition. *See* Ignition systems.

- Corona discharge locators, 80, 103.
- Coupling coefficient  $k$ , **10 et seq.**, **13 et seq.**, 123, 162, 190 et seq.  
 effective (transducer) –  $k_{eff}$ , 123, 163, 190.  
 – material coupling coefficient of PXE, **11 et seq.**  
 planar or radial mode –  $k_p$ , 13.  
 thickness mode –  $k_t$ , 13.
- Coupling factor. *See* Coupling coefficient.
- Creep, in piezoelectric ceramics, 45. *See also* Hysteresis.
- Curie temperature, 4, 18, 19.
- Deflection**  
 – of flexure elements. *See* Flexure elements.  
 – of light beams. *See* Light beam deflectors and choppers.
- Delay lines, **146 et seq.**  
 transducer materials for –, 21, 154.
- Depolarization. *See* Depoling.
- Depoling, 15.  
 electrical –, 16, 52.  
 mechanical –, 16, 26, 52.  
 thermal –, 15.
- Detectors (mechano-electrical), 48.
- Diaphragm transducers, 41, 47, 81.
- Dielectric  
 – constant. *See* Permittivity.  
 – displacement  $D$ , **8 et seq.**  
 – loss factor,  $\tan \delta$ , 18, 19, 123, 159.
- Dipoles (in piezoceramics), 5.
- Direction dependence (of piezoelectric parameters), 11.
- Directivity (of acoustic transducers)  
 – in air, 85.  
 – in water, 109.  
 – shear wave in a solid delay line, 150.
- Disc transducers  
 high power –, 143.  
 low power –, 81.
- Domains (ferroelectric), 4.
- Doppler effect, 80, 97.
- Echo sounder, 108 et seq.**  
 – directivity characteristic, 109, 110, 115.  
 – indicator or display stage, 108.  
 – maximum range, 109.  
 – operating frequency, 109.  
 – receiver stage, 120.

- resolution or minimum measuring distance, 109.
  - transducer, 110.
  - transmitter stage, 118.
- Edge-clamped mounting of diaphragm transducers, 82, 85.
- Edge-pinned mounting of diaphragm transducers, 106.
- Effective coupling coefficient  $k_{eff}$ . *See* Coupling coefficient.
- Efficiency, 11. *See also* Electroacoustic efficiency.
- Electrical
- behaviour (of a piezoelectric medium), 8 **et seq.**
  - behaviour (of a piezoelectric transducer), 64 *et seq.*, 88, 157 *et seq.*
  - depoling. *See* Depoling.
  - energy (in a stressed piezoelectric medium), 26.
  - impedance of a piezoelectric transducer. *See* Impedance.
  - matching. *See* Matching.
  - quality factor  $Q_e$ . *See* Quality factor. *See also* Dielectric loss factor.
- Electric
- dipole, 1, 4 *et seq.*
  - field strength, 6 *et seq.*, 200. *See also* Maximum permissible electrical field strength.
- Electroacoustic
- behaviour. *See* Electroacoustic transducers.
  - efficiency, 123.
  - energy (in a stressed piezoelectric medium), 26.
  - transducers for gases, 78 *et seq.*
  - transducers for liquids, 108 *et seq.*, 123 *et seq.*
- Electrodes, 5, 170.
- Electro-mechanical
- behaviour of flexure elements, 45.
  - conversion, 7.
  - coupling coefficient. *See* Coupling coefficient.
- Encapsulation
- of delay lines, 157.
  - of echo sounder transducer, 111.
  - of ignition unit, 34.
  - of piezoelectric resonators, 68.
  - of ultrasound air transducer, 87.
- Ends clamped mounting of flexure elements, 42.
- Ends pinned mounting of flexure elements, 42, 47, 49, 50.
- Energy trapping (in PXE resonators), 76.
- Equivalent circuits, 157.
- flexure elements, 52.
  - resonators, 68.
  - tuned transducers, 165.
  - ultrasound air transducers, 88.

- Far field (of acoustic beam), 85, 114, 151.
- Fatigue strength
- of epoxy glues, 134, 135.
  - of metals and alloys, 131, 132.
  - of PXE, 134, 135.
- Feedback plates (for frequency control), 17.
- Ferroelectric materials, 4 et seq.
- Field strength. *See* Electric field strength.
- Filters (electrical), 64 et seq.
- Fine movement control, 17, 22, 43.
- Flashover (PXE high voltage generators), 25, 35.
- Flaw detectors, 3.
- Flexure elements.
- available displacement or deflection, 44.
  - available force, 44.
  - bimorph (bilaminar element) -, 40 et seq.
  - disc -, 42, 47, 81 et seq., 110.
  - mounting methods, 42, 81.
  - multimorph -, 41 et seq.
  - non-resonant operation of -, 45.
  - parallel operation of -, 42.
  - plate -, 81, 87.
  - resonant operation of -, 49.
  - trimorph (trilaminar element) -, 41.
- Four-channel ultrasonic receiver, 98.
- Four-channel ultrasonic transmitter, 94.
- Fraunhofer region. *See* Far field.
- Frequency constant  $N$ , 14 et seq.
- Fresnel region. *See* Near field.
- Gas appliances (ignition of).** *See* Ignition systems.
- Generator action (piezoelectric), 6.
- application examples, 6.
- Glues, *See* Bonding techniques.
- Gramophone pick-up. *See* Pick-up elements.
- Half-value distances (of ultrasonic beams in air),** 81, 90.
- Half-wave resonators. *See* Resonators.
- Helmholtz resonator, 104.
- High intensity transducers, 123.
- non-pre-stressed -, 134, 143, 170.
  - pre-stressed -, 136, 170.
- High power transducers. *See* High intensity transducers.
- High tension lead (of ignition unit), 33.

Housing. *See* Encapsulation.

Hydrophones, 17, 116.

Hysteresis (in PXE), 17, 45.

Ignition systems (piezoelectric), 23.

  impact –, 30, 36.

  internal insulation of –, 35.

  static (squeeze) –, 23, 35.

Impedance

  acoustic –, 30, 42, 112, 124 et seq.

  electrical –, 68, 89, 159 et seq.

Intercom systems (ultrasonic), 80.

Intruder alarm systems, 78, 79, **97**.

Isopaustic glass (in delay lines), 148, 158.

Lead zirconate titanate, 17.

Leak detectors, 80, 103.

Light beam deflectors and choppers, 43, 62.

Liquid level sensors, 44, 59.

  liquid damped –, 61.

  tuning fork –, 59.

Losses, electrical, mechanical. *See* Quality factor.

Low-frequency filters, 44.

Matching

  acoustic or mechanical –, 53, 112, 134, **164**.

  electrical –, 90, 113, 120, **164**.

Material parameters of PXE, 8 et seq.

Maximum

  – admittance frequency  $f_m$ . *See* Minimum impedance frequency.

  – impedance frequency  $f_n$ , 68, **159**.

  – output (from flexure elements)

    – non-resonant operation, 52.

    – resonant operation, 53.

  – permissible electric field strength for PXE  $E_{max}$ , 7, 52.

  – permissible mechanical stress for PXE, 26, 52, 134.

  – permissible operating power, 53, 142.

Mechanical

  – behaviour of a piezoelectric medium, 9.

  – depoling. *See* Depoling.

  – energy of a piezoelectric transducer  $W_m$ , **24** et seq.

  – pre-stress, **136** et seq.

  – quality factor  $Q_m$ . *See* Quality factor.

  – resonance, 8.

- resonant frequency
- - of a disc or diaphragm, 82, 106.
- - of a flexure bar, 50.
- stress  $T$ , 7 et seq. *See also* Maximum permissible mechanical stress for PXE.
- Mechano-electrical
  - behaviour of flexure elements, 48.
  - conversion, 7.
  - transducers, 43.
- Medical equipment (application of PXE), 2.
- Metal
  - disc transducers, 81, 143.
  - end piece
  - - in high intensity sandwich transducers, 126.
  - - in PXE ignition units, 34.
- Microphones, 2, 17, 43.
  - telephone -, 106.
  - ultrasonic -, 78 et seq., **87**.
- Minimum
  - admittance frequency  $f_n$ . *See* Maximum impedance frequency  $f_n$ .
  - impedance frequency  $f_m$ , 68, **159**.
- Monolithic filters (PXE), 76.
- Motor action, 7. *See also* Electro-mechanical.
  - application examples, 7.
- Moulding compound, 34, 113. *See also* Encapsulation.
- Movement detectors. *See* Doppler effect.
- Multimorph. *See* Flexure elements.
- Multi-stage filters, 64, 71.
  
- Near field (of acoustic beam), 151.
- Nodes-supported mounting
  - of flexure bars, 42, 48, 50.
  - of flexure discs and plates, 82, 87.
- Non-destructive testing, 3.
- Non-resonant operation (of flexure elements). *See* Flexure elements.
  
- Optical scanners. *See* Light beam deflectors and choppers.
- Ovens (ignition of gas by PXE). *See* Ignition systems.
- Overtones, 51, 65, 86, 111.
  
- Parallel
  - operation of bimorph. *See* Flexure elements.
  - resonant frequency  $f_p$ . *See* Resonant frequency.
- Pascal (unit of pressure or stress), 6, 199.
- Permittivity (dielectric constant), 8 et seq.

- absolute –, 12.
  - of free space or vacuum, 12.
  - relative –, 12.
- Pick-up elements, 2, 17, 43, 49, 51, 54.
- Piezoelectric
- ceramic, 1, 4 et seq.
  - charge constant  $d$ , 7 et seq.
  - coupling coefficient. *See* Coupling coefficient.
  - equations, 8 et seq.
  - materials, 1, 4 et seq.
  - properties, 1, 4 et seq.
  - temperature dependence of properties. *See* Stability.
  - voltage constant  $g$ , 7 et seq.
- Piezoelectricity
- in ferroelectric ceramics, 1, 4 et seq.
  - range of application, 2, 3.
- Planar coupling coefficient  $k_p$ . *See* Coupling coefficient.
- Pocket lighters (with PXE ignition). *See* Ignition systems.
- Poling
- direction for different transducer modes, 42, 150, 158, 194, 195.
  - field, 5, 7.
  - treatment, 5.
  - voltage, 6.
- Polarization. *See* Poling.
- Potassium sodium niobate, PXE11. *See* PXE11.
- Power limit for operation of piezoelectric transducers, 53, 142.
- Pre-stress. *See* Mechanical pre-stress.
- Pressure sensors, 17.
- Proximity switch (ultrasonically remote controlled), 98.
- PXE4, 17, 23, 26, 28, 36, 52, 131, 137, 139, 171, 172, 173.
- PXE5, 17, 48, 49, 50, 52, 54, 61, 62, 81, 85, 103, 171, 174, 175.
- PXE6, 21, 64, 66, 70, 176, 177.
- PXE7, 21, 153, 154, 158, 178, 179.
- PXE11, 17, 21, 153, 154.
- PXE21, 21, 23, 26, 28, 31, 38, 180, 181, 182, 183.
- PXE22, 21, 23, 26, 28, 31, 38, 184, 185, 186, 187.
- PXE41, 21, 23, 26, 28, 31, 36, 38, 111, 131, 137, 139, 171, 188, 189.
- PXE42, 22, 131.
- PXE51, 22, 48, 50, 54.
- Quality control if PXE, 1.
- Quality factor  $Q$
- electrical –  $Q_e$ , 18, 19, 123. *See also* Dielectric loss factor.
  - mechanical –  $Q_m$ , 16, 18, 19, 52, 123, 162.

Quartz, 1.

**Radial mode**

- coupling. *See* Coupling coefficient.
- resonator, 65.
- vibration, 14.

Radio receiver (applications of PXE resonators), 64 et seq.

Record player pick-up. *See* Pick-up elements.

Relays (using PXE), 43.

**Remanent**

- deflection. *See* Creep.
- polarization. *See* Poling.

Remote control. *See* Ultrasonic applications.

Resonance range, 44, 159.

Resonant frequency, **159** et seq.

- anti -. *See* Resonant frequency, parallel.
- mechanical -, 49, 85, 106.
- parallel -, 88, 92, 93, 97, **162**, 190,
- series -, 68, 88, 92, **159**.

Resonant operation (of flexure elements). *See* Flexure elements.

**Resonators**

- 450 kHz to 480 kHz -, 65.
- 10,7 MHz -, 66.
- half-wave -, 123 et seq.
- planar or radial mode -, 14, 65.
- thickness mode -, 14, 66.

Safety belt security system, 105.

Sandwich transducer. *See* High intensity transducers.

**Series**

- operation of bimorph. *See* Flexure elements.
- resonant frequency  $f_s$ . *See* Resonant frequency, series.

**Shear**

- mode, 12, 21, 150.
- transducer, 153.
- waves, 150.

Side lobes (of sound field), 110.

Single-channel ultrasonic transmitter, 93.

**Soldering**

- equipment, 23.
- prescription or technique (for PXE), 170.

Sonar, 17.

**Sound**

- field plotter, 115.

- pressure, 85, 89, 92, 93, 94, 116.
  - transducers or generators, 43, **78** et seq.
- Spark
- energy, 38.
  - gap (for gas ignition), 25.
- Square bimorph PXE flexure elements. *See* Flexure elements, plate.
- Stability (of properties of PXE)
- temperature, 16, **172**.
  - time (aging), 16, **20**.
- Strain
- gauges, 43.
  - relative deformation  $S$ , 7 et seq.
  - to-stress ratio. *See* Compliance.
- Strength
- compressive –, 18, 19.
  - fatigue –, 131, 135.
  - tensile –, 18, 19.
- Stress
- gauges, 43.
  - maximum permissible for PXE, **26**, 52, 134.
- Subscripts, 11.
- Superscripts, 9 et seq.
- Switches, 43.
- Table lighters (PXE ignition of). *See* Ignition systems.
- $\tan \delta$ . *See* Dielectric loss factor.
- Telephone microphones. *See* Microphones.
- Temperature dependence of PXE properties, 16, 172.
- Thermal depoling. *See* Depoling.
- Thickness
- coupling coefficient  $k_t$ . *See* Coupling coefficient.
  - mode resonator, 66, 111, 194, 195.
  - shear mode resonator, 67, 150, 194, 195.
- Three-stage hybrid filter, 71.
- Tone generator, 103 et seq., 105.
- Total energy  $W_T$  (of a piezoelectric transducer), 24 et seq.
- Transducer
- echo sounder –, 108 et seq.
  - flexure mode –, 40 et seq., 78 et seq.
  - half-wave –, 123 et seq.
  - high power or intensity –. *See* High intensity transducers.
  - shear mode –, 146 et seq.
  - ultrasonic –, for air, 78 et seq.
  - ultrasonic –, for water, 108 et seq., 123 et seq.

Trilaminar elements, trimorphs. *See* Flexure elements.

Ultrasonic applications

- beams in air, 78 et seq.
- cleaning, 137, 143.
- delay lines, 146.
- drilling and machining (high intensity transducers), 2, **137**.
- echo sounders, 108.
- medical, 2.
- non-destructive testing, 3.
- remote control, 78, **98**.
- welding (high intensity transducers), 2, **137**.

Ultrasound. *See* Ultrasonic applications.

Vacuum permittivity  $\epsilon_0$ . *See* Permittivity.

Vibratory motors, 43, 54.

Vibrational modes

- flexure modes, 42, 81.
- general, 194, 195.

Voltage constant, piezoelectric, *g*, 7.

**Argentina**  
FAPESA I.y.C.  
Av. Crovara 2550  
Tel 652-7438/7478  
BUENOS AIRES

**Australia**  
Philips Industries Ltd.  
Elcoma Division  
67-71 Mars Road  
Tel. 42 1261  
LANE COVE, 2066, N.S.W.

**Austria**  
Österreichische Philips  
Bauelemente Industrie G.m.b.H.  
Zieglergasse 6  
Tel. 93 26 22  
A-1072 VIENNA

**Belgium**  
M.B.L.E.  
80, rue des Deux Gares  
Tel. 23 00 00  
B-1070 BRUSSELS

**Brazil**  
IBRAPE S.A.  
Av. Paulista 2073-S/Loja  
Tel. 278-1111  
SAO PAULO, SP.

**Canada**  
Philips Electron Devices  
116 Vanderhoof Ave.  
Tel. 425-5161  
TORONTO 17, Ontario

**Chile**  
Philips Chilena S.A.  
Av. Santa Maria 0760  
Tel. 39-40 01  
SANTIAGO

**Colombia**  
SADAPE S.A.  
Calle 19, No. 5-51  
Tel. 422-175  
BOGOTA D.E. 1

**Denmark**  
Miniwatt A/S  
Emdrupvej 115A  
Tel. (01) 69 16 22  
DK-2400 KØBENHAVN NV

**Finland**  
Oy Philips Ab  
Elcoma Division  
Kaivokatu 8  
Tel. 1 72 71  
SF-00100 HELSINKI 10

**France**  
R.T.C.  
La Radiotechnique-Compelec  
130 Avenue Ledru Rollin  
Tel. 357-69-30  
F-75540 PARIS 11

**Germany**  
Valvo G.m.b.H.  
Valvo Haus  
Burchardstrasse 19  
Tel. (040) 3296-1  
D-2 HAMBURG 1

**Greece**  
Philips S.A. Hellénique  
Elcoma Division  
52, Av. Syngrou  
Tel. 915 311  
ATHENS

**Hong Kong**  
Philips Hong Kong Ltd.  
Components Dept.  
11th Fl., Din Wai Ind. Bldg  
49 Hoi Yuen Rd  
Tel. K-42 82 05-8  
KWUNTONG

**India**  
INBELEC Div. of  
Philips India Ltd.  
Band Box House  
254-D, Dr. Annie Besant Rd  
Tel. 457 311-5  
Prabhadevi, BOMBAY-25-DD

**Indonesia**  
P.T. Philips-Ralin Electronics  
Elcoma Division  
Djalan Gadjah Mada 18  
Tel. 44 163  
DJAKARTA

**Ireland**  
Philips Electrical (Ireland) Ltd.  
Newstead, Clonskeagh  
Tel. 69 33 35  
DUBLIN 14

**Italy**  
Philips S.p.A.  
Sezione Elcoma  
Piazza IV Novembre 3  
Tel. 69 94  
I-20124 MILANO

**Japan**  
NIHON PHILIPS  
32nd Fl., World Trade Center Bldg.  
5, 3-chome, Shiba Hamamatsu-cho  
Minato-ku  
Tel. (435) 5204-5  
TOKYO

**Mexico**  
Electrónica S.A. de C.V.  
Varsovia No. 36  
Tel. 5-33-11-80  
MEXICO 6, D.F.

**Netherlands**  
Philips Nederland B.V.  
Afd. Elonco  
Boschdijk 525  
Tel. (040) 79 33 33  
NL-4510 EINDHOVEN

**New Zealand**  
EDAC Ltd.  
70-72 Kingsford Smith Street  
Tel. 873 159  
WELLINGTON

**Norway**  
Electronica A.S.  
Middelthunsgate 27  
Tel. 46 39 70  
OSLO 3

**Peru**  
CADESA  
Jr. ilo, No. 216  
Apartado 10132  
Tel. 27 73 17  
LIMA

**Philippines**  
EDAC  
Philips Industrial Dev. Inc.  
2246 Pasong Tamo Street  
Tel. 88 94 53 (to 56)  
MAKATI-RIZAL

**Portugal**  
Philips Portuguesa S.A.R.L.  
Av. Eng. Duharte Pacheco 6  
Tel. 68 31 21  
LISBOA 1

**Singapore**  
Philips Singapore Private Ltd.  
8th Fl., International Bldg  
360 Orchard Road  
Tel. 37 22 11  
SINGAPORE-9

**South Africa**  
EDAC (Pty.) Ltd.  
South Park Lane  
New Doornfontein  
Tel. 24/6701-2  
JOHANNESBURG

**Spain**  
COPRESA S.A.  
Balmes 22  
Tel. 232 66 80  
BARCELONA 7

**Sweden**

ELCOMA A.B.  
Lidingövägen 50  
Tel. 08/67 97 80  
S-10 250 STOCKHOLM 27

**Switzerland**

Philips A.G.  
Edenstrasse 20  
Tel. 01/44 22 11  
CH-8027 ZUERICH

**Taiwan**

Philips Taiwan Ltd.  
3rd Fl., San Min Building  
57-1, Chung Shan N. Rd, Section 2  
P.O. Box 22978  
Tel. 553101-5  
TAIPEI

**Turkey**

Türk Philips Ticaret A.S.  
EMET Department  
Gümüssuyu Cad. 78-80  
Tel. 45.32.50  
Beyoğlu, ISTANBUL

**United Kingdom**

Mullard Ltd.  
Mullard House  
Torrington Place  
Tel. 01-580 6633  
LONDON WC1E 7HD

**United States**

Ferroxcube Corporation,  
P. O. Box 359,  
Mt. Marion Rd.  
SAUGERTIES, N.Y. 12477

**Uruguay**

Luzilectron S.A.  
Rondeau 1567, piso 5  
Tel. 9 43 21  
MONTEVIDEO

**Venezuela**

C.A. Philips Venezolana  
Elcoma Dept.  
Av. Principal de los Ruices  
Edif. Centro Colgate, Apdo 1167  
Tel. 36.05.11  
CARACAS

Notes

## Notes

## Notes



## Notes

